Magnetic pyrochlore oxides

Jason S. Gardner*

NIST Center for Neutron Research, National Institute of Standards and Technology, Gaithersburg, Maryland 20899-6102, USA and Indiana University, 2401 Milo B. Sampson Lane, Bloomington, Indiana 47408-1398, USA

Michel J. P. Gingras†

Department of Physics and Astronomy, University of Waterloo, Waterloo, Ontario, Canada N2L 3G1 and Canadian Institute for Advanced Research, 180 Dundas Street West, Toronto, Ontario, Canada M5G 1Z8

John E. Greedan‡

Department of Chemistry and Brockhouse Institute for Materials Research, McMaster University, Hamilton, Ontario, Canada L8S 4M1

(Published 26 January 2010)

Within the past 20 years or so, there has occurred an explosion of interest in the magnetic behavior of pyrochlore oxides of the type $A_2^{3+}B_2^{4+}O_7$, where A is a rare-earth ion and B is usually a transition metal. Both the A and B sites form a network of corner-sharing tetrahedra which is the quintessential framework for a geometrically frustrated magnet. In these systems the natural tendency to form long-range ordered ground states in accord with the third law of thermodynamics is frustrated, resulting in some novel short-range ordered alternatives, such as spin glasses, spin ices, and spin liquids, and much new physics. This article attempts to review the myriad of properties found in pyrochlore oxides, mainly from a materials perspective, but with an appropriate theoretical context.

DOI: 10.1103/RevModPhys.82.53 PACS number(s): 74.25.Ha, 75.40.Cx, 75.25.−j

CONTENTS

I. Introduction 54
A. Overview 54
B. Motivation for the study of frustration 55
C. Historical perspective 56
D. Theoretical background 57
II. Materials 59
A. Crystal structure 60
1. Space group and atomic positions 60
2. Local environment of the A and B sites 60
3. Alternative views of the pyrochlore structure 61
4. Phase stability 62
B. Sample preparation and characterization 62
C. Metal-insulator transitions in the oxide pyrochlores 63
III. Experimental Results 64
A. Long-range ordered phases 64
1. $Gd_2Ti_2O_7$ and $Gd_2Sn_2O_7$ 65
2. $Er_2Ti_2O_7$ 66
3. $Tb_2Sn_2O_7$ 68
4. $A_2Ru_2O_7$ (A=Y, Gd, Dy, Ho, Er, and Tl) 68
5. $A_2Mn_2O_7$ (A=Sc, Y, Tb–Lu, and Tl) 70
a. $Tl_2Mn_2O_7$ 71
b. $Y_2Mn_2O_7$ 72
c. $Ho_2Mn_2O_7$ and $Yb_2Mn_2O_7$ 75
6. $A_2Ir_2O_7$ (A=Nd–Yb) 75
7. $A_2Mo_2O_7$ (A=Gd, Nd, and Sm) 77
a. $Gd_2Mo_2O_7$ 77
b. $Nd_2Mo_2O_7$ 78
c. $Sm_2Mo_2O_7$ 79
d. $A_2(MoB)_2O_7$ 79
B. Spin-glass phases 79
1. $Y_2Mo_2O_7$ and $Tb_2Mo_2O_7$ 80
a. $Y_2Mo_2O_7$ 80
b. $Tb_2Mo_2O_7$ 83
c. Other $A_2Mo_2O_7$ 84
C. Spin-ice phases 84
1. $Dy_2Ti_2O_7$ and $Ho_2Ti_2O_7$ 87
2. $A_2Sn_2O_7$ (A=Pr,Dy, and Ho) 92
3. $Ho_{2+x}Ti_{2-x}O_{7-\delta}$: Stuffed spin ice 92
D. Spin-liquid phases 93
1. $Tb_2Ti_2O_7$ 93
2. $Yb_2Ti_2O_7$ 96
3. $Er_2Sn_2O_7$ 97
4. $Pr_2Ir_2O_7$ 97
E. External perturbations 98
1. Magnetic field 98
a. $Gd_2Ti_2O_7$ 98
b. Spin ice 98
c. $Tb_2Ti_2O_7$ 99
2. High pressure 99

*jsg@nist.gov
†gingras@gandalf.uwaterloo.ca
‡greedan@univmail.cis.mcmaster.ca

a. $Tb_2Ti_2O_7$ 100
b. $A_2Mo_2O_7$ (A=Gd and Tb) 100
IV. Conclusions 101
Acknowledgments 101
References 101

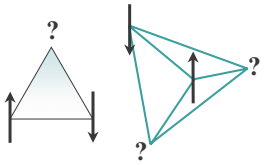

FIG. 1. (Color online) Antiferromagnetically coupled spins arranged on a triangle or tetrahedron are geometrically frustrated.

I. INTRODUCTION

A. Overview

Competing interactions, or frustration, are common in systems of interacting degrees of freedom. The frustration arises from the fact that each of the interactions in competition tends to favor its own characteristic spatial correlations. A more operational definition classifies a system as frustrated whenever it cannot minimize its total classical energy by minimizing the interaction energy between each pair of interacting degrees of freedom, pair by pair. Frustration is ubiquitous in condensed matter physics. It arises in liquid crystals, in superconducting Josephson junction arrays in a magnetic field, in molecular crystals such as solid N_2, and in magnetic thin films. Frustration is important outside the realm of condensed matter physics in, for example, the competition between nuclear forces and long-range electrostatic Coulomb interactions between protons which is believed to lead to the formation of a so-called "nuclear pasta" state of spatially modulated nuclear density in stellar interiors. This enhances the scattering cross section for neutrinos with nuclear matter and may be a factor in the mechanism of supernovae explosions. Yet, perhaps, the most popular context for frustration is in magnetic systems. This review is concerned with the many interesting and often exotic magnetic and thermodynamic phenomena that have been observed over the past 20 years in a broad family of geometrically frustrated magnetic materials, the pyrochlore oxides. Before launching into the review *per se*, we first outline what is meant by geometric magnetic frustration and comment on the scientific motivation for investigating geometrically frustrated magnetic systems.

Although the details will be provided later, here we give the reader an introduction to the key issues in frustrated magnetic systems. One can distinguish two classes of frustrated magnetic systems: those in which the frustration is *geometric* and those in which it is *random*. The simplest example of geometric frustration is that of Ising spins which can only point in two possible (up or down) directions, interacting via nearest-neighbor antiferromagnetic exchange and which lie at the vertices of an equilateral triangle, as shown in Fig. 1. Under those conditions, it is impossible for the three spins to align mutually antiparallel to each other. When many triangles are condensed to form an edge-sharing triangular lattice, a massive level of configurational spin disorder results, giving rise to an extensive residual zero temperature entropy and no phase transition down to absolute zero temperature (Houtappel, 1950; Wannier, 1950, 1973). This example is one of geometric frustration since it is the regular periodic structure of the (here triangular) space lattice that imposes the constraint inhibiting the development of a long-range ordered state given antiferromagnetic interactions between the spins. The same system with Ising spins on a triangular lattice, but with ferromagnetic interactions, is not frustrated and displays a second order phase transition to long-range order at nonzero temperature.

One can distinguish two types of random frustration. The first one arises due to competing interactions among degrees of freedom in full thermodynamic equilibrium, as in the case of liquid crystals and the nuclear pasta mentioned above. Although it is not commonly referred to as such, one could speak of "dynamical frustration" or "annealed frustration" by analogy to annealed disorder. Since there is rarely only one type of interaction setting a sole characteristic length scale in any realistic system, annealed frustration is really the norm. In this context, the most dramatic signature of dynamical frustration occurs when multiple length scales develop as in modulated phases of condensed matter, for example, the case of stripes in the copper-oxide superconducting materials or in the case of re-entrant phase transitions as in some liquid crystal materials. In other words, a system with competing interactions will often attempt to resolve the underlying frustration by developing nontrivial spatial correlations, such as modulated structures, whenever full dynamical equilibrium is maintained. We return to the topic of multiple dynamical degrees of freedom and annealed frustration when discussing the role that lattice degrees of freedom may play in geometrically frustrated magnetic systems.

The other case of random frustration arises when the randomness is "quenched," i.e., frozen in. This occurs when a subset of the degrees of freedom evolves on a time scale that is, for all practical purposes, infinitely long compared to the predominant degrees of freedom under focus. Consider the example above of the triangular lattice Ising antiferromagnet. There the position of the atoms is quenched and only the magnetic (spin) degrees of freedom are dynamical. This is an example of quenched frustration. However, the frustration in that case is said to be geometric, not random. Quenched random frustration arises in systems where the frozen degrees of freedom (e.g., positions of the magnetic atoms) are not related by periodic translational invariance. One example of random frustration is that of magnetic iron (Fe) atoms in a gold (Au) matrix. In AuFe, the interaction between the Fe moments is mediated by conduction electrons via the Rudermann-Kittel-Kasuya-Yoshida (RKKY) $J_{RKKY}(r)$ interaction, which can be either ferro-

magnetic or antiferromagnetic depending on the distance r between two magnetic Fe atoms. Depending on their relative separation distance, some trios of Fe spins will have either one or three of their J_{RKKY} interactions antiferromagnetic and will therefore be frustrated. Because the atomic positions are frozen in, this is an example of *quenched random frustration*. Quenched random frustration is a crucial ingredient in the physics of spin-glass materials (Binder and Young, 1986). These systems exhibit a transition from a paramagnetic state of thermally fluctuating spins to a glasslike state of spins frozen in time but random in direction. Random frustration can also arise when the magnetic moments in an otherwise disorder-free geometrically frustrated system are diluted or substituted with nonmagnetic atoms (Villain 1979; Binder and Young, 1986).

While it is common to invoke exchange interactions between spins as the source of their magnetic coupling, there are cases (discussed below) where magnetostatic dipole-dipole interactions play a crucial role. Because of their long-range nature and angular dependence, dipolar interactions are intrinsically frustrated, irrespective of the lattice dimensionality or topology. Indeed, two dipole moments $\boldsymbol{\mu}_1$ and $\boldsymbol{\mu}_2$ at positions $\boldsymbol{r}_1$ and $\boldsymbol{r}_2$ ($\boldsymbol{r}_{12}=\boldsymbol{r}_2-\boldsymbol{r}_1$) reach their minimum energy for $\boldsymbol{\mu}_1\|\boldsymbol{\mu}_2\|\boldsymbol{r}_{12}$. Obviously, this condition cannot be met for any system of more than two dipole moments that are not all located on a perfectly straight line. As a result, even systems where long-range collinear ferromagnetism is due to dipolar interactions are in fact frustrated and display quantum mechanical zero-point fluctuations (Corruccini and White, 1993; White *et al.* 1993). This example illustrates that even systems which achieve a seemingly simple conventional long-range order can be subject to frustration of their underlying microscopic interactions. Being intrinsically frustrated, the introduction of randomness via the substitution of dipole-carrying atoms by nonmagnetic (diamagnetic) species can lead for sufficiently large dilution to a spin-glass phase (Villain, 1979; Binder and Young, 1986).

B. Motivation for the study of frustration

Magnetism and magnetic materials are pervasive in everyday life from electric motors to hard disk data storage. From a fundamental perspective, magnetic materials and theoretical models of magnetic systems have, since the original works of Ising and Potts, offered physicists perhaps the best test bench to investigate the broad fundamental concepts, even at time universal ones, underlying collective phenomena in nature. The reasons for this are threefold. First, from an experimental perspective, magnetic materials present themselves in various aspects. They can be metallic, insulating, or semiconducting. As well, the magnetic species may reside on crystalline lattices which are spatially anisotropic, providing examples of quasi-one- or quasi-two-dimensional systems and permitting an exploration of the role that spatial dimensionality plays in phase transitions. Second, and perhaps most importantly, magnetic

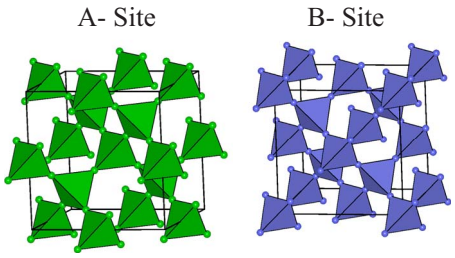

FIG. 2. (Color online) The A and B sublattices of the cubic pyrochlore materials. Either or both sublattices can be magnetic.

materials can be investigated via a multitude of experimental techniques that can probe many aspects of magnetic and thermodynamic phenomena by exploring spatial and temporal correlations over a range of several decades of length or time scales. Finally, from a theoretical view point, magnetic materials can often be described by well-defined microscopic Hamiltonian models which, notwithstanding the mathematical complexity commonly associated in solving them, allow in principle to develop a theoretical framework that can be used to interpret experimental phenomena. This close relationship between theory and experiment has been a key characteristic of the systematic investigation of magnetism since its incipiency. Such a symbiotic relationship between experiment and theory has been particularly strong in the context of investigations of frustrated magnetism systems. Indeed, a number of experimental and theoretical studies in frustrated magnetic systems were originally prompted by theoretical proposals. We mention two. The first pertains to the proposal that frustrated antiferromagnets with a noncollinear ordered state may display a transition to a paramagnetic state belonging to a different ("chiral") universality class from conventional O(N) universality for collinear magnets (Kawamura, 1988). The second, perhaps having stimulated the largest effort, is that some frustrated quantum spin systems may lack conventional semiclassical long-range order altogether and possess instead a quantum disordered "spin-liquid" state breaking no global spin or lattice symmetries (Anderson, 1973, 1987).

Systems where magnetic moments reside on lattices of corner-sharing triangles or tetrahedra are subject to geometric magnetic frustration, as illustrated in Fig. 1, and are expected to be ideal candidates for exhibiting large quantum mechanical spin fluctuations and the emergence of novel, exotic, magnetic ground states.

The cubic pyrochlore oxides, $A_2B_2O_7$, have attracted much attention over the past 20 years because the A and B ions reside on two distinct interpenetrating lattices of corner-sharing tetrahedra as shown in Fig. 2. Henceforth, we refer to the lattice of corner-sharing tetrahedra simply as the pyrochlore lattice, as has become customary since the mid-1980s. If A, B, or both are magnetic and the nearest-neighbor exchange interaction is antiferromagnetic, the system is highly geometrically frustrated. As a result, antiferromagnetically coupled classical Heisenberg spins on the pyrochlore lattice do not

develop long-range order at any nonzero temperature, opening up new avenues for novel intrinsically quantum mechanical effects to emerge at low temperatures.

In all real systems, interactions other than isotropic nearest neighbor exchange are at play. Exchange beyond nearest neighbors, symmetric and antisymmetric (Dzyaloshinskii-Moriya) exchanges, dipolar interactions, and magnetoelastic couplings are all concrete examples of corrections to the isotropic nearest-neighbor exchange part of the Hamiltonian, $\mathcal{H}_H$. These additional interactions, $\mathcal{H}'$, are typically weaker than $\mathcal{H}_H$ and often two or more terms in $\mathcal{H}'$ compete to dictate the development of the spin-spin correlations as the system is cooled from the paramagnetic phase. The specific details pertaining to the material under consideration determine whether the perturbations $\mathcal{H}'$ are ultimately able to drive the system into a semiclassical long-range ordered state or whether quantum fluctuations end up prevailing. It is for this reason that many magnetic pyrochlore oxides have been found to display a gamut of interesting and unconventional magnetic and thermodynamic behaviors. Examples of phenomena exhibited by $A_2B_2O_7$ materials include spin glass freezing in $Y_2Mo_2O_7$, spin-liquid behavior in $Tb_2Ti_2O_7$, disordered spin-ice (not to be confused with spin-glass) phenomenology in $Ho_2Ti_2O_7$ and $Dy_2Ti_2O_7$, ordered spin ice in $Tb_2Sn_2O_7$, order by disorder in $Er_2Ti_2O_7$, unconventional anomalous Hall effect in metallic $Nd_2Mo_2O_7$, superconductivity in $Cd_2Re_2O_7$, and the Kondo-like effect in $Pr_2Ir_2O_7$ to name a few.

The above examples illustrate the broad diversity of phenomena exhibited by pyrochore oxides. There exist a number of general reviews concerned with pyrochlore structure materials such as those by Subramanian *et al.* (1983), Greedan (1992), and Subramanian and Sleight (1993) and more focused reviews, for example, on the rare-earth titanates (Greedan, 2006). Pyrochlore structure materials are often featured in more general reviews of geometrically frustrated magnetic materials, such as those by Ramirez (1994), Schiffer and Ramirez (1996), Greedan (2001), and others (Diep, 1994, 2004; Gaulin, 1994). The purpose of this review article is to provide a comprehensive review of both experimental and theoretical investigations of the $A_2B_2O_7$ materials over the past 20 years or so. Whenever possible, we outline promising avenues for future work. Thus, space limitations preclude detailed discussion of other very interesting highly frustrated magnetic materials based on lattices of corner-shared triangles such as kagome systems and garnets, or the spinels and Laves phases, which are also based on the pyrochlore lattice. However, we refer to those materials in specific contexts whenever appropriate in order to either contrast or relate to the behavior observed in the pyrochlore oxides.

This review is organized as follows. After a historical overview and some generalities on geometrically frustrated magnets we review and discuss experimental data from the most static (i.e., long-range ordered phases) to the most dynamic (i.e., spin-liquid phases). Finally, we report on salient results from experiments performed under the influence of applied magnetic field or pressure. We conclude the review with a discussion of perceived avenues for future research.

C. Historical perspective

The term frustration, meaning the inability of a plaquette of spins with an odd number of antiferromagnetic bonds to adopt a minimum energy collinear spin configuration, first appeared in a paper on spin glasses by Toulouse (1977) and soon after in one by Villain (1977). However, it is said that the concept of frustration as a key ingredient in the physics of spin glasses was first introduced by Anderson who apparently wrote on a blackboard at a summer school in Aspen in 1976 "Frustration is the name of the game" (Chandra and Coleman 1995; Harrison, 2004). It is interesting that the notion of frustration, random frustration to be more precise, had to await the discovery of spin glasses before it was introduced in magnetism.

Geometrically frustrated antiferromagnets, without being labeled as such, had been studied much earlier. In 1950, Houtappel (1950) and Wannier (1950) investigated the exact solution of the Ising antiferromagnet on the triangular lattice, finding that no transition to long range order occurs at positive temperature and that the system possesses an extensive ground state entropy. Soon after, following on a previous work by Néel (1948), Yafet and Kittel (1952) investigated the problem of antiferromagnetic spin arrangements in spinel ferrite materials and the role of magnetic interactions between the octahedral and the tetrahedral sites in determining the ground state spin structure, where the octahedral sites form a pyrochlore lattice. Motivated by the problem of magnetic ordering for spins on the octahedral sites of normal spinels and the related one of ionic ordering in inverse spinels, Anderson (1956) investigated the physics of antiferromagnetically coupled Ising spins on what we now recognize as the pyrochlore lattice. This work appears to have been the first to identify clearly the peculiar magnetic properties of this system and, in particular, noted the existence of a macroscopic number of ground states and the connection with the problem of the zero-point proton entropy in hexagonal water ice previously investigated by Pauling (1935). We return to the connection between geometrically frustrated Ising spins on the pyrochlore lattice and the water ice problem later.

Quantum mechanics made its first noticeable entry in the realm of geometrically frustrated magnetism in 1973 when Anderson (1973) proposed that a regular two-dimensional triangular lattice of spins $S=1/2$ coupled via nearest-neighbor antiferromagnetic exchange could, instead of displaying a three sublattice 120° Néel ordered state, possess an exotic *resonating valence bond* liquid of spin singlets. This proposal was further examined and its conclusion was supported by more detailed calculations by Fazekas and Anderson (1974). While Anderson (1973) had written that there were no experimental realizations of an $S=1/2$ antiferromagnet with isotropic exchange, the situation would change dramati-

cally almost 25 years later with the 1987 discovery of the copper-oxide-based high-temperature superconductors, some of which possess a parent insulating state with antiferromagnetically coupled $S=1/2$ spins (Anderson, 1987).

The discovery of spin glasses by Cannella and Mydosh (1972) prompted a flurry of experimental and theoretical activity aimed at understanding the nature of the observed spin freezing and determining whether a true thermodynamic *spin-glass* phase transition occurs in these systems. Villain (1979) investigated the general problem of insulating spin glasses and the role of weak dilution of the B-site pyrochlore lattice in spinels. The extensive ground state degeneracy characterizing this system for classical Heisenberg spins interacting via nearest-neighbor antiferromagnetic exchange, J, was noted. Villain speculated that such a system would remain in a paramagneticlike state down to zero temperature, giving rise to a state at temperatures $T \ll J$ that he called a *collective paramagnet*—a classical spin liquid of sorts. Villain (1979) also considered the case of tetragonal spinels where there are two exchange couplings, J and J', perpendicular and parallel to the tetragonal axis. More recently, theoretical (Yamashita and Ueda, 2000; Tchernyshyov *et al.*, 2002) and experimental (Lee *et al.*, 2000) studies investigated the cubic to tetragonal distortion in spinels, which leads to a relief of the magnetic frustration and allows the system to develop long-range magnetic order. Villain discussed how the effect of a *weak* dilution of the magnetic moments may be dramatically different in the case of cubic spinels compared to those with a slight tetragonal distortion. In particular, he argued that in the case of the cubic spinel, weak dilution would leave the system a collective paramagnet, while for the tetragonal spinel, the ground state would be glassy.

While there had been some experimental studies on noncollinear magnets between the work of Villain and the mid-to-late 1980s (Coey, 1987), the high level of research activity in the field of frustrated magnetism really only started following the discovery of the unconventional magnetic properties of $SrCr_{9-x}Ga_{3+x}O_{19}$ by Obradors *et al.* (1988). In the context of oxide pyrochlores, experimental and theoretical interests developed in the mid-1980s with reports of spin-glass behavior in the apparently well-ordered material $Y_2Mo_2O_7$ (Greedan *et al.*, 1986) and accelerated rapidly after 1990.

D. Theoretical background

The amount of theoretical work dedicated to the topic of highly frustrated systems, particularly quantum spin systems, has exploded over the past ten years. It is beyond our scope here to discuss more than a fragment of this work. We refer the interested reader to Diep (2004) and Lacroix *et al.* (2010). In this section, we present the simplest and most generic theoretical arguments of relevance to the pyrochlore systems. The focus of the discussion is on the effects of perturbations on a nearest-neighbor Heisenberg pyrochlore antiferromagnet.

One simple and highly convenient measure of the level of frustration in magnetic systems is the so-called frustration index f (Ramirez, 1994), defined as

$$f \equiv |\theta_{\mathrm{CW}}|/T^*. \tag{1}$$

Here θ_{CW} is the Curie-Weiss temperature, defined from the high-temperature paramagnetic response of the system, i.e., the high-temperature, linear part of the inverse dc susceptibility. The temperature T^* is the critical temperature T_c (or Néel temperature T_N) at which the system ultimately develops long-range spin order. In the case of freezing into a glassy state, which may correspond to a genuine thermodynamic spin-glass transition, T^* would be the freezing temperature T_f. The more frustrated a system is, the lower T^* is compared to θ_{CW}; hence an ideal spin-liquid system would have $f=\infty$. In most real materials there are, however, perturbative interactions, $\mathcal{H}'$, that ultimately intervene at low temperature and lead to the development of order out of the spin-liquid state. The rest of this section discusses some of the most common perturbations.

Anderson (1956) and Villain (1979) were the first to anticipate the absence of long-range order at nonzero temperature in the Ising (Anderson, 1956) and the Heisenberg (Villain, 1979) pyrochlore antiferromagnets. The Hamiltonian for the Heisenberg antiferromagnet model is

$$\mathcal{H}_H = -J\sum_{\langle i,j\rangle} \boldsymbol{S}_i \cdot \boldsymbol{S}_j, \tag{2}$$

where we take for convention that $J<0$ is antiferromagnetic while $J>0$ is ferromagnetic. The spins $\boldsymbol{S}_i$ can be, at least within the model, taken as either classical and of fixed length $|\boldsymbol{S}_i|=1$ or quantum. A model with $n=1$, 2, or 3 components of $\boldsymbol{S}$ corresponds to the Ising, XY, and Heisenberg model, respectively. Since the pyrochlore lattice has cubic symmetry, the Ising and XY models with a uniform global Ising easy axis direction $\hat{z}$ or XY global plane are not physical. One can, however, define local $\hat{z}_i$ Ising directions or local XY planes with normal $\hat{z}_i$ that are parallel to the four cubic $\langle 111\rangle$ directions.

A mean field theory calculation for the Heisenberg Hamiltonian by Reimers, Berlinsky, and Shi (1991) provided indirect confirmation of the result of Anderson and Villain by finding that a nearest-neighbor model with classical Heisenberg spins on the pyrochlore lattice has two (out of four) branches of exactly degenerate soft (critical) modes throughout the Brillouin zone. In other words, there is an extensive number of soft modes in this system and no unique state develops long-range order at the mean field critical temperature. In early Monte Carlo simulations, Reimers (1992) found no sign of a transition in this system either to long-range order or to a more complex type, such as nematic order, down to a temperature of $J/20$, where J is the nearest-neighbor antiferromagnetic exchange constant. This conclusion was further confirmed in numerical studies by Moessner and

Chalker (1998a, 1998b). The behavior of the nearest-neighbor pyrochlore antiferromagnet differs markedly from that of the nearest-neighbor classical Heisenberg antiferromagnet on the two-dimensional kagome lattice where coplanar order by disorder develops as the temperature drops below $\sim J/100$ (Chalker *et al.*, 1992; Reimers and Berlinsky, 1993). However, the Mermin-Wagner-Hohenberg theorem forbids a phase transition at nonzero temperature in the kagome Heisenberg antiferromagnet. While no transition is seen in the pyrochlore Heisenberg system (Reimers, 1992; Moessner and Chalker, 1998a, 1998b), the pyrochlore lattice with easy-plane (XY) spins, where the easy planes are perpendicular to the local $\langle 111 \rangle$ directions, displays a phase transition to long-range order (Bramwell *et al.*, 1994; Champion *et al.*, 2003). Finally, in agreement with Anderson's prediction (Anderson, 1956), Monte Carlo simulations find that the Ising antiferromagnet or, equivalently, the Ising ferromagnet with local $\langle 111 \rangle$ directions, which is the relevant model to describe spin-ice materials, does not order down to the lowest temperature (Harris, Bramwell, Holdsworth, and Champion, 1998).

Moessner and Chalker (1998a, 1998b) investigated the conditions under which an n-component classical spin $\vec{S}_i$ with $|\vec{S}_i|=1$ arranged on a lattice of corner-sharing units of q sites and interacting with $q-1$ neighbors in each unit can exhibit thermally induced order by disorder. Their analysis allows one to rationalize why the Heisenberg $n=3$ kagome antiferromagnet develops coplanar order and why the XY pyrochlore antiferromagnet (with spins in a global XY plane) develops collinear order (Moessner and Chalker, 1998a). From their analysis, one would predict a phase transition to long-range nematic order for $q=3$, $n=3$ in three spatial dimensions. Interestingly, the situation $q=3$, $n=3$ arises in the $S=1/2$ $Na_4Ir_3O_8$ hyperkagome (Okamoto *et al.*, 2007) and $Gd_3Ga_5O_{12}$ garnet (Schiffer *et al.*, 1994; Schiffer, Ramirez, Huse, *et al.*, 1995; Petrenko *et al.*, 1998; Dunsiger *et al.*, 2000; Yavors'kii *et al.*, 2006). Moving away from the strictly nearest-neighbor model, one would generally expect interactions beyond nearest neighbors to drive a transition to an ordered state at least for classical spins (Reimers, 1992). While this has been studied via Monte Carlo simulations (Reimers *et al.*, 1992; Mailhot and Plumer, 1993), it has not been the subject of many investigations. In that context, we note that Pinettes *et al.* (2002) studied a classical Heisenberg pyrochlore antiferromagnet with an additional exchange interaction J' that interpolates between the pyrochlore lattice ($J'=0$) and the face-centered-cubic lattice ($J'=J$). It is found that for J'/J as low as $J'/J \sim 0.01$, the system orders into a collinear state whose energy is greater than the classical incommensurate ground state predicted by mean field theory. A Monte Carlo study of another classical model of a pyrochlore lattice with antiferromagnetic nearest-neighbor exchange and ferromagnetic next-nearest-neighbor exchange finds an ordered state with mixed ordered and dynamical character (Tsuneishi *et al.*, 2007). Because the pyrochlore lattice lacks bond inversion symmetry, Dzyaloshinsky-Moriya spin-spin interactions arising from spin-orbit coupling are allowed and can give rise to various ordered states depending on the orientation of the Dzyaloshinsky-Moriya vector (Elhajal *et al.*, 2005).

As discussed below, a number of pyrochlore materials exhibit glassy behavior where the spins freeze at low temperature into a state where their orientation is random in space but frozen in time (Binder and Young, 1986). It is not yet fully understood whether this glassy behavior is due to the intrinsic nature of the systems considered, as is the case for the spin ices, or if it originates from random disorder (e.g., antisite disorder, random bonds, or other) as in conventional random disorder spin glasses (Binder and Young, 1986). Only a few theoretical studies have explored the effect of random disorder in antiferromagnetic pyrochlores with classical Heisenberg spins and with small and homogoneously random deviations of exchange J_{ij} from the average antiferromagnetic exchange J (Bellier-Castella *et al.*, 2001; Saunders and Chalker, 2007). Interestingly, random bonds on a single tetrahedron lift the degeneracy and drive an order by (random) disorder to a collinear spin arrangement. However, on the lattice, the system remains frustrated and there is no global order by disorder (Bellier-Castella *et al.*, 2001). Considering this model in more detail, Saunders and Chalker (2007) found compelling evidence of a conventional spin-glass transition. Sagi *et al.* (2005) investigated how coupling with the spins to the lattice may lead to a freezing behavior and trapping of the spins into metastable states in an otherwise disorder-free nearest-neighbor classical pyrochlore antiferromagnet. Villain (1979) discussed the role of nonmagnetic impurities on the pyrochlore lattice antiferromagnet. He argued that the collective paramagnetic behavior of the otherwise disorder-free system should survive up to a finite concentration of impurities. A similar conclusion was reached on the basis of heuristic arguments and simulations for the site-diluted two-dimensional kagome Heisenberg antiferromagnet (Shender *et al.*, 1993). It would be valuable if the problems of site-disorder and dilute random bonds in the antiferromagnetic pyrochlore lattice were explored in more detail. We note in passing that the problem of disorder in quantum variants of the kagome Heisenberg antiferromagnet has attracted some attention (Läuchli *et al.*, 2007).

In insulating $A_2B_2O_7$, where A is a $4f$ rare-earth trivalent ion, the inter-rare-earth exchange interactions are often small, contributing only 10^0–10^1 K to the Curie-Weiss θ_{CW} temperature. This is because the unfilled magnetically active $4f$ orbitals are strongly shielded by the $5s$, $5p$, and $5d$ orbitals and their direct exchange overlap or superexchange overlap is small. At the same time, trivalent rare earth ions often possess large magnetic moments and hence the magnetostatic dipole-dipole energy scale is significant compared to θ_{CW} and needs to be incorporated into Eq. (2),

$$\mathcal{H}_{\rm int} = -\frac{1}{2}\sum_{(i,j)} \mathcal{J}_{ij}\boldsymbol{J}_i\cdot\boldsymbol{J}_j + \left(\frac{\mu_0}{4\pi}\right)\frac{(g_{\rm L}\mu_{\rm B})^2}{2r_{\rm nn}^3}\sum_{(i,j)}\frac{\boldsymbol{J}_i\cdot\boldsymbol{J}_j - 3\boldsymbol{J}_i\cdot\hat{\boldsymbol{r}}_{ij}\hat{\boldsymbol{r}}_{ij}\cdot\boldsymbol{J}_j}{(r_{ij}/r_{\rm nn})^3}. \quad (3)$$

Here we have taken the opportunity to generalize Eq. (2) to the case where the total angular momentum $\boldsymbol{J}_i = \boldsymbol{L}_i + \boldsymbol{S}_i$ is included. $g_{\rm L}$ is the Landé factor and $\boldsymbol{r}_j - \boldsymbol{r}_i = |\boldsymbol{r}_{ij}|\hat{\boldsymbol{r}}_{ij}$, where $\boldsymbol{r}_i$ is the position of magnetic ion i. In general, one needs to include the role of the single-ion crystal field, $\mathcal{H}_{\rm cf}$, to the full Hamiltonian $\mathcal{H} = \mathcal{H}_{\rm cf} + \mathcal{H}_{\rm int}$.

A mean field study of $\mathcal{H}_{\rm int}$, with $\mathcal{H}_{\rm cf}=0$ and with only nearest-neighbor antiferromagnetic $\mathcal{J}_{\rm nn}$ and dipolar interactions of approximately 20% the strength of $\mathcal{J}_{\rm nn}$, was done by Raju *et al.* (1999) to investigate the type of order expected in $Gd_2Ti_2O_7$. The assumption $\mathcal{H}_{\rm cf}=0$ is a reasonable first approximation for $Gd_2Ti_2O_7$ since the electronic ground state of Gd^{3+} is ${}^8S_{7/2}$ with $L=0$. Raju *et al.* (1999) argued that this model has an infinite number of soft modes with arbitrary ordering wave vector along [111] and that the transition at ~1 K could possibly proceed via order by disorder. However, Palmer and Chalker (2000) argued that quartic terms in the mean field Ginzburg-Landau theory would select a $\mathbf{k}_{\rm ord}=000$ ordering wave vector at the critical temperature T_c that also corresponds to the zero temperature classical ground state. Subsequent mean field calculations (Enjalran and Gingras, 2003; Cépas and Shastry, 2004) showed that there are in fact two very closely spaced transitions and that the transition at the highest temperature is at a unique ordering wave vector ($\mathbf{k}_{\rm ord}=\frac{1}{2}\frac{1}{2}\frac{1}{2}$) that had been missed in previous calculations (Raju *et al.*, 1999; Palmer and Chalker, 2000). A Monte Carlo simulation (Cépas *et al.*, 2005) found a single first order transition. It appears likely that the small temperature separation between the two transitions that is predicted by mean field theory is not resolved in the Monte Carlo simulation. Irrespective of the subtleties associated with the transition, it is generally accepted that the classical ground state of the nearest-neighbor pyrochlore Heisenberg antiferromagnet with weak dipolar interactions is the so-called Palmer-Chalker ground state (Palmer and Chalker, 2000; Enjalran and Gingras, 2003; Cépas and Shastry, 2004; Del Maestro and Gingras, 2004, 2007; Wills *et al.*, 2006). Starting from the Palmer-Chalker ground state, a $1/S$ expansion calculation shows that all conventional magnetic spin-wave-like excitations of this system are gapped and that the $1/S$ quantum fluctuations are negligible (Del Maestro and Gingras, 2004, 2007). For Ho- and Dy-based pyrochlore oxides, the crystal-field Hamiltonian $\mathcal{H}_{\rm cf}$ produces a single-ion ground state doublet and the system maps onto a classical dipolar Ising model. We return to this model when reviewing the problem of spin ice in Sec. III.C.

Another important perturbation of relevance to real materials is the coupling between spin and lattice degrees of freedom. Spin-lattice coupling can lead to a redistribution of the frustration among the magnetic bonds such that the energy cost for distorting the lattice is more than compensated by the energy difference between that of the more strongly coupled antiparallel spins on the compressed bonds compared to the higher energy (frustrated, parallel) spins on the dilated bonds (Yamashita and Ueda, 2000; Tchernyshyov *et al.*, 2002). It is anticipated that such coupling can lead to a global lifting of magnetic degeneracy and drive a transition to long-range magnetic order that is accompanied by a cubic to tetragonal lattice deformation. Villain (1979) also discussed a number of significant differences in the thermodynamic properties and the response to random disorder of a tetragonal spinel compared to that of a cubic spinel. The problems of magnetic order, lattice distortion, coupling to an external magnetic field, and magnetization plateaus in oxide spinels are currently very topical ones (Lee *et al.*, 2000; Tchernyshyov *et al.*, 2002; Penc *et al.*, 2004; Bergman *et al.*, 2006). However, in pyrochlore oxides, interest in the role of the lattice degrees of freedom is just starting to attract attention (Sagi *et al.*, 2005; Ruff *et al.*, 2007).

We close with a discussion of the quantum $S=1/2$ pyrochlore Heisenberg antiferromagnet. This is obviously an extremely difficult problem and there is no concensus yet about the nature of the ground state. It appears to have been first studied by Harris *et al.* (1991) who found indicators that the system may form a dimerized state at low temperature. Applying perturbation theory to the density matrix operator, Canals and Lacroix (1998, 2000) found evidence for a quantum spin liquid in the $S=1/2$ pyrochlore antiferromagnet. From exact diagonalizations on small clusters, they also found that the singlet-triplet gap is filled with a large number of singlets similar to what is observed in the $S=1/2$ kagome lattice antiferromagnet (Lecheminant *et al.*, 1997). Calculations using the contractor-renormalization method (Berg *et al.*, 2003) found a ground state that breaks lattice symmetry, analogous to that suggested by Harris *et al.* (1991), and with a singlet-triplet gap filled with singlets, similar to Canals and Lacroix (1998). Moving away from strictly numerical approaches, analytical calculations based on large-N (Moessner *et al.*, 2006; Tchernyshyov *et al.*, 2006) and large-S expansions (Hizi and Henley, 2007) as well as variational calculations away from an exact dimer covering ground state solution (Nussinov *et al.*, 2007) have been recently carried out.

II. MATERIALS

While this review is focused on the three-dimensional pyrochlore lattice, which is shown in Fig. 2, there are of course other lattice types which provide the conditions for geometric frustration. Among these, in two spatial dimensions are the edge-sharing and corner-sharing triangular lattices—the latter best known as the kagome lattice—and in three spatial dimensions one has garnets, langasites, and face-centered-cubic lattices among others. There exists considerable literature devoted to these materials which lies outside the scope of this work.

A network of corner-sharing tetrahedra is found in several common mineral types in nature. The octahedrally coordinated B site of the spinel class of minerals (AB_2O_4) forms a network of corner-sharing tetrahedra. The A and B sites can be filled by many ions, but when the B site is occupied by a trivalent magnetic transition metal ion, magnetic frustration can play a role in its bulk properties. The trivalent chromates have recently sparked considerable interest (Lee *et al.*, 2000, 2002; Ueda *et al.*, 2005; Matsuda *et al.*, 2007). Another common family of materials that contain a network of corner-sharing tetrahedra is the cubic Laves phases, such as YMn_2 (Shiga *et al.*, 1993; Ballou, 2001).

As already emphasized, in this review we restrict ourselves to the cubic pyrochlore oxides with the general formula $A_2B_2O_7$, where A is a trivalent rare earth which includes the lanthanides, Y, and sometimes Sc and B is either a transition metal or a p-block metal ion. It should be mentioned that it is possible to form $A_2^{2+}B_2^{5+}O_7$ $(2+,5+)$ pyrochlores; however, these are not common and have not been studied in great detail. Most of this review will deal with the $(3+,4+)$ variety of pyrochlores, but when appropriate the $(2+,5+)$ will be discussed.

A. Crystal structure

1. Space group and atomic positions

Pyrochlore materials take their name from the mineral $NaCaNb_2O_6F$, pyrochlore, the structure of which was first reported by von Gaertner (1930). The name, literally "green fire," alludes to the fact that the mineral shows a green color upon ignition. Most synthetic pyrochlores of interest here are oxides that crystallize in the space group $Fd\bar{3}m$ (No. 227). As pointed out by Subramanian and Sleight (1993), confusion can exist due to the fact that there are four possible choices for the origin. Currently, standard practice is to formulate oxide pyrochlores as $A_2B_2O_6O'$ and to place the B ion at 16c (the origin of the second setting for $Fd\bar{3}m$ in the International Tables of Crystallography), A at 16d, O at 48f, and O′ at 8b, as shown in Table I. Note that there is only one adjustable positional parameter x for the O atom in 48f. There are at least two important implications of these structural details. One concerns the topology of the 16c and 16d sites and the other the coordination geometry of the O ligands about the two metal sites. Both the 16c and 16d sites form a three-dimensional array of corner-sharing tetrahedra, as shown in Fig. 2, thus giving rise to one of the canonical geometrically frustrated lattices.

2. Local environment of the A and B sites

The coordination geometry about the two metal sites is controlled by the value of x for the O atom in the 48f site. For $x=0.3125$ one has a perfect octahedron about 16c and $x=0.375$ gives a perfect cube about 16d. In fact x is usually found in the range of 0.320–0.345 and the two geometries are distorted from the ideal polyhedra. For a typical pyrochlore the distortion about the B ion or 16c site is relatively minor. The $\bar{3}m$ (D_{3d}) point symmetry requires that all six B-O bonds must be of equal length. The O-B-O angles are distorted only slightly from the ideal octahedral values of 90° ranging between 81° and 100°. The distortion of the A-site geometry from an ideal cube is very large. This site is depicted in Fig. 3 and is best described as consisting of a puckered six-membered ring of O atoms with two O′ atoms forming a linear O′-A-O′ stick oriented normal to the average plane of the six-membered ring. The A-O and A-O′ bond distances are very different. While typical A-O values are 2.4–2.5 Å, in accord with the sum of the ionic radii, the A-O′ bonds are among the shortest known for any rare-earth oxide, ≈2.2 Å. Thus, the A site has very pronounced axial symmetry, the unique axis of which is along a local ⟨111⟩ direction. This in turn has profound implications for the crystal field at the A site which determines much of the physics at play in pyrochlore materials where the A ion is magnetic.

TABLE I. The crystallographic positions for the space group $Fd\bar{3}m$ (No. 227) suitable for the cubic pyrochlore $A_2B_2O_6O'$ with origin at 16c.

Atom	Wyckoff position	Point symmetry	Minimal coordinates
A	16d	$\bar{3}m$ (D_{3d})	$\frac{1}{2}, \frac{1}{2}, \frac{1}{2}$
B	16c	$\bar{3}m$ (D_{3d})	0, 0, 0
O	48f	mm (C_{2v})	$x, \frac{1}{8}, \frac{1}{8}$
O′	8b	$\bar{4}3m$ (T_d)	$\frac{3}{8}, \frac{3}{8}, \frac{3}{8}$

Recall that the spin-orbit interaction is large in rare-earth ions and the total angular momentum $\boldsymbol{J}=\boldsymbol{L}+\boldsymbol{S}$ is a good quantum number. For a given ion one can apply Hund's rules to determine the isolated (usually) electronic ground state. Electrostatic and covalent bonding

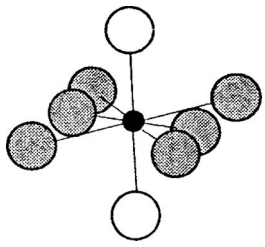

FIG. 3. The coordination geometry of the A site by O (shaded spheres) and O′ (open spheres) atoms. The O′-A-O′ unit is oriented normal to the average plane of a puckered six-membered ring. This bond is one of the shortest seen between a rare earth and oxygen ions.

effects originating from the local crystalline environment, the so-called crystal field (CF), lift the $2J+1$ degeneracy of the ground state. A discussion of modern methods for calculation of the CF for *f*-element ions is beyond the scope of this review but is described, for example, by Hüfner (1978). For our purposes we will assume the single-ion energy levels, the wave functions, the eigenvectors, and the eigenenergies of the CF Hamiltonian $\mathcal{H}_{\rm cf}$ have been suitably determined either through *ab initio* calculations or from optical or neutron spectroscopy [see, for example, Rosenkranz *et al.* (2000) and more recently Mirebeau *et al.* (2007)].

$\mathcal{H}_{\rm cf}$ can be expressed in terms of either the so-called tensor operators or the "operator equivalents" due to Stevens (1952). The two approaches are contrasted by Hüfner (1978). While the tensor operators are more convenient for *ab initio* calculations, the latter are better suited to our purposes here. In this formalism, $\mathcal{H}_{\rm cf}$ is expressed in terms of polynomial functions of J_{iz} and $J_{i\pm}$, with $J_{i\pm}=J_{ix}\pm J_{iy}$, which are components of the $\boldsymbol{J}_i$ angular momentum operator. The most general expression for $\mathcal{H}_{\rm cf}$ is

$$\mathcal{H}_{\rm cf}=\sum_i \sum_{l,m} B_l^m O_l^m(\boldsymbol{J}_i), \tag{4}$$

where, for example, the operator equivalents are $O_2^0=3J_z^2-J(J+1)$ and $O_6^6=J_+^6+J_-^6$. The full CF Hamiltonian for $-3m$ (D_{3d}) point symmetry involves a total of six terms for $l=2$, 4, and 6 (Greedan, 1992). In fact, due to the strong axial symmetry of the *A* site, described previously, it can be argued that the single $l=2$ term B_2^0 plays a major role in the determination of the magnetic anisotropy of the ground state. In the Stevens formalism, $B_2^0=A_2^0\langle r^2\rangle\alpha_J(1-\sigma_2)$, where A_2^0 is a point charge lattice sum representing the CF strength, $\langle r^2\rangle$ is the expectation value of r^2 for the $4f$ electrons, σ_2 is an electron shielding factor, and α_J is the Stevens factor (Stevens, 1952). This factor changes sign in a systematic pattern throughout the lanthanide series, being positive for *A* = Sm, Er, Tm, and Yb and negative for all others. So, the sign of B_2^0 depends on the product $\alpha_J A_2^0$ and A_2^0 is known from measurements of the electric field gradient from, for example, ^{155}Gd Mössbauer studies, to be positive for pyrochlore oxides (Barton and Cashion, 1979). Thus, B_2^0 should be positive for *A* = Sm, Er, Tm, and Yb and negative for all others. From the form of B_2^0 above, it is clear that states of different $|M_J\rangle$ do not mix and that the energy spectrum will consist of a ladder of states with either $|M_{J_{(\rm min)}}\rangle$ ($B_2^0>0$) or $|M_{J_{(\rm max)}}\rangle$ ($B_2^0<0$) as the ground state. Note that the former constitutes an easy plane and the latter an easy axis with respect to the quantization axis which is $\langle 111\rangle$ for pyrochlores. A comparison of the known anisotropy for the $A_2Ti_2O_7$ and $A_2Sn_2O_7$ materials, that is, easy axis for *A* = Pr, Nd, Tb, Dy, and Ho and easy plane for *A* = Er and Yb with the sign of B_2^0, shows a remarkable agreement with this simple argument. [Note that only the Stevens formalism works here. The tensor operator definition of B_2^0 is $B_2^0=A_2^0\langle r^2\rangle$, so this quantity is always positive for pyrochlore oxides, independent of the rare earth *A*. We do not maintain that the actual ground state wave function can be obtained within such a simple model (although the agreement for *A* = Dy and Ho is remarkable), rather that the overall anisotropy can be predicted without a detailed calculation.]

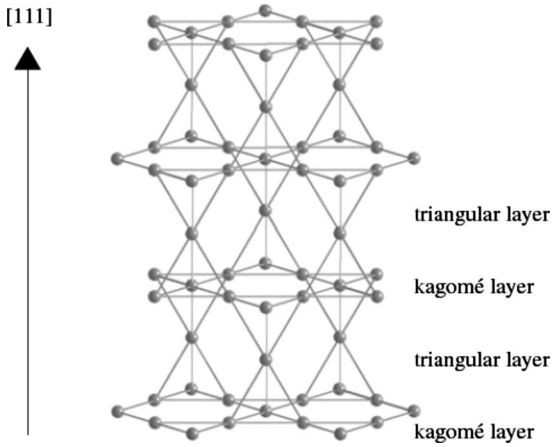

FIG. 4. Alternating kagome and triangular planar layers stacked along a [111] direction of the pyrochlore lattice.

3. Alternative views of the pyrochlore structure

An important feature of the pyrochlore structure relevant to the central theme of this review is the fact that the 16*c* or 16*d* sites form layers stacked along a [111] direction, as shown Fig. 4. From this perspective, the pyrochlore lattice is seen to consist of alternating kagome and triangular planar layers. From the viewpoint of chemical bonding, the pyrochlore structure can be described either as an ordered defect fluorite (CaF_2) or as two interpenetrating networks, one of composition B_2O_6, which is a network of corner-sharing metal-oxygen octahedra (topologically equivalent to that found in the perovskite structure), and the other of composition A_2O', which forms a zigzag chain through the large channels formed by the B_2O_6 network. These models have been described in several previous reviews and the discussion here focuses on a few important issues. While there is a topological relationship with the perovskites, the pyrochlore lattice is considerably more rigid. For example, the *B*-O-*B* angle in which the O atom is shared between two octahedra is restricted to a very narrow range in pyrochlores, usually from about 127° to 134°, with only little influence from the size of the *A* ion. This angle can range from 180° to 140° in perovskites where there is a strong variation with the radius of the *A* ion. The interpenetrating network description allows an understanding of the formation of so-called defect or "rattling" pyrochlores, such as KOs_2O_6, in which the entire A_2O' network is missing and where the large K^+ ion occupies the 8*b* site which is normally occupied by O′ in the standard pyrochlore structure. The disordered fluorite model is useful in

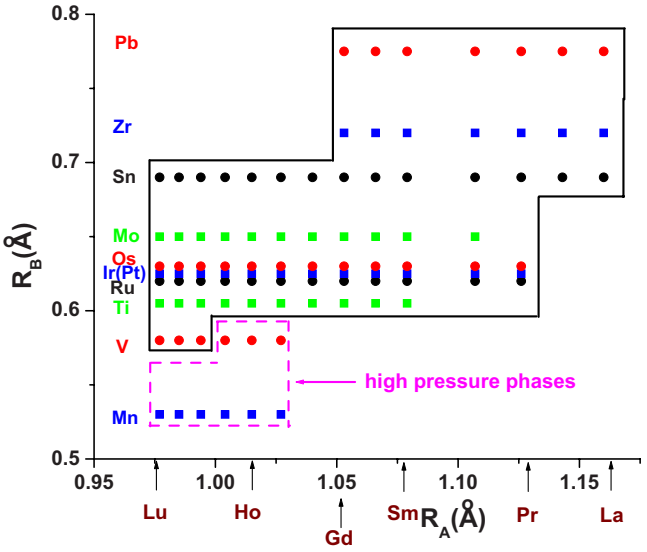

FIG. 5. (Color online) A structure-field or stability-field map for $A_2B_2O_7$ materials. The B=Pt series are also high-pressure phases. Adapted from Subramanian and Sleight, 1993.

cases where a disordered defect fluorite structure phase competes with the ordered pyrochlore, such as for the $A_2Zr_2O_7$ series where A/B site mixing is observed.

4. Phase stability

There are over 15 tetravalent ions that can reside on the B site of a cubic pyrochlore at room temperature. Pyrochlore oxides of most interest here are formed with a rare-earth ion in the A site and transition or p-block elements in the B site. The rare-earth elements form a series in which the trivalent state predominates and through which the ionic radius decreases systematically with increasing atomic number (the so-called lanthanide contraction). Nonetheless, it is uncommon to find that the pyrochlore phase is stable for all A for a given B.

The most efficient way to display the range of stability of pyrochlores in the space of the ionic radii is through a structure-field map or structure-stability map. Figure 5 is an abridged version of a comprehensive map by Subramanian and Sleight (1993). It is worth noting that the B=Sn series is the only one to form for all rare earth ions. There would also appear to be minimal and maximal ionic radius ratios, A^{3+}/B^{4+}, which define the stability limits for pyrochlore phases of this type. For B ions with very small radii, such as Mn^{4+}, the pyrochlore phase can be prepared only using high-pressure methods. This is in strong contrast to perovskites of the type $A^{2+}Mn^{4+}O_3$ which can be prepared easily under ambient oxygen pressures. The first series stable under ambient pressure is that for B=V but only for the three smallest members, Lu, Yb, and Tm. The series can be extended using high-pressure synthesis (Troyanchuk, 1990). For the largest B ion, Pb^{4+}, the smallest rare earth for which a stable pyrochlore is found appears to be Gd. Thus, an ambient pressure stability range defined in terms of radius ratios (RRs), A^{3+}/B^{4+}, would extend between 1.36 and 1.71 with marginal stability expected as those limits are approached. There are exceptions, for example, $Pr_2Ru_2O_7$ is clearly stable with a RR of 1.82, yet $Pr_2Mo_2O_7$ does not exist with a RR=1.73.

Also of relevance to this review are issues of defect formation in pyrochlores. This is an active area of research in materials science where defect pyrochlores which show high ionic conductivities are of interest. While the defect levels are often small and difficult to quantify via experiment, some computational guidelines have appeared recently (Minervini *et al.*, 2002). The general trend is that defect concentrations are predicted to increase as the RR approaches its lower limit, for example, as the B radius increases within any given series, and that the predicted levels are generally of the order of 1% or less.

B. Sample preparation and characterization

Polycrystalline samples of pyrochlore oxides readily form by a standard solid state process, where stoichiometric proportions of high purity (>99.99%) rare earth and transition metal oxides are calcined at 1350 °C over several days in air with intermittent grindings. Elements known to exist in the cubic (3+,4+) pyrochlore phase are highlighted in the Periodic Table shown in Fig. 6. Several series of compounds with particularly volatile elements, such as tin, require excess material to account for losses during the heating processes and others require heating under special atmospheres to form the desired oxidation state. For example, the molybdates require a vacuum furnace or a reducing atmosphere to form the Mo^{4+} state and the rare-earth manganese (IV) oxide pyrochlores are not stable at ambient pressure and require a high-pressure synthesis technique (Subramanian *et al.*, 1988). Specialized growth conditions will be discussed below as relevant. When high chemical homogeneity is required, the sol-gel method (Kido *et al.*, 1991) has been successful.

Crystals of a several oxide pyrochlores were grown in the 1960s and 1970s by flux methods (Garton and Wanklyn, 1968). The size and quality of the crystals grown by these methods vary, and it is often difficult to obtain voluminous crystals, especially for neutron scattering experiments. The "floating zone" method of crystal growth was first used by Gardner *et al.* (1998) to produce large single crystals of $Tb_2Ti_2O_7$. Later the entire titanate series was produced by others (Balakrishnan *et al.*, 1998; Tang *et al.*, 2006; Zhou *et al.*, 2007) and within the last few years several groups have started to grow many other pyrochlores in image furnaces including molybdates, ruthenates, and stannates (Miyoshi *et al.*, 2002; Taguchi *et al.*, 2002; Wiebe *et al.*, 2004). Single crystals have also been produced by other methods including vapor transport (He *et al.*, 2007), hydrothermal techniques (Chen and Xu, 1998), and KF flux (Millican *et al.*, 2007).

Most oxide pyrochlores are cubic at room temperature with a lattice parameter between 9.8 and 10.96 Å (Subramanian *et al.*, 1983). Of these, the titanates are

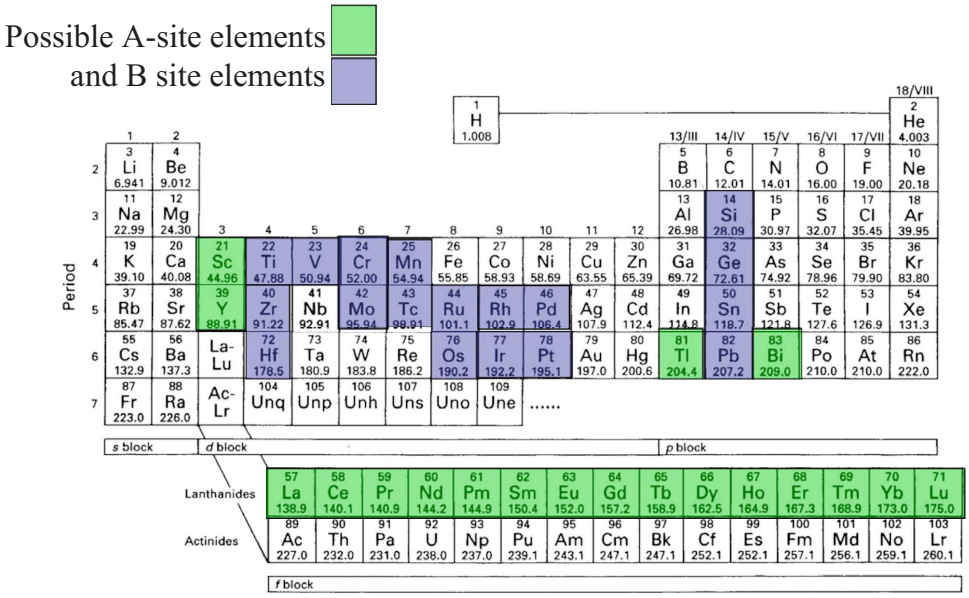

FIG. 6. (Color online) Elements known to produce the (3+,4+) cubic pyrochlore oxide phase.

probably the most studied, followed by the zirconates, but many are still poorly represented in the literature. Both the titanate and zirconate pyrochlores were first reported by Roth (1956). Since then, over 1000 papers have been published on the two families.

C. Metal-insulator transitions in the oxide pyrochlores

Two types of metal-insulator (MI) transitions occur in the oxide pyrochlore family. First are those that, as a function of a thermodynamic variable (e.g., temperature, magnetic field, or pressure), change their transport properties, for example, $Tl_2Mn_2O_7$ (Fujinaka *et al.*, 1979). Second, there is the *series* of compounds where the room temperature character changes from metal to insulator as the rare-earth ion changes, for example, the molybdate (Greedan *et al.*, 1986) or iridate series (Yanagishima and Maeno, 2001). There appears to be little controversy over the first class of MI transition; however, for the second type the exact position of this transition is a topic of debate. For example, in the molybdenum pyrochlore series, studies of their bulk properties have indicated a strong correlation between the magnetism and electrical transport properties, i.e., in early studies the ferromagnets were found to be metallic while the paramagnets were insulating (Greedan *et al.*, 1987; Ali *et al.*, 1989). Indeed, the dependence of the lattice constant a_0 on the A^{3+} radius showed a distinct break at the MI boundary (see Fig. 7). In some subsequent studies, however, $Gd_2Mo_2O_7$ is clearly insulating (Cao *et al.*, 1995; Kézsmárki *et al.*, 2004). The initial studies were carried out on polycrystalline samples, prepared between 1300 and 1400 °C and, in at least one case, in a CO/CO_2 "buffer gas" mixture which fixes the oxygen partial pressure during synthesis (Greedan *et al.*, 1986). Several subsequent studies have used single crystals grown by various methods above 1800 °C, including melt and floating zone growths (Raju and Gougeon, 1995; Moritomo *et al.*, 2001; Kézsmárki *et al.*, 2004). While the polycrystalline samples have been fairly well characterized, including elemental analysis, thermal gravimetric weight gain and measurement of the cubic lattice constant a_0, this is less true of the single crystals. The differences between polycrystalline and single-crystalline samples can be monitored most simply using the unit cell constant as shown in Fig. 8 in which unpublished data (Raju and Gougeon, 1995) for a selection of single crystals of $Gd_2Mo_2O_7$ are plotted. Note that as a_0 increases the samples become more insulating. In all cases, a_0 for the crystals exceeds that for the metallic, polycrystalline sample which is 10.337(1) Å. From accurate structural data for the powders and single crystals, it has been determined that the increase in a_0 correlates with an increase in the Mo-O distance as shown in Fig. 8. The most likely origin of this systematic increase is the substitution of the larger Mo^{3+} for Mo^{4+} which can arise from oxygen deficiency in the crystals, resulting in the formula $Gd_2Mo_{2-2x}{}^{4+}Mo_{2x}{}^{3+}O_{7-x}$. Note that other defect mechanisms, such as vacancies on either the *A* or Mo

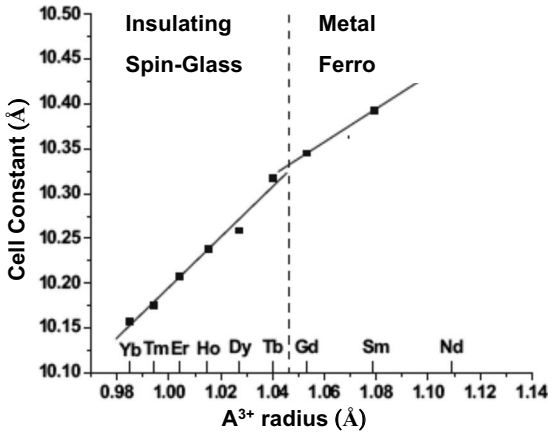

FIG. 7. Variation in unit cell constant and physical properties of the series $A_2Mo_2O_7$ with the A^{3+} radius. From Ali *et al.*, 1989.

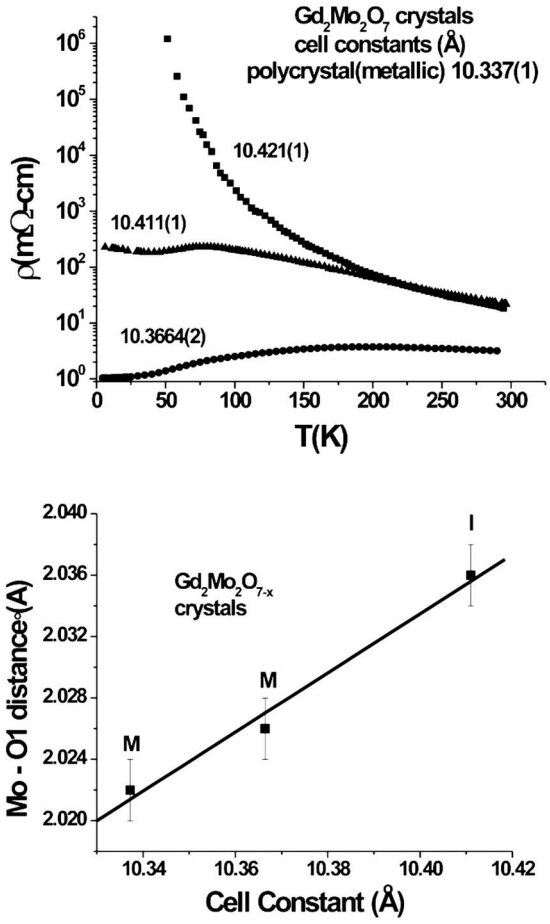

FIG. 8. Variation of electrical resistivity and Mo-O1 distances with unit cell constant for oxygen deficient $Gd_2Mo_2O_{7-x}$ single crystals. Top: Comparison of electrical resistivity data for three single crystals of as $Gd_2Mo_{2-2x}^{4+}Mo_{2x}^{3+}O_{7-x}$ a function of unit cell constant, a_0. Bottom: Variation in the Mo-O distance with increasing cell constant for $Gd_2Mo_2O_{7-x}$ crystals.

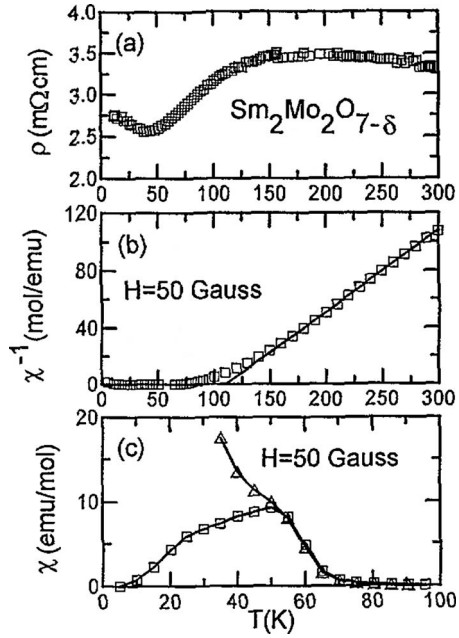

FIG. 9. Properties of an oxygen deficient single crystal of $Sm_2Mo_2O_{7-x}$. (a) Metallic behavior. (b) Inverse susceptibility showing a positive ferromagnetic (FM) Curie-Weiss temperature. (c) Susceptibility showing T_c=65 K and a zero field cooled (squares) and a field cooled (triangles) divergence at 50 K. From Cao *et al.*, 1995.

sites, would result in the oxidation of Mo^{4+} to the smaller Mo^{5+}, which would lead to a reduction in a_0. Further evidence for this mechanism comes from the fact that the crystal with the intermediate cell constant in Fig. 8 was obtained from the most insulating crystal by annealing in a CO/CO_2 buffer gas at 1400 °C for 1–2 days. Thus, insulating single crystals of $Gd_2Mo_2O_7$ are oxygen deficient. This analysis is fully consistent with Kézsmárki *et al.* (2004) who found that $Gd_2Mo_2O_7$ is insulating but can be doped into the metallic state by 10% Ca substitution on the Gd site. Ca doping will of course add holes to the Mo states which compensate for the electron doping due to the oxygen deficiency in the "as grown" crystals. After considering all studies, we conclude that the MI boundary for stoichiometric $A_2Mo_2O_7$ is indeed between A=Gd and Tb.

Single crystals for the other ferromagnetic metals, A=Nd and Sm, are also reported and these are subject to the same oxygen deficiency and electron doping but, as they are farther from the MI boundary, the effects on the physical properties are less drastic. For example, the transport, optical, and magnetic properties, reported by Cao *et al.*, 1995) for $Sm_2Mo_2O_7$ were for an oxygen deficient crystal with a_0=10.425(1) Å, Fig. 9, whereas polycrystalline samples have a_0=10.391(1) Å. While the material is still metallic (albeit a poor metal), the ferromagnetic Curie temperature is reduced by ~30 to 65 K relative to the powder which has T_c=95 K (Sato, Yan, and Greedan, 1986). Note also the zero field cooled (ZFC)/field cooled (FC) divergence below 50 K which suggests a spin-glassy component. Similar results were reported for other A=Sm single crystals, a_0 =10.4196(1) Å, for example, by Moritomo *et al.* (2001) and Park *et al.* (2003), which also show T_c~65 K and a ZFC/FC divergence below 20 K.

The oxide pyrochlores can display a wide range of bulk properties including oxygen ion conductivity, superconductivity, ferroelectricity, and unusual magnetic behavior (e.g., spin liquid and spin ice). However, these are intimately related to their stoichiometry, electrical, and crystallographic properties, as shown in the previous discussion. Whenever possible, we encourage one to measure and report these basic properties at room temperature, especially the lattice constant.

III. EXPERIMENTAL RESULTS

A. Long-range ordered phases

Many magnetic oxide pyrochlores enter a long-range ordered state. These ordered phases are often promoted by single-ion anisotropy, anisotropic spin-spin interactions, and/or further neighbor exchange interactions.

Despite the fact that they develop long-range order, these systems are still of significant interest, providing magnetic systems with axial and planar symmetry, quantum order-by-disorder transition, polarized moments, and partially ordered systems, for example.

1. $Gd_2Ti_2O_7$ and $Gd_2Sn_2O_7$

Antiferromagnetically coupled Heisenberg spins on a pyrochlore lattice are expected to be highly frustrated because the exchange energy can be minimized in an infinite number of ways. Classical (Moessner and Chalker, 1998a) and quantum (Canals and Lacroix, 1998, 2000) calculations showed that the system should remain in a collective paramagnetic state with short-range spin-spin correlations at any nonzero temperature. As discussed in Sec. I.D, Raju *et al.* (1999) reported an infinite number of degenerate spin configurations near the mean field transition temperature when dipolar interactions are considered. However, Palmer and Chalker (2000) showed that a four-sublattice state with the ordering vector $\mathbf{k}_{\mathrm{ord}}=000$ could be stabilized. More recent mean field theory calculations (Enjalran and Gingras, 2003; Cépas and Shastry, 2004) found a higher temperature second order transition to a phase with three ordered sublattices and one disordered one. At a slightly lower temperature another transition was found to the Palmer-Chalker state. In contrast, Monte Carlo simulations by Cépas *et al.* (2005) found a single strongly first order transition to the Palmer-Chalker state. As shown below, the experimental situation is even more complex.

The $S=7/2$ Gd^{3+} ion, with its half-filled $4f$ shell and zero orbital momentum, is the best example of a Heisenberg spin among the rare-earth ions. The bulk susceptibility for both $Gd_2Ti_2O_7$ and $Gd_2Sn_2O_7$ follows the Curie-Weiss law with an effective moment close to the theoretical limit of $7.94\mu_B$ for the free ion (Raju *et al.*, 1999; Bondah-Jagalu and Bramwell, 2001) and a Curie-Weiss temperature of $\theta_{\mathrm{CW}}\sim-10$ K. Both compounds, however, enter a magnetically ordered state at $\approx$1 K, resulting in a frustration index, f, of about $f\sim10$.

Early specific heat and ac susceptibility measurements showed that $Gd_2Ti_2O_7$ entered an ordered phase at 0.97 K (Raju *et al.*, 1999). A subsequent specific heat study showed two transitions in zero applied field, at 0.97 and 0.7 K (Ramirez *et al.*, 2002), and additional phase transitions, induced in applied fields. These phases were later confirmed by single-crystal magnetization work by Petrenko *et al.* (2004).

The nature of these ordered states is hard to determine by neutron diffraction due to the high absorption cross section of gadolinium. However, a small, enriched, sample of $^{160}Gd_2Ti_2O_7$ has been studied. In an initial work at 50 mK, a partially ordered noncollinear antiferromagnetic structure was proposed (Champion *et al.*, 2001). This unusual spin configuration had 3/4 of the Gd^{3+} spins ordered within kagome planes, separated by the triangular plane of Gd ions (see Fig. 4), which remain disordered down to the lowest temperature. This model was later modified when the diffuse scattering

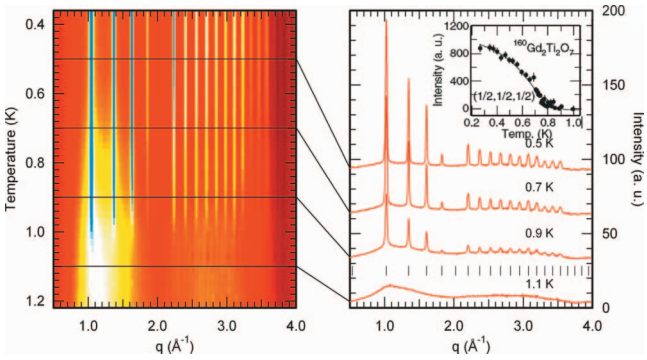

FIG. 10. (Color) Low temperature magnetic neutron powder diffraction data for $Gd_2Ti_2O_7$. Left: False color map of the temperature dependence of the magnetic diffraction from $Gd_2Ti_2O_7$. As temperature is lowered, the broad diffuse scattering centered at 1.2 Å^{-1} sharpens into peaks. Right: Diffraction patterns at specific temperatures are shown along with tic marks indicating where Bragg reflections should be for the proposed ground state (see main text). At the lowest temperatures the $\frac{1}{2}\frac{1}{2}\frac{1}{2}$ reflection has some intensity and this is highlighted in the inset. From Stewart, Ehlers, and Gardner, 2004.

and a new magnetic reflection at $\frac{1}{2}\frac{1}{2}\frac{1}{2}$ were observed and studied (Stewart, Ehlers, Wills, *et al.*, 2004). The magnetic scattering from $^{160}Gd_2Ti_2O_7$ is shown in Fig. 10. Very broad diffuse scattering is seen above 1 K. Below this temperature, Bragg peaks occur at the reciprocal lattice positions indicated by the tick marks (vertical bars) in the right panel. The lowest angle magnetic reflection, the very weak $\frac{1}{2}\frac{1}{2}\frac{1}{2}$ peak at $|\mathbf{Q}|=0.6$ Å^{-1}, only gains intensity below the second transition. At all temperatures, diffuse magnetic scattering is observed which diminishes as the temperature decreases and the Bragg peaks grow. The diffuse magnetic scattering, centered at $|\mathbf{Q}|\approx1.2$ Å^{-1}, indicates that the correlation length of the disordered spins is $\approx$3.5 Å, the nearest-neighbor distance and not 7 Å appropriate for the model proposed earlier by Champion *et al.* (2001). This picture of two different Gd moments is consistent with ^{155}Gd Mössbauer experiments (Bonville, Hodges, Ocio, *et al.*, 2003). Most interestingly, this is not the state proposed by Palmer and Chalker (2000). There is currently no theoretical explanation for the ordered phases of $Gd_2Ti_2O_7$.

The isostructural stannate $Gd_2Sn_2O_7$ has received comparatively less attention. As mentioned above, the paramagnetic properties are similar to $Gd_2Ti_2O_7$ (Matsuhira, Hinatsu, *et al.*, 2002). However, only one transition (at 1.0 K) and only one Gd moment have been observed in $Gd_2Sn_2O_7$ (Bonville, Hodges, Ocio, *et al.*, 2003). Recent neutron diffraction measurements by Wills *et al.* (2006), shown in Fig. 11, have confirmed that $Gd_2Sn_2O_7$ undergoes only one transition down to the lowest temperatures and that the ground state is the one predicted theoretically by Palmer and Chalker (2000) for a Heisenberg pyrochlore antiferromagnet with dipolar interactions.

The difference in these two materials highlights the extreme sensitivity of the ground state to small changes

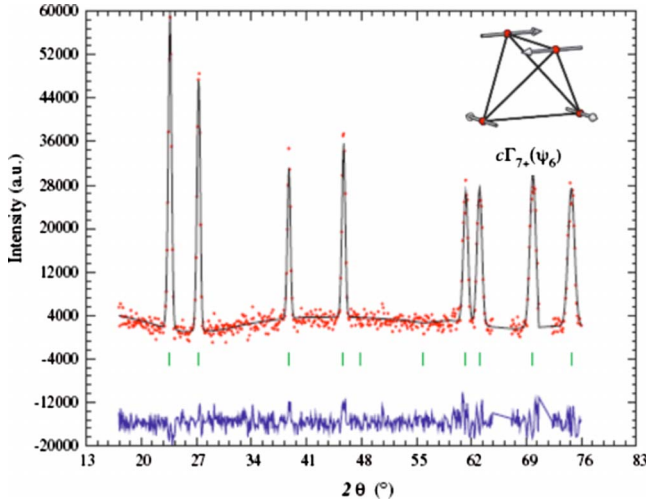

FIG. 11. (Color online) Neutron powder diffraction pattern from $Gd_2Sn_2O_7$ at 0.1 K after a nuclear background (1.4 K) data set was subtracted (Wills *et al.*, 2006). Inset: one of the three Γ_{7+} basis vectors that describe the data (see fit), consistent with the Palmer-Chalker model (Palmer and Chalker, 2000).

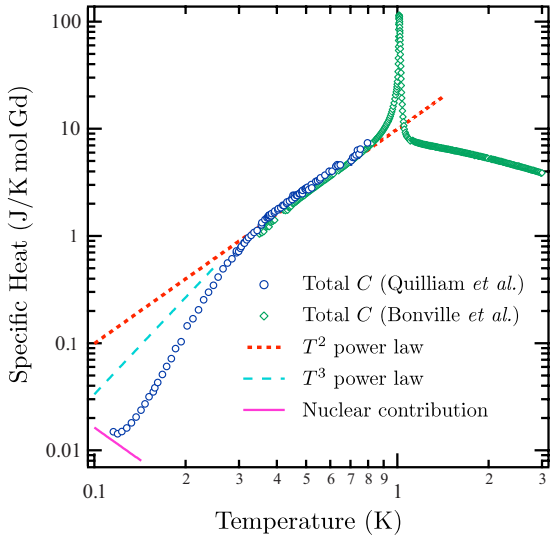

FIG. 12. (Color online) Specific heat of $Gd_2Sn_2O_7$ from Quilliam *et al.*, 2007 (circles) and Bonville, Hodges, Ocio, *et al.*, 2003 (diamonds). The T^2 power law (dotted line) and a conventional T^3 power law (dashed line) for a three-dimensional antiferromagnet are plotted. The upturn seen below 150 mK results from the nuclear electric quadrupole interaction (Quilliam *et al.*, 2007).

in composition and of the consequential details in the spin-spin interactions in these highly frustrated materials. Wills *et al.* (2006) proposed that a different relative magnitude in the two types of third-neighbor superexchange interaction may be responsible for the different ground states in these otherwise very similar Gd compounds (Del Maestro and Gingras, 2007).

To understand the magnetic ground states further and the true cause of the differences between $Gd_2Ti_2O_7$ and $Gd_2Sn_2O_7$ one has to investigate the excitation spectrum. Specific heat is a bulk probe that often provides a reliable insight into the low lying excitations. The specific heat, C_v, of these two compounds just below the transition temperature is described well by an anomalous power law, $C_v \propto T^2$, which had been presumed to be associated with an unusual energy dependence of the density of states (Raju *et al.*, 1999; Ramirez *et al.*, 2002; Bonville, Hodges, Bertin, *et al.*, 2003; Bonville, Hodges, Ocio, *et al.*, 2003). Electron spin resonance (Hassan *et al.*, 2003; Sosin, Smirnov, Prozorova, Balakrishnan, and Zhitomirsky, 2006; Sosin, Smirnov, Prozorova, Petrenko, *et al.*, 2006), Mössbauer (Bertin *et al.*, 2002), muon spin relaxation (Bonville, Hodges, Bertin, *et al.*, 2003; Yaouanc *et al.*, 2005; Dunsiger *et al.*, 2006), and neutron spin echo (Ehlers, 2006) have provided many interesting results. In all these measurements, spin fluctuations were observed much below the ordering temperature of the compound, seemingly consistent with the unusual energy dependence of the density of states invoked to interpret the specific heat measurements. Sosin, Smirnov, Prozorova, Balakrishnan, and Zhitomirsky (2006) and Sosin *et al.* (2008) failed to confirm the unusually large planar anisotropy measured by Hassan *et al.* (2003), however, they found a small gap ≈1 K that coexists with a paramagnetic signal in $Gd_2Ti_2O_7$; no paramagnetic spins were observed at low temperatures in $Gd_2Sn_2O_7$. Recently Quilliam *et al.* (2007) remeasured the specific heat of $Gd_2Sn_2O_7$ and found that the $C_v \propto T^2$ behavior does not hold below 400 mK (see Fig. 12) and that C_v decreases exponentially below 350 mK, providing evidence for a gapped spin-wave spectrum due to anisotropy resulting from single-ion effects and long-range dipolar interactions (Del Maestro and Gingras, 2007).

The current experimental understanding of these Heisenberg antiferromagnets is at this time incomplete. $Gd_2Sn_2O_7$ appears to be a good example of the model considered by Palmer and Chalker (2000), and $Gd_2Ti_2O_7$ is perhaps a small perturbation from this. However, an explanation for the low lying excitations as probed by muon spin relaxation in both compounds still eludes theorists (Del Maestro and Gingras, 2007). Understanding these ubiquitous, low-temperature spin dynamics in a relatively simple model magnet, such as the Gd-based Heisenberg-like antiferromagnet on the pyrochlore lattice, would likely help elucidate the nature of the low-temperature spin dynamics in other frustrated magnets. We discuss in Sec. III.E.1 some recent work on $Gd_2Ti_2O_7$ in a magnetic field.

2. $Er_2Ti_2O_7$

The Er^{3+} single-ion crystal-field ground state in $Er_2Ti_2O_7$ is a Kramers doublet with magnetic moments of $3.8\mu_B$ and $0.12\mu_B$ perpendicular and parallel to the local ⟨111⟩ axis, respectively. $Er_2Ti_2O_7$, like $Yb_2Ti_2O_7$, is a realization of an *XY*-like system on the pyrochlore lattice. However, while $Yb_2Ti_2O_7$ has a small ferromagnetic Curie-Weiss temperature ($\theta_{CW} \sim +0.75$ K) (Hodges *et al.*, 2002), $Er_2Ti_2O_7$ has a large negative Curie-Weiss temperature ($\theta_{CW} \sim -22$ K) (Champion *et al.*, 2003) and

FIG. 13. Ground state spin configuration determined for $Er_2Ti_2O_7$ (Poole *et al.*, 2007). In a macroscopic sample six symmetry equivalent spin configurations will coexist.

is therefore a pyrochlore XY antiferromagnet. The lowest lying crystal-field states of $Er_2Ti_2O_7$ are at 6.38 meV (74.1 K) and 7.39 meV (85.8 K) above the ground states (Champion *et al.*, 2003).

Specific heat measurements show a sharp feature at approximately $T_N \sim 1.2$ K (Blöte *et al.*, 1969; Siddharthan *et al.*, 1999; Champion *et al.*, 2003). Neutron scattering below T_N confirms the existence of a Néel long-range ordered state with propagation vector $\mathbf{k}_{\text{ord}} = 000$. The neutron scattering data strongly suggest a second order phase transition at T_N, with the scattered intensity I vanishing at T_N as $I(T) \propto (T_N - T)^{2\beta}$ with critical exponent $\beta \approx 0.33$, characteristic of the three-dimensional XY model.

As the transition is continuous, the system is expected to order in only one of the irreducible representations of the Er^{3+} site representation. A refinement of the magnetic structure finds that only the two basis vectors ψ_2 or ψ_3 of Γ_5 or a superposition of both is consistent with the observed magnetic intensitites of the Bragg peaks. Results from a spherical neutron polarimetry study find that the zero magnetic field ordered state is described almost entirely by ψ_2 with very little admixing from ψ_3. The spin configuration corresponding to ψ_2 is shown in Fig. 13 (Poole *et al.*, 2007). The experimental observations of (i) an ordering into the noncoplanar ψ_2 structure via (ii) a second order phase transition are both surprising.

As discussed in Secs. I.D and III.A.1, isotropic exchange plus dipolar interactions select by themselves a state with spins perpendicular to the local ⟨111⟩ axes. Hence, easy-plane (XY) anisotropy should further enhance the stability of this state. This was explicitly shown in calculations (Del Maestro and Gingras, 2007) pertaining to $Gd_2Sn_2O_7$ which does display a Palmer-Chalker ground state (Wills *et al.*, 2006). However, a Palmer-Chalker ground state for $Er_2Ti_2O_7$ is seemingly robustly rejected by recent neutron polarimetry experiments (Poole *et al.*, 2007). Since nearest-neighbor antiferromagnetic exchange, dipolar interactions, and the XY nature of the magnetic moments should conspire together to produce a Palmer-Chalker ground state in $Er_2Ti_2O_7$, other interactions or effects must be at play to stabilize the experimentally observed ψ_2 ground state (Poole *et al.*, 2007).

An early numerical study of the classical XY antiferromagnet on the pyrochlore lattice had found a strongly first order transiton into a long-range ordered state with propagation vector $\mathbf{k}_{\text{ord}} = 000$ (Bramwell *et al.*, 1994). This finding was subsequently confirmed by another study (Champion *et al.*, 2003; Champion and Holdsworth, 2004). In earlier work, Bramwell *et al.* (1994) identified only a macroscopic degeneracy of discrete ground states, while there is in fact a continuous degree of freedom for antiferromagnetically coupled XY spins on a single tetrahedron, resulting in a continuous ground state degeneracy for a macroscopic sample (Champion *et al.*, 2003; Champion and Holdsworth, 2004). Monte Carlo simulations of a classical ⟨111⟩ pyrochlore XY antiferromagnet found that the degeneracy is lifted by an order-by-disorder transition driven by thermal fluctuations with the system developing long-range order in the same ψ_2 state as found experimentally in $Er_2Ti_2O_7$. The Monte Carlo results can be rationalized on the basis of a classical spin-wave calculation (Champion and Holdsworth, 2004). There it is found that there are zero energy spin-wave modes over planes in the Brillouin zone for which the spin-wave wave vector $\boldsymbol{q}$ obeys $\boldsymbol{q} \cdot \mathbf{a} = 0$ and $\boldsymbol{q} \cdot (\mathbf{b} - \mathbf{c}) = 0$, where $\mathbf{a}$, $\mathbf{b}$, and $\mathbf{c}$ are the basis vectors of the primitive rhombohedral unit cell of the pyrochlore lattice.

On the basis of the results from Monte Carlo and classical spin-wave calculations, Champion and Holdsworth (2004) proposed that the ψ_2 in $Er_2Ti_2O_7$ is perhaps stabilized by zero point quantum fluctuations, arguing that their effects are captured by the classical spin-wave argument. However, many problems remain with this interpretation. As mentioned above, the transition at $T_N \sim 1.2$ K is second order in the experiment while simulations show a strong first order transition (Champion and Holdsworth, 2004). The density of zero energy classical spin-wave states is also a constant, a result that is incompatible with the experimental specific heat data which show a T^3 temperature dependence below 1 K. Inelastic neutron scattering reveals no evidence for such low lying excitations required to generate the T^3 temperature dependence of the specific heat. The experimental results and models presented above suggest a well established long-range ordered ground state for $Er_2Ti_2O_7$. Yet, muon spin relaxation data reveal that below T_N the muon polarization relaxation rate remains large ($2 \times 10^6\ \mu s^{-1}$) and essentially temperature independent down to 20 mK, indicative of a dynamic ground state (Lago *et al.*, 2005). This behavior reminds one of low-temperature muon data in several pyrochlores including the "ordered" Gd pyrochlores and the "dynamic" $Tb_2Ti_2O_7$.

Unlike $Er_2Ti_2O_7$, $Er_2(GaSb)O_7$ does not appear to order down to 50 mK (Blöte *et al.*, 1969). It is not clear at this stage whether the randomness on the B sites leads to a disordered and glassy phase, i.e., an XY-like spin glass. Results on $Er_2Sn_2O_7$ will be discussed in Sec. III.D.3.

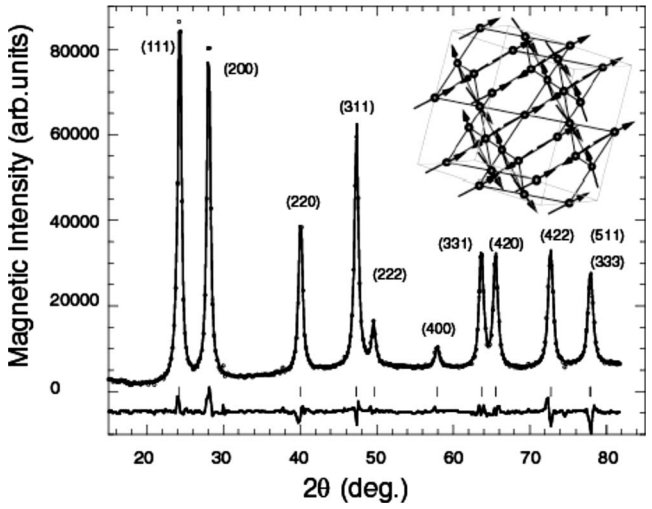

FIG. 14. Magnetic scattering from $Tb_2Sn_2O_7$ at 100 mK. Inset: The proposed ordered spin-ice structure with spins canted off the ⟨111⟩ by 13°. The broad scattering at the base of the Bragg reflections is indicative of spin clusters which reach ≈200 Å at base temperature. From Mirebeau *et al.*, 2005.

3. $Tb_2Sn_2O_7$

Until recently the magnetic and electrical properties of the stannates had received little attention. This is probably due to the slightly more problematic synthesis and the lack of large, high-quality, single crystals.

Like many frustrated magnets, the high-temperature ($T>40$ K) inverse susceptibility is very linear. In $Tb_2Sn_2O_7$, this yields a Curie-Weiss temperature of $\theta_{CW}\sim -12$ K and an effective moment of $9.8\mu_B$, which agrees well with the value of $9.72\mu_B$ for the $^7F_6$ ground state of Tb^{3+} (Bondah-Jagalu and Bramwell, 2001). Reminiscent of the cooperative paramagnet $Tb_2Ti_2O_7$ (see Sec. III.D), the inverse susceptibility deviates downward at ≈30 K upon cooling. However, on cooling further, the system enters a frozen ferromagnetic state at 0.87 K. This was first reported by Matsuhira, Hinatsu, *et al.* (2002) from low-temperature susceptibility measurements and then by Mirebeau *et al.* (2005) who determined the magnetic structure from neutron diffraction measurements. Mirebeau *et al.* (2005) observed a crossover from antiferromagnetic correlations to ferromagnetic correlations at 2 K. This was followed, at a lower temperature, by a transition into an ordered state and the appearance of Bragg peaks (see Fig. 14). Rietveld analysis determined that the spins are canted by 13.3° off the local ⟨111⟩ directions with an ordered moment of $5.9\mu_B$, significantly reduced from the free ion moment of $9\mu_B$, presumably due to crystalline electric field effects.

Ferromagnetically coupled spins on the pyrochlore lattice fixed along the local ⟨111⟩ directions give rise to a highly degenerate state that has become known as the spin-ice state (see Sec. III.C). By comparing the Tb^{3+} moment value deduced from neutron diffraction ($5.9\mu_B$) to the smaller value deduced from the nuclear specific heat ($4.5\mu_B$) Mirebeau, Apetrei, Goncharenko, and Moessner (2006) suggested that slow collective fluctuations, on the time scale of 10^{-4}–10^{-8} s, coexist with the ordered state at the lowest temperatures (Mirebeau, Apetrei, Goncharenko, and Moessner, 2006).

Subsequently, Bert *et al.* (2006) and Dalmas de Réotier *et al.* (2006) suggested that the ground state is not static. They claimed that the absence of any oscillations, even at the shortest times, in the muon spin relaxation spectrum precludes the existence of a static moment. Dalmas de Réotier *et al.* (2006) argued that both neutron and muon data are consistent with a characteristic spin relaxation time of $\approx 10^{-10}$ s, while Bert *et al.* (2006) suggested that the dynamics result from fluctuations of clusters of correlated spins with the ordered spin-ice structure. The results from the neutron spin echo study of Chapuis *et al.* (2007) suggest no spin dynamics below 0.8 K.

Mirebeau, Apetrei, Goncharenko, and Moessner (2006) suggested that the ≈3% expansion in the lattice constant between $Tb_2Sn_2O_7$ and $Tb_2Ti_2O_7$ results in the dipolar interaction overcoming the weakened exchange interaction allowing $Tb_2Sn_2O_7$ to freeze. Clearly more experimental work is needed on this compound to determine the exact nature of the ground state. From inelastic neutron scattering studies, Mirebeau *et al.* (2007) found that the composition of the first two crystal-field levels of $Tb_2Sn_2O_7$ are inverted when compared to those of $Tb_2Ti_2O_7$. This cannot be explained by simple calculations of the local point-charge crystal-field environment and more work is needed to clarify this issue.

4. $A_2Ru_2O_7$ (A=Y, Gd, Dy, Ho, Er, and Tl)

All but the largest, A=La and Ce, rare-earth ruthenates as well as A=Bi and A=Tl form as cubic pyrochlores (Bertaut *et al.*, 1959; Subramanian *et al.*, 1983; Yoshii and Sato, 1999). The lattice parameters vary from 10.07 to 10.355 Å across the rare-earth series with the A=Bi and Tl compounds at the high end of this range. Crystals of several ruthenates have been made by hydrothermal, vapor transport, and floating zone methods (Sleight and Bouchard, 1972; Zhou *et al.*, 2007). Historically, the ruthenium pyrochlore oxides have been extensively studied for their novel conductivity (Pike and Seager, 1977; Carcia *et al.*, 1982) and catalytic activity (Horowitz *et al.*, 1983), but until recently little was known about their magnetic properties. Most of the ruthenates are semiconductors at room temperature with hopping energies of ~0.1 eV, but the Bi based sample is metallic with Pauli paramagnetism. Ru^{4+} (low spin $4d^4$) has an $S=1$ moment and the Ru sublattice appears to order between 70 and 160 K, depending on the rare earth (see Fig. 15). However, θ_{CW} for $Y_2Ru_2O_7$ is reported to be −1250 K although it is not clear that this was obtained in the paramagnetic regime (Gurgul *et al.*, 2007). Studies of diamagnetic A=Y and Lu provide evidence of the magnetic nature of the Ru^{4+} ion. These indicate a magnetic transition at ≈75 K, leading to a high frustration index, $f\approx 17$. The magnetic susceptibilities measured under ZFC and under FC conditions show a different temperature dependence (see Fig. 15). This is

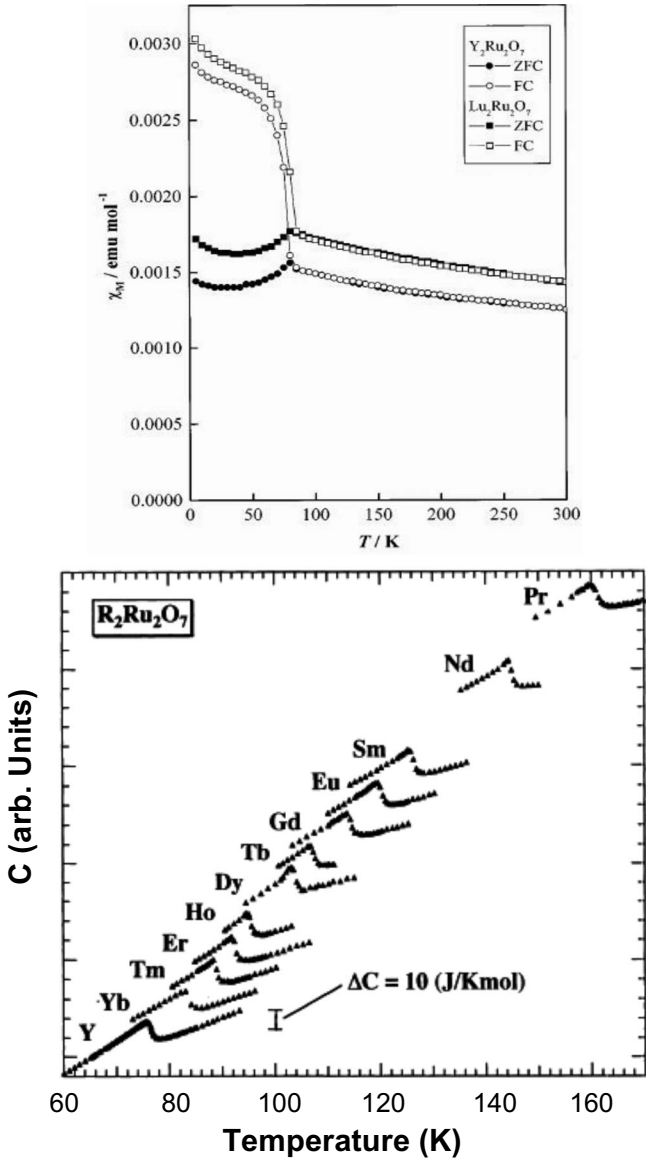

FIG. 15. Magnetic susceptibility and heat capacity results for various $A_2Ru_2O_7$ pyrochlores. Top: The temperature dependence of the susceptibility for Y and Lu ruthenate. Both data sets show the Ru^{4+} moments ordering at ≈75 K. From Taira *et al.*, 1999. Bottom: Heat capacity measurements over the entire rare-earth ruthenate series showing how the Ru^{4+} ordering temperature increases as the size of the rare-earth ion decreases. From Ito *et al.*, 2001.

consistent with the observation of a canted antiferromagnetic structure from neutron diffraction (Ito *et al.*, 2001; Kmieć *et al.*, 2006). Inelastic neutron scattering measurements by van Duijn *et al.* (2008) reveal the development of a large gap in the excitation spectrum below the ordering temperature.

$Er_2Ru_2O_7$ and $Gd_2Ru_2O_7$ have been studied by powder neutron diffraction (Taira *et al.*, 2003) and Mössbauer (Gurgul *et al.*, 2007). In both cases, the Ru sublattice orders at the temperature indicated by the peak in the specific heat plotted in Fig. 15. This long-range ordered state is a $\mathbf{k}_{ord}=000$ type. This is also true for $Y_2Ru_2O_7$ (Ito *et al.*, 2001). In the Er and Gd ruthenates, the rare-earth moment is polarized by the ordered Ru sublattice via the rare-earth-Ru^{4+} exchange interactions. This reveals itself in a small but finite moment on the *A* site as soon as the ruthenium orders. This moment grows with decreasing temperature before the rare-earth ion orders in its own right at 10 K (Er) and 40 K (Gd). A refinement of the low-temperature (3 K) neutron diffraction data from $Er_2Ru_2O_7$ suggests that the magnetic moments, both Er and Ru, are in a plane oriented toward the same [100] direction but antiparallel to each other. The refined moments for Ru^{4+} saturate at the theoretical limit for the $S=1$ ion ($2\mu_B$) at 90 K, but at 3 K the moment on the Er site is only $4.5\mu_B$, 50% of the predicted value, and is probably reduced by crystalline electric field effects, although the signal has not yet saturated at the lowest temperature studied (see Fig. 16).

Since Bansal *et al.* (2002) reported a possible spin-ice ground state (see Sec. III.C) in $Ho_2Ru_2O_7$ and $Dy_2Ru_2O_7$, there have been several studies of the magnetic behavior of $Ho_2Ru_2O_7$ (Bansal *et al.*, 2003; Wiebe *et al.*, 2004; Gardner *et al.*, 2005). In this compound, unlike the other heavy rare-earth ruthenates, a small difference is seen between FC and ZFC when the rare-earth ion orders. This happens at 1.4 K when the Ho^{3+} sublattice enters a long-range ordered state, unlike a true spin-ice material. Lower temperature ($T<20$ K) specific heat (see Fig. 17) also highlights this transition. As seen in a number of geometrically frustrated systems, a broad feature (centered here at ≈3 K) precedes the sharp lambdalike transition at a slightly lower temperature. These features are related to the buildup of short- and long-range correlations between Ho spins. The ordered spin ice has the holmium moments canted off the local ⟨111⟩ axes presumably due to the local fields generated by the ordered Ru^{4+} sublattice. The ordered structure of $Gd_2Ru_2O_7$ is similar to $Ho_2Ru_2O_7$. In both cases the full moment of the rare-earth ion was not measured at the lowest temperatures investigated (Wiebe *et al.*, 2004; Gurgul *et al.*, 2007).

The magnetic entropy associated with $Ho_2Ru_2O_7$ at these low temperatures reaches neither $R\ln 2$ (expected for a completely ordered doublet system) nor $R(\ln 2 - \frac{1}{2}\ln\frac{3}{2})$ (expected for spin ice). In fact, the magnetic entropy of $Ho_2Ru_2O_7$ (Gardner *et al.*, 2005) resembles that of the dipolar spin ices in an applied field of 1 T. Several neutron scattering (Wiebe *et al.*, 2004; Gardner *et al.*, 2005) and ac susceptibility (Gardner *et al.*, 2005) experiments have investigated the spin dynamics in $Ho_2Ru_2O_7$. The nature of the Ho moments is governed by the crystalline electric field levels which are slightly perturbed from those measured in $Ho_2Ti_2O_7$ (Rosenkranz *et al.*, 2000) especially after the ordering of the Ru^{4+} sublattice (Gardner *et al.*, 2005). This is most apparent in neutron spin echo measurements where a 35 K change in the gap to the first excited state is observed once the Ru^{4+} ions order (Gardner *et al.*, 2005) (see Fig. 18).

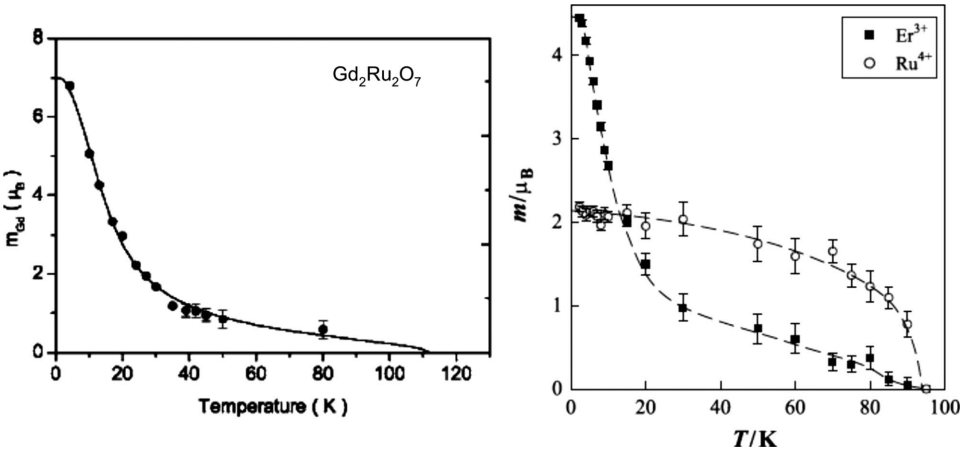

FIG. 16. Temperature dependence of magnetic moments in $Gd_2Ru_2O_7$ and $Er_2Ru_2O_7$. Left: The temperature dependence of the Gd moment from Gd Mössbauer on $Gd_2Ru_2O_7$. From Gurgul *et al.*, 2007. Right: The temperature dependence of the Ru^{4+} and Er^{3+} moments in $Er_2Ru_2O_7$ as measured by neutron diffraction. From Taira *et al.*, 2003.

While $Tl_2Ru_2O_7$ is cubic with a room temperature lattice parameter of 10.18 Å and, when cooled below 120 K, it transforms to an orthorhombic structure. Concomitantly, a metal-insulator transition occurs and the resistivity changes by five orders of magnitude. A sudden drop in the susceptibility also occurs at this temperature (Lee *et al.*, 2006). These data have been interpreted as the three-dimensional analog to the more commonly known one-dimensional $S=1$ Haldane gap system (Haldane, 1983). Specifically, it is believed that the structural phase transition creates effective $S=1$ chains of Ru ions which do not dimerize. These chains are arguably created due to the orbital ordering of the Ru $4d$ electrons.

Three $(2+,5+)$ pyrochlores of interest are $Cd_2Ru_2O_7$ (Wang and Sleight, 1998), $Ca_2Ru_2O_7$ (Munenaka and Sato, 2006), and $Hg_2Ru_2O_7$ (Yamamoto *et al.*, 2007), with an $S=3/2$ Ru^{5+} ion and nonmetallic transport properties. $Hg_2Ru_2O_7$, like $Tl_2Ru_2O_7$, has a metal-insulator transition that is concomitant with a structural phase transition. Single crystals of $Ca_2Ru_2O_7$ have been grown by the hydrothermal method (Munenaka and Sato, 2006) and the effective paramagnetic moment is only $0.36\mu_B$, about one order of magnitude smaller than the theoretical value for the $S=3/2$ ion. At 23 K, there is clear irreversibility between FC and ZFC susceptibilities, indicative of a spin-glass transition and reminiscent of $Y_2Mo_2O_7$ (Greedan *et al.*, 1986).

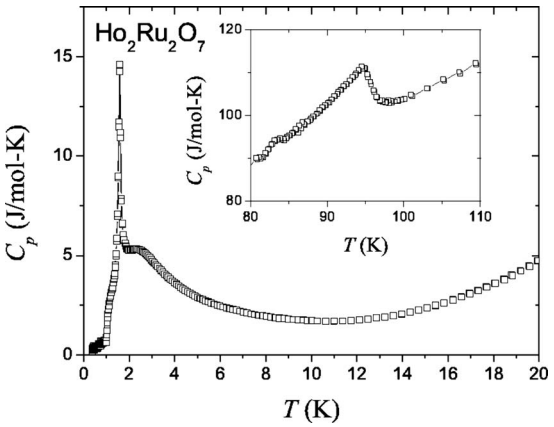

FIG. 17. Specific heat of polycrystalline $Ho_2Ru_2O_7$ as a function of temperature around the Ru^{4+} (inset) and Ho^{3+} (main) ordering temperatures. From Gardner *et al.*, 2005.

5. $A_2Mn_2O_7$ (A=Sc, Y, Tb–Lu, and Tl)

The rare-earth manganese (IV) pyrochlores are not stable at ambient pressure at any temperature and must be prepared using-high pressure methods. The earliest published report is by Fujinaka *et al.* (1979) who synthesized the pyrochlores $A_2B_2O_7$ with A=Y, Tl and B=Cr, Mn using temperatures in the range of 1000–1100 °C and pressures from 3 to 6 GPa. Reports of the high-pressure synthesis of several $A_2Mn_2O_7$ phases appeared from the groups of Subramanian *et al.* (1988) and Troyanchuk and Derkachenko (1988) about ten years later. Troyanchuk and Derkachenko (1988) prepared the phases A=Sc, Y, In, Tl, and Tb–Lu with pressures between 5 and 8 GPa and temperatures of 1000–1500 °C. Subramanian *et al.* (1988) were able to prepare A=Y and Dy-Lu using much lower pressures and temperatures with a hydrothermal method in sealed gold tubes including $NaClO_3$, NaOH, and H_2O at 3 kbar (0.3 GPa) and 500 °C. Greedan, Raju, and Subramanian (1996)

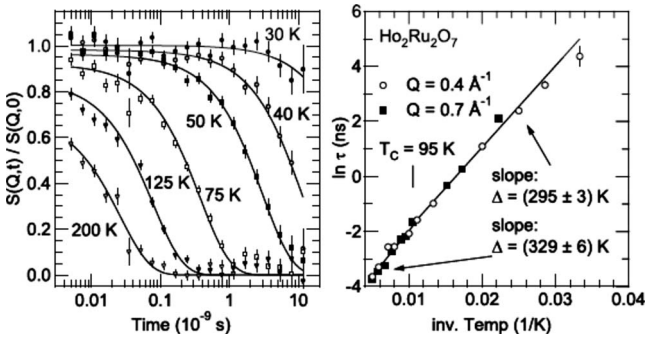

FIG. 18. Neutron spin echo spectra from $Ho_2Ru_2O_7$ at $|\mathbf{Q}|=0.4$ Å^{-1} as measured on NG5 neutron spin echo spectrometer at NIST (left) and the dependence of the relaxation time on temperature (right) from two different positions in reciprocal space. The lines through the spectra on the left are a simple exponential, where the characteristic relaxation time is used in the Arrhenius plot on the right. From Gardner *et al.*, 2005.

synthesized A=Sc using a tetrahedral anvil press at 850 °C and 60 kbar (6 GPa). Subsequently, Shimakawa *et al.* (1999) used a hot isostatic press apparatus at 1000–1300 °C and only 0.4 kbar (0.04 GPa) for the series A=In, Y, and Lu while the A=Tl material required 2.5 GPa and 1000 °C in a piston-cylinder apparatus (Shimakawa *et al.*, 1999).

The unit cell constants from all known preparations of $A_2Mn_2O_7$ phases along with preliminary magnetic characterization data are collected in Table II for A=Sc, Y, Lu, In, and Tl, i.e., where only the Mn sublattice is magnetic. Given the variety of preparative conditions, the agreement among the various groups for these key parameters is excellent, suggesting that sample to sample compositional variation is small. As seen in the case of the molybdate pyrochlores (Sec. II.C), both the unit cell constant a_0 and T_c are very sensitive to composition. All of these materials appear to be ferromagnets, consistent with the observation of a positive Curie-Weiss temperature and an apparent Curie temperature as shown, for example, in Fig. 19 for $Tl_2Mn_2O_7$ (Raju *et al.*, 1994). Note, however, that there appear to be two separate classes of ferromagnetic materials if sorting is done by the ratio θ_{CW}/T_c. The compounds A=Tl and In have T_c values of 120 K and θ_{CW}/T_c ratios of about 1.25–1.3. Mean field theory gives $T_c=\theta_{CW}$ for a ferromagnet. Empirically, for most ferromagnets this ratio is larger than 1, with typical values between 1.1 and 1.2 as shown in Table III for some selected ferromagnetic insulators. One can also estimate a theoretical ratio calculated using the Rushbrooke-Wood relationship for T_c and the mean field theory for θ_{CW}, assuming the same exchange constant J (nearest neighbors only) and $S=3/2$, appropriate for Mn^{4+}, which gives $T_c/\theta_{CW}=1.4$ (Rushbrooke and Wood, 1958). The A=Sc, Y, and Lu compounds show corresponding ratios within the range of 3–4, values well outside those seen for typical ferromagnets and well outside the expected theoretical limits. This suggests that these phases present a much more complex situation than that of a simple ferromagnet. Interestingly, when the A element has a magnetic moment (A=Tb–Yb), the properties, especially the θ_{CW}/T_c ratio, return to typical simple ferromagnetic levels just above 1 as shown in Table IV.

TABLE III. Comparison of the Curie-Weiss and ordering temperatures for selected ferromagnetic insulators.

	θ_{CW} (K)	T_c (K)	θ_{CW}/T_c
EuO	80	69	1.2
EuS	19	16.6	1.2
$Lu_2V_2O_7$	83	74	1.1
$YTiO_3$	33	29	1.1

a. $Tl_2Mn_2O_7$

$Tl_2Mn_2O_7$ has attracted considerable attention following the discovery of giant magnetoresistance (GMR) (Cheong *et al.*, 1996; Shimakawa *et al.*, 1996; Subramanian *et al.*, 1996). While this topic is outside the main area of this review, having little to do with geometric frustration, some comments are in order. Figure 19 shows the evidence for this effect (Shimakawa *et al.*, 1996). It was soon realized that the mechanism for this GMR must be different from that for the well-studied perovskite manganates (Schiffer, Ramirez, Bao, and

TABLE II. Collected values for unit cell constants a_0, measured Curie temperatures T_c, and Curie-Weiss temperatures θ_{CW} for $A_2Mn_2O_7$ phases with A=Sc, Y, Lu, In, and Tl.

A	a_0 (Å)	T_c (K)	θ_{CW} (K)	θ_{CW}/T_c	Reference
Sc	9.586(3)	15			Troyanchuk and Derkachenko, 1988
Sc	9.5965(4)	20(1)	77(3)	3.9	Greedan, Raju, and Subramanian, 1996
Y	9.912(3)				Fujinaka *et al.*, 1979
Y	9.912(3)				Troyanchuk and Derkachenko, 1988
Y	9.901	20(5)	50(10)	2.5	Subramanian *et al.*, 1988
Y	9.919(2)	15(1)	42(2)	2.8	Reimers, Greedan, *et al.*, 1991
Y	9.91268(3)	15	50	3.3	Shimakawa *et al.*, 1999
Lu	9.814(3)	9			Troyanchuk and Derkachenko, 1988
Lu	9.815	23(5)	70(10)	3.0	Subramanian *et al.*, 1988
Lu	9.82684(3)	15	60	4.0	Shimakawa *et al.*, 1999
In	9.717(3)	132			Troyanchuk and Derkachenko, 1988
In	9.727(1)	120	150	1.25	Raju *et al.*, 1994
In	9.70786(9)	120	155	1.29	Shimakawa *et al.*, 1999
Tl	9.890(3)	120			Fujinaka *et al.*, 1979
Tl	9.892(1)	121(1)	155	1.28	Raju *et al.*, 1994
Tl	9.89093(7)	122	175	1.43	Shimakawa *et al.*, 1999

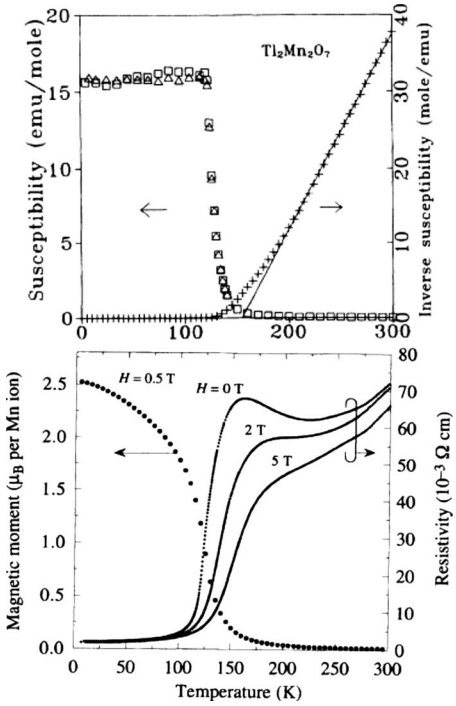

FIG. 19. Ferromagnetism and giant megnetoresistance in $Tl_2Mn_2O_7$. Top: Magnetic properties of $Tl_2Mn_2O_7$ showing evidence for ferromagnetic order in 0.005 T (Raju *et al.*, 1994). Bottom: Evidence for a giant magnetoresistance effect in $Tl_2Mn_2O_7$ (Shimakawa *et al.*, 1996).

Cheong, 1995). In the latter, double exchange between Mn^{3+} and Mn^{4+} is in part involved in both the metallic behavior and the ferromagnetism. From a combination of accurate measurements of Mn-O1 distances and core level spectroscopies, it was determined that only Mn^{4+} is present in $Tl_2Mn_2O_7$ (Rosenfeld and Subramanian, 1996; Subramanian *et al.*, 1996; Kwei *et al.*, 1997). The ferromagnetism arises from superexchange, not double exchange, and the metallic properties are due to accidental overlap between the Tl 6*s* band and the Mn 3*d* band. The coupling between magnetic and transport properties results from abnormally strong incoherent scattering of the conduction electrons due to large spin fluctuations which accompany the FM ordering, and GMR in $Tl_2Mn_2O_7$ arises from the large field dependence of T_c. Interestingly, doping of the Tl site with In or Sc, the parent compounds of which are both insulating, greatly enhances the GMR effect as does doping with Tl vacancies or even Cd (Cheong *et al.*, 1996; Ramirez and Subramanian, 1997; Alonso *et al.*, 2000; Velasco *et al.*, 2002).

Neutron diffraction confirmed the ferromagnetic long-range order for this material, finding an ordered moment of $2.91(4)\mu_B$ per Mn^{4+} ion, in excellent agreement with the $3.0\mu_B$ expected for an $S=3/2$ state. Small angle neutron scattering is fully consistent with the formation of domain walls and spin waves below $T_c=123.2(3)$ K (Raju *et al.*, 1994; Lynn *et al.*, 1998). These results are of interest when compared to data from the insulating materials with $A=$Y, Ho, and Yb below.

b. $Y_2Mn_2O_7$

As shown by Reimers, Greedan, *et al.* (1991), this material exhibits many of the features of a ferromagnet, including an apparent $T_c\approx16(1)$ K from dc magnetization studies and saturation with applied magnetic field at low temperatures (see Fig. 20). Note that saturation is not reached even at $\mu_0H=4$ T and that the moment is close to $2\mu_B$ rather than the $3\mu_B$ expected for an $S=3/2$ ion.

Behavior quite atypical of ferromagnetism is found in the ac susceptibility and the heat capacity as shown in Figs. 20 and 21. While χ' does indeed show a sharp increase below 16 K, the dominant feature is a broad maximum centered at about 7 K which shows a strong frequency dependence, typical of spin glassiness. Controversy exists concerning measurements of the specific

TABLE IV. Collected values for unit cell constants a_0, Curie temperatures T_c, and Curie-Weiss temperatures θ_{CW} for $A_2Mn_2O_7$ phases with $A=$Tb–Yb.

A	a_0 (Å)	T_c (K)	θ_{CW} (K)	θ_{CW}/T_c	Reference
Tb	9.972(3)	38			Troyanchuk and Derkachenko, 1988
Dy	9.929	40(5)	43(2)	1.08	Subramanian *et al.*, 1988
Ho	9.906(3)	24			Troyanchuk and Derkachenko, 1988
Ho	9.905	37(5)	33(5)	1	Subramanian *et al.*, 1988
Ho	9.907(1)	37(1)	37(1)	1.0	Greedan, Raju, Maignan, *et al.*, 1996
Er	9.888(3)	24			Troyanchuk and Derkachenko, 1988
Er	9.869	35(5)	40(5)	1.15	Subramanian *et al.*, 1988
Tm	9.852(3)	14			Troyanchuk and Derkachenko, 1988
Tm	9.847	30(5)	56(8)	1.8	Subramanian *et al.*, 1988
Yb	9.830(3)	22			Troyanchuk and Derkachenko, 1988
Yb	9.830	35(5)	41(3)	1.17	Subramanian *et al.*, 1988
Yb	9.838(1)	37(1)	44(1)	1.19	Greedan, Raju, Maignan, *et al.*, 1996

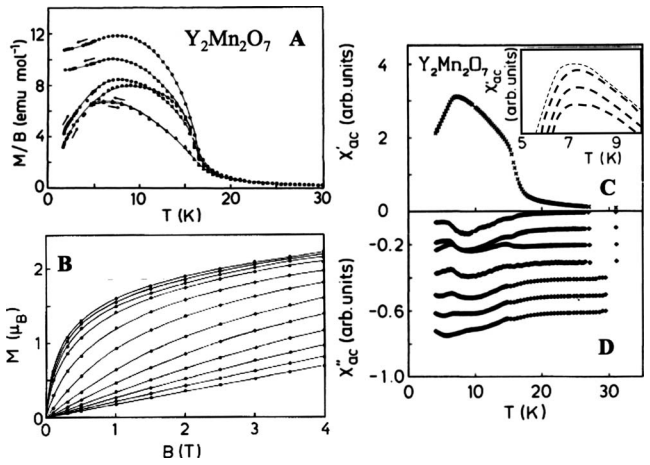

FIG. 20. Bulk properties of $Y_2Mn_2O_7$. Top left: dc susceptibility showing $T_c = 16$ K in 0.15 mT (circle), 0.56 mT (square), and 10 mT (triangle). Bottom left: Magnetization vs applied field at various temperatures (K) from top to bottom: 1.8, 5, 7.5, 10, 15, 20, 25, 30, 35, 40, 45, and 50 K. Right: ac susceptibility. (C) $\chi' = 20$ Hz. The inset shows the χ' maximum for various frequencies from top to bottom: 20, 100, 200, and 1000 Hz. (D) χ'' at various frequencies from top to bottom: 20, 40, 80, 100, 200, 500, and 1000 Hz. The curves are each shifted by −0.1 from the preceding one. From Reimers, Greedan, *et al.*, 1991.

heat. Reimers, Greedan, *et al.* (1991) reported no lambda-type anomaly near 16 K and a linear temperature dependence below 7 K, behavior again typical of spin glasses. They also reported that about 60% of the total entropy of $R \ln 4$ (attained by 100 K) is removed above 16 K. Shimakawa *et al.* (1999) found a lambda anomaly at 15 K which they interpreted as evidence for long-range ferromagnetic order. Figure 21 compares both results and those for a nonmagnetic, lattice matched material, $Y_2Sn_2O_7$. Although the agreement in the data between the two groups is good, apart from the weak lambda anomaly, Fig. 21 shows considerable magnetic heat capacity both above and below the lambda feature when compared to $Y_2Sn_2O_7$. Clearly, this is not consistent with a simple ferromagnetic transition. Even the observation of a lambda anomaly in the specific heat has no guarantee of a phase transition to a conventional long-range ordered state as has been demonstrated for other pyrochlores such as $Yb_2Ti_2O_7$ and the garnet, $Yb_3Ga_5O_{12}$ (Blöte *et al.*, 1969; Hodges *et al.*, 2002; Dalmas de Réotier, *et al.*, 2003). While the results of Fig. 21 cannot be easily reconciled, the claim by Shimakawa *et al.* (1999) that the heat capacity demonstrates an ordered state is not substantiated and should be investigated further.

Neutron scattering data from Greedan *et al.* (1991) and Reimers, Greedan, *et al.* (1991) also provided evidence for a quite complex ground state. Elastic scattering data show mainly broad features below 50 K (see Fig. 22). Enhanced magnetic scattering forms below 15 K at nuclear Bragg positions corresponding to the 111 and 222 at 13.9° and 28.0°, respectively. These data were further analyzed via Fourier transformation to give the real-space spin-spin correlation function which suggested that the nearest-neighbor exchange was weakly antiferromagnetic while further neighbor exchange is strongly ferromagnetic. This is consistent with the observed positive Curie-Weiss temperatures and the apparent failure to order in a simple ferromagnetic ground state.

Small angle neutron scattering (SANS) data from Greedan *et al.* (1992) and Greedan, Raju, Maignan, *et al.* (1996) are also unusual and in fact unprecedented. These are compared with corresponding data for ferromagnetic $Tl_2Mn_2O_7$ in Fig. 23 (Raju *et al.*, 1994; Lynn *et al.*, 1998). At $|\mathbf{Q}| = 0.030$ Å^{-1} the ferromagnet ($Tl_2Mn_2O_7$) shows a decrease in scattering intensity with decreasing temperature below T_c which is ascribed to scattering from spin waves which diminish in intensity as the long-range order is established and the cluster size moves out

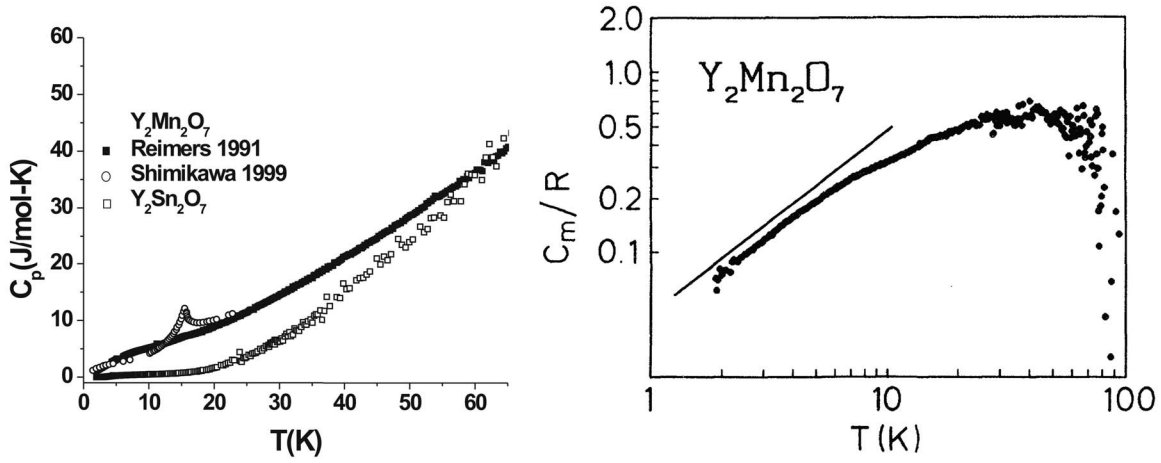

FIG. 21. Heat capacity for $Y_2Mn_2O_7$. Left: Comparison of the total heat capacity for $Y_2Mn_2O_7$ reported by Reimers, Greedan, *et al.* (1991) (filled black squares) and Shimakawa *et al.* (1996) (open circles) and the diamagnetic material $Y_2Sn_2O_7$ (open squares). Right: The magnetic component of the heat capacity. Note the absence of a sharp peak and the linear dependence at low temperatures. From Reimers, Greedan, *et al.*, 1991).

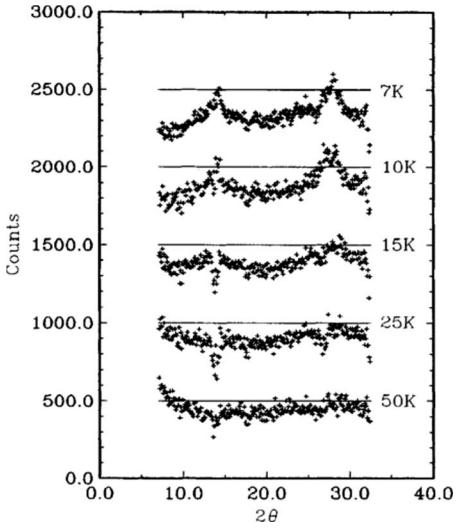

FIG. 22. Neutron diffraction data for $Y_2Mn_2O_7$ showing difference plots (data at 200 K subtracted) at various temperatures. Note the buildup of broad peaks at the 111 and 222 Bragg positions. From Reimers, Greedan, *et al.*, 1991.

of the SANS resolution window. On the other hand, the behavior of $Y_2Mn_2O_7$ is the opposite, showing an increase below the apparent ordering temperature of

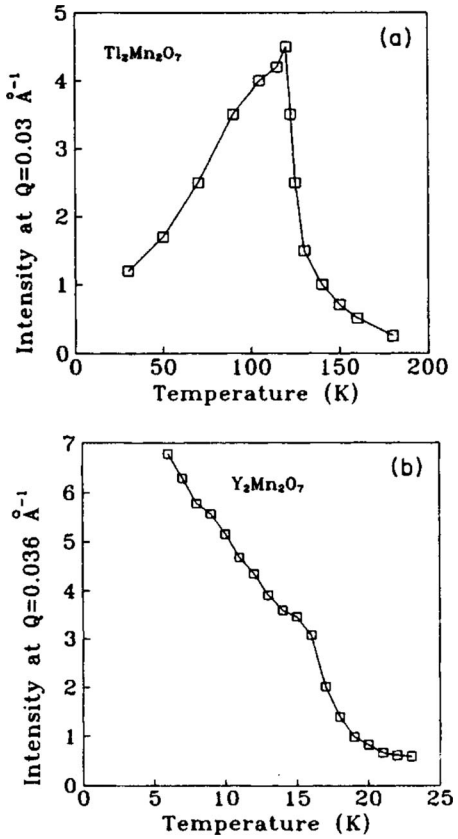

FIG. 23. Comparison of the temperature dependence of the total SANS intensity data for the ferromagnet $Tl_2Mn_2O_7$ and $Y_2Mn_2O_7$ at $|\mathbf{Q}|=0.03$ Å^{-1} (Raju *et al.*, 1994; Greedan, Raju, Maignan, *et al.*, 1996). Similar results for $Tl_2Mn_2O_7$ were obtained by Lynn *et al.*, 1998.

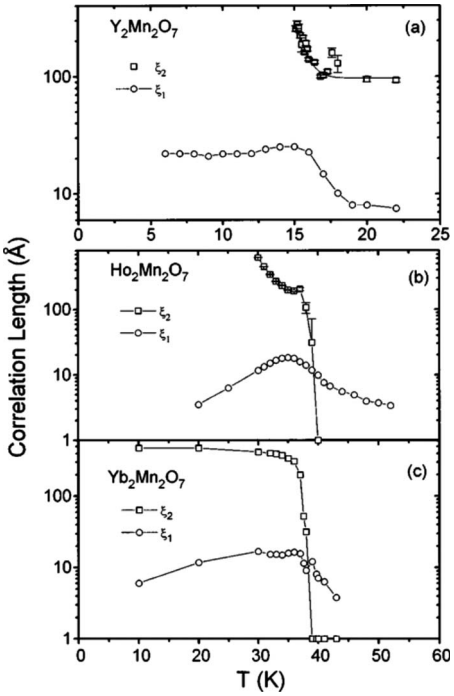

FIG. 24. Temperature dependence of the correlation lengths ξ_1 and ξ_2 for $Y_2Mn_2O_7$, $Ho_2Mn_2O_7$, and $Yb_2Mn_2O_7$. From Greedan, Raju, Maignan, *et al.*, 1996.

15 K, indicating that the population of subcritical clusters does not diminish significantly at low temperatures. In addition, the full range of the data cannot be fitted to a simple Lorentzian as is normally the rule for ferromagnets as, for example, in $Tl_2Mn_2O_7$ (Lynn *et al.*, 1998), but only to a Lorentzian plus Lorentzian-squared ($L+L^2$) law which involves two correlation lengths ξ_1 and ξ_2,

$$S(Q) = A/(Q + 1/\xi_1) + B/(Q + 1/\xi_2)^2. \quad (5)$$

The $L+L^2$ law is often found for systems in which there is competition between ferromagnetic order and random-field disorder and where ξ_1 is associated with the ferromagnetic correlations and ξ_2 with the random fields (Aharony and Pytte, 1983; Arai *et al.*, 1985; Rhyne, 1985). As shown in Fig. 24, for $Y_2Mn_2O_7$ the two correlation lengths differ by nearly one order of magnitude over the temperature range investigated. ξ_1 shows a buildup through a rounded maximum to a value near 20 Å. Similar broad maxima are found in nearly ferromagnetic metallic glasses (Rhyne, 1985; Rhyne and Fish, 1985). ξ_2 quickly diverges to a resolution limited value below 15 K. The most straightforward interpretation is that ξ_1 measures the temperature evolution of ferromagnetic correlations that never realize a long-range ordered state due to the intervention of random fields as monitored by ξ_2. In this case, both tendencies have onsets near the same temperature. Note that there is no anomaly near 7 K, the maximum in the real part of the ac susceptibility. While a detailed understanding of the SANS results for this material is not yet available, there is little in these data to indicate that $Y_2Mn_2O_7$ behaves as a conventional ferromagnet.

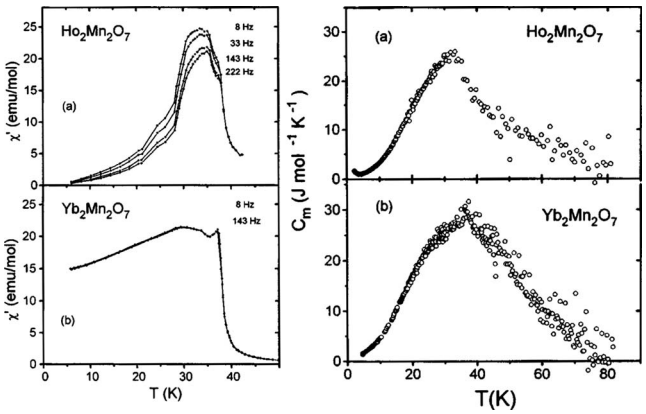

FIG. 25. Bulk properties of $Yb_2Mn_2O_7$ and $Ho_2Mn_2O_7$. Left column is the real part of the ac susceptibility and right column is the magnetic component of the heat capacity. From Greedan, Raju, Maignan, *et al.*, 1996.

c. $Ho_2Mn_2O_7$ and $Yb_2Mn_2O_7$

Among the remaining $A_2Mn_2O_7$ pyrochlores only those with A=Ho and Yb have been studied in detail (Greedan, Raju, Maignan, *et al.*, 1996). As seen from Table III, the θ_{CW}/T_c ratio is within the range typically seen for ferromagnets and both show positive Curie-Weiss temperatures which indicate ferromagnetic rather than ferrimagnetic correlations between the two sublattices. The apparent T_c values are significantly higher than those for A=Y, Lu, or Sc indicating that the A-Mn exchange has a strong influence on the ordering temperature. Unlike $Y_2Mn_2O_7$, both materials show magnetic saturation at 5 K for modest applied fields $\mu_0 H > 2$ T with values of $12.4\mu_B$ and $9.2\mu_B$ per formula unit for A=Ho and Yb, respectively. Assuming ferromagnetic A-Mn coupling and that the Mn-sublattice moment saturates with the full spin-only value of $3.0\mu_B$ per Mn^{4+}, the A sublattice saturation moments are $3.2\mu_B$ and $1.6\mu_B$ per Ho^{3+} and Yb^{3+} ions, respectively. These are considerably smaller than the full saturation moments $g_L J$ for free Ho^{3+} ($10.0\mu_B$) and Yb^{3+} ($4.0\mu_B$) and indicate the strong influence of crystal fields on the ground state. A similar Yb moment is found in the isostructural compound $Yb_2V_2O_7$ (Soderholm *et al.*, 1980).

In addition to dc susceptibility and magnetization, ac susceptibility, heat capacity, and neutron scattering data are available but these do not lead straightforwardly to a consistent interpretation. For example, the real part of the ac susceptibility data shown in Fig. 25 indicates divergent behavior for the two materials. While there is an apparent T_c at 38(1) K with a broad maximum just above at 30 K for both materials, the data for $Ho_2Mn_2O_7$ show a strong frequency dependence while those for $Yb_2Mn_2O_7$ do not. Thus, the $Ho_2Mn_2O_7$ phase appears to show a so-called re-entrant spin-glass state where glassy behavior develops at a temperature below T_c.

Heat capacity (see Fig. 25) and neutron scattering (see Fig. 26) data seem to suggest a very complex magnetic ground state for both materials. No lambda anomaly

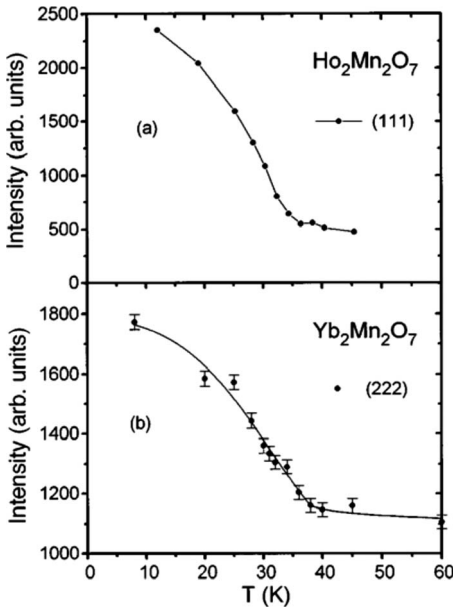

FIG. 26. Temperature dependence of magnetic Bragg peaks for $Yb_2Mn_2O_7$ and $Ho_2Mn_2O_7$ showing order-parameter-like behavior and an apparent T_c of 38(1) K for both. From Greedan, Raju, Maignan, *et al.*, 1996.

consistent with true long-range order has been observed but resolution limited magnetic Bragg peaks are seen for both materials, the temperature dependence of which is order-parameter-like and consistent with T_c=38(1)K for both compounds. However, the magnetic structure for $Yb_2Mn_2O_7$ and $Ho_2Mn_2O_7$ is still unknown. SANS data are similar to those for $Y_2Mn_2O_7$ in that the $L+L^2$ law holds and the two correlation lengths have different temperature dependences (see Fig. 24). Interestingly, the B coefficient in Eq. (5), which measures the contribution from the L^2 term associated with the ξ_2 correlation length, shows a temperature dependence akin to that of an order parameter for all three materials.

More work on the ordered manganese pyrochlores is needed to understand fully their magnetic ground states. The role of random fields arising from the geometrically frustrated Mn sublattice, but whose microscopic origin is not understood, plays an important role in the determination of the magnetic ground state which appears to be rather inhomogeneous. The A=Y, Ho, and Yb compounds do not behave like simple ferromagnets and studies of their spin dynamics are warranted. In addition, diffraction studies using modern instruments should be performed on A=Ho and Yb to determine the ordered component of the ground state.

6. $A_2Ir_2O_7$ (A=Nd–Yb)

In the rare-earth iridium (IV) pyrochlores, iridium has an electronic configuration $5d^5$ which is expected to be low spin, resulting in an $S=1/2$ system, thus this series of considerable interest. The pyrochlore structure is reported to be stable for A=Pr–Lu, one of the widest stability ranges for any pyrochlore system (Subramanian

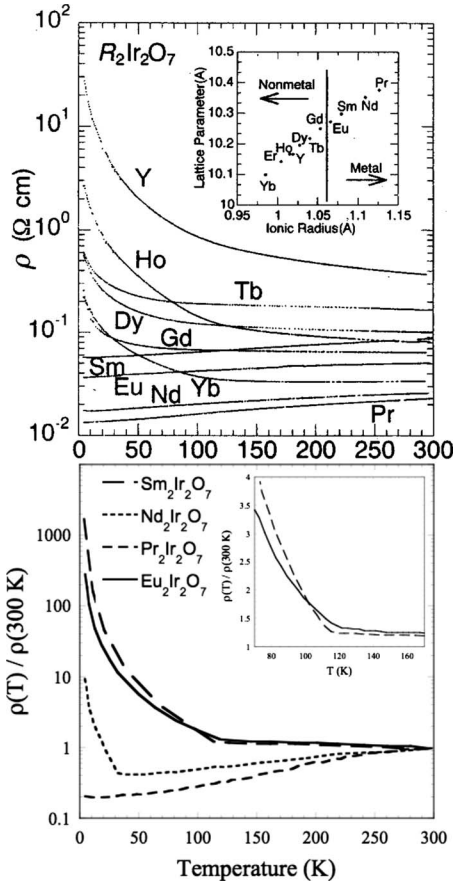

FIG. 27. Electrical resistivity for the $A_2Ir_2O_7$ series. Top: Resistivity data for the $A_2Ir_2O_7$ series showing the metal-insulator crossover between A=Eu and Gd (Yanagishima and Maeno, 2001). Bottom: Evidence for metal-insulator transitions with decreasing temperature for A=Eu, Sm, and Nd but not for Pr. From Matsuhira *et al.*, 2007.

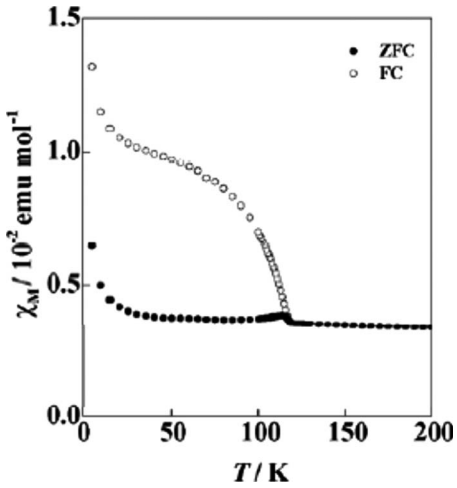

FIG. 28. Magnetic susceptibility for $Sm_2Ir_2O_7$ showing evidence for a magnetic anomaly near 120 K. From Taira *et al.* 2001.

and Sleight, 1993). This series of compounds not only shows a metal-insulator (MI) transition across the rare-earth series at room temperature, such as that discussed in Sec. II.C for the molybdates, but several individual compounds do show a MI transition as a function of temperature. These materials were first studied in the early 1970s by Sleight and Bouchard (1972), but have not been studied systematically until fairly recently. Early reports on the electrical transport behavior were contradictory. Lazarev and Shaplygin (1978) reported room temperature resistivities in the range of poor metals, while Subramanian and Sleight (1993) argued that the entire series of compounds were low activation energy semiconductors. Also, among the earliest measurements were specific heat studies for A=Er and Lu which showed no magnetic anomalies up to 20 K but a rather large gamma coefficient which is not expected for materials reported to be insulating (Blacklock and White, 1980). Interest in these materials was rekindled in 2001 with the report of magnetic anomalies above 100 K for the A=Y, Lu, Sm, and Eu series members by Taira *et al.* (2001) and the study of Yanagishima and Maeno (2001) who found a crossover from metallic to insulating behavior with decreasing A radius and with the metal-insulator boundary between A=Eu and Gd. Representative results are shown in Fig. 27.

There exists a controversy concerning the connection between the magnetic and metallic properties of these materials. Initial reports by Yanagishima and Maeno (2001) indicated that the metallic series members, A=Pr, Nd, Sm, and Eu were not magnetic. This is contradicted by Taira *et al.* (2001), as can be seen in Fig. 28, where the metallic $Sm_2Ir_2O_7$ also shows a magnetic transition.

In subsequent work, it was found that hole doping of $Y_2Ir_2O_7$ by substitution of Ca^{2+} for Y^{3+} induces an insulator to metal transition at doping levels of about 15 at. % (Fukazawa and Maeno, 2002). The magnetic transition disappears with the onset of metallic behavior. One other important issue addressed here is the apparent large gamma coefficient of the specific heat which persists at low temperatures, first noted by Blacklock and White (1980). Fukazawa and Maeno (2002) found gamma, the Sommerfeld parameter, to tend toward zero, 0.0(5) mJ/K^2 mol Ir, at 0.4 K and thus concluded that $Y_2Ir_2O_7$ is indeed a Mott insulator.

Nonetheless, the issue of the persistence of magnetic order into the metallic samples remains an important question. Another attempt to address this problem was reported by Matsuhira *et al.* (2007). They investigated the correlation between sample quality and their transport and magnetic properties. These studies have revealed MI transitions as the temperature is lowered for A=Eu, Sm, and Nd. However, $Pr_2Ir_2O_7$ appears to remain metallic down to the lowest temperatures investigated (see Fig. 27). We return to $Pr_2Ir_2O_7$ in Sec. III.D.4. For one compound, $Sm_2Ir_2O_7$, the onset temperatures for both the MI and magnetic transition were shown to be identical, suggesting that the two phenomena are intimately connected. The samples showing these effects were prepared by a different route than those from Yanagishima and Maeno (2001) and Fukazawa and

Maeno (2002) which involved firing of the starting materials in air. Matsuhira *et al.* (2007) used Pt tubes in evacuated silica with a 10% excess of IrO_2 and many regrinding sequences. X-ray powder diffraction showed single phase samples with well resolved $K\alpha_1/K\alpha_2$ splittings at high angles, indicative of good crystallinity. No evidence for changes in the diffraction pattern was observed below the apparent MI transitions from which they suggested that these are continuous rather than first order. The nature of the magnetic transition is still unclear. The observation of a lambda-type anomaly in the specific heat at the metal-insulator transition temperature indicated by the susceptibility is evidence for a long-range ordered antiferromagnetic ground state but more work is needed. For $S=1/2$ systems, neutron diffraction can be a challenge but studies on a single crystal should be definitive. Clearly, studies of this interesting pyrochlore series are at an early stage and more work is needed to resolve the discrepancies among the various groups.

Related 5d pyrochlores. Little has been reported about other pyrochlore oxides based on 5*d* transition elements. The synthesis of $B=$Os ($5d^4$) and Pt ($5d^6$) pyrochlores with $A=$Pr–Lu (including Sc and In for $B=$Pt) has been reported (Hoekstra and Gallagher, 1968; Lazarev and Shaplygin, 1978). The $B=$Pt series can only be prepared using high pressures, 4 GPa, and high temperatures, 1200 °C (Hoekstra and Gallagher, 1968). Room temperature electrical resistivity values are reported for the $B=$Os series and all are in the range for poor metals, similar to the initial reports for the $B=$Ir compounds described above. $Cd_2Os_2O_7$ was first studied by Sleight *et al.* (1974) and later by others for its unusual MI transition at 226 K (Mandrus *et al.*, 2001). This suggests that a closer study of this series could be very interesting.

7. $A_2Mo_2O_7$ ($A=$Gd, Nd, and Sm)

The earliest report of the existence of rare-earth molybdenum pyrochlores appears to be that of McCarthy (1971) from a study of the Eu-Mo-O and Sm-Mo-O phase diagrams in which the pyrochlore compounds were observed. Hubert (1974) was the first to report magnetic susceptibility for $Y_2Mo_2O_7$ in the range of 300–1000 K. Ranganathan *et al.* (1983) synthesized the series $A=$Gd–Lu along with solid solutions in which the *A* site contained various ratios of Nd/Yb and Nd/Er and reported magnetic susceptibility and limited electrical transport data for 77–300 K. The observation of positive Curie-Weiss (θ_{CW}) temperatures led them to suggest that some of these materials might be ferromagnets, for example, $Sm_2Mo_2O_7$ (Mandiram and Gopalakrishnan, 1980). Samples rich in Nd appeared to be metallic as well (Ranganathan *et al.*, 1983). This situation was clarified by Greedan *et al.* (1987) who showed that Mo (IV) pyrochlores for $A=$Nd, Sm, and Gd were indeed ferromagnets with $T_c=97$, 93, and 83 K, respectively, which was attributed to the ordering of the Mo (IV) moments, an unprecedented observation. As mentioned in Sec. II.C, there is a link between the ionic radius of the *A* ion and the electrical transport properties of the molybdenum pyrochlores which in turn are strongly correlated to the magnetic properties.

The existing evidence appears to support the view that the properties of ferromagnetism and metallic behavior are fundamentally linked in these materials. A proposal for the origin of the ferromagnetism (and antiferromagnetism for $Y_2Mo_2O_7$) has been advanced by Solovyev (2003). While the argument is complex and has a number of elements, the key idea is that the Mo t_{2g} states are split by the axial crystal-field component into a_{1g} and e_g states. These states are affected differently by systematic changes in crystal structure in proceeding from $A=$Nd to Y. For $A=$Nd and Gd, the e_g band is found to be relatively broad and can support itinerant spin up electrons rather in analogy to the double exchange mechanism in the manganate perovskites which selects a ferromagnetic ground state. However, for $Y_2Mo_2O_7$, the e_g states become more localized, while the a_{1g} band broadens. This is found to favor an antiferromagnetic ground state. The marked differences in magnetism and transport properties are surprising given that the structural changes in moving from $A=$Nd $\rightarrow$Gd$\rightarrow$Y are very subtle. For example, the Mo-O-Mo bond angle changes from 131.4° (Nd) to 130.4° (Gd) to 127.0° (Y) (Reimers *et al.*, 1988; Moritomo *et al.*, 2001).

a. $Gd_2Mo_2O_7$

$Gd_2Mo_2O_7$ has attracted much interest due to its position near the metal-insulator (MI) boundary (see Fig. 7) in this molybdate series. As mentioned in Sec. II.C, the electrical transport properties are dependent on the stoichiometry of the sample (see Fig. 8). Stoichiometric samples are ferromagnetic and metallic with T_c near 80 K. These show a giant negative magnetoresistance exceeding 40% below 15 K (Troyanchuk *et al.*, 1998). Insulating samples are oxygen deficient and electron doped. It has been shown by Hanasaki *et al.* (2006) that insulating samples of $Gd_2Mo_2O_7$ can be driven metallic by application of high pressure with the MI boundary occurring between 3 and 4 GPa (see Sec. III.E.2). Extensive specific heat studies have been carried out on polycrystalline samples for both $A=$Sm and Gd by Schnelle and Kremer (2004). Unlike previous studies by Raju *et al.* (1992), clear maxima were observed for both materials near 75 K, indicative of long-range magnetic order on the Mo sublattice. For $Gd_2Mo_2O_7$, a steplike anomaly at 11.3 K superimposed on a dominant Schottky peak suggests partial ordering of the Gd spins, which was supported by measurement of the entropy.

Until quite recently, there had been little information regarding the magnetic structure of either the $A=$Sm or Gd molybdate pyrochlores due to the high neutron absorption cross sections for both elements. Mirebeau, Apetrei, Goncharenko, Andreica, *et al.* (2006) solved this problem with the use of ^{160}Gd substituted materials. The room temperature unit cell constant for this sample is 10.3481(2) Å, which indicates only a slight oxygen deficiency. The magnetic diffraction pattern at 1.7 K is

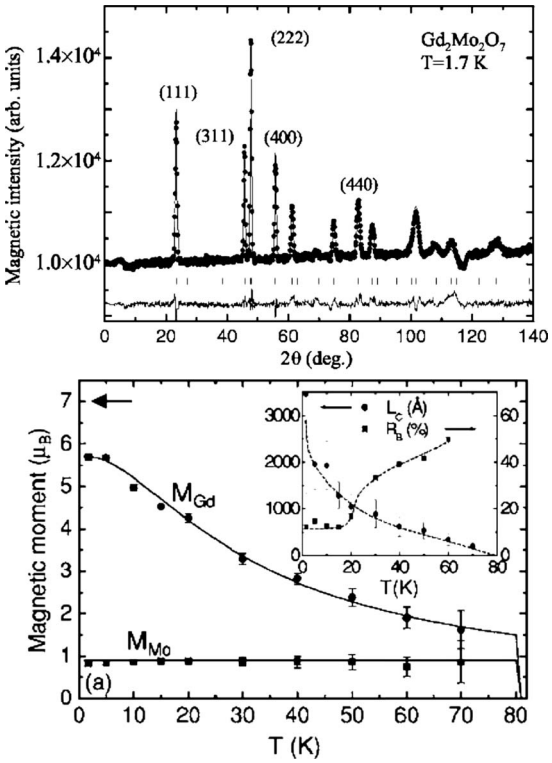

FIG. 29. Neutron powder diffraction results for $Gd_2Mo_2O_7$. Top: The magnetic scattering at 1.7 K after a 90 K data set has been subtracted. The solid line is a fit to a model with collinear ferromagnetic coupling between Gd and Mo moments. Bottom: The temperature dependence of the ordered moments for the Gd and Mo sublattices. The inset shows the temperature development of the correlation lengths (L) obtained from the widths of the Bragg peaks. From Mirebeau, Apetrei, Goncharenko, Andreica, *et al.*, 2006.

shown in Fig. 29 along with the temperature dependence of the sublattice moments and correlation lengths. The absence of a (200) reflection is consistent with a collinear magnetic structure and the best fit occurs for a ferromagnetic coupling of the Gd and Mo sublattices. This agrees with the earliest magnetization studies of Sato *et al.* (1986) who found that the bulk saturation moment could only be understood in terms of a ferromagnetic Gd-Mo coupling.

From the bottom panel of Fig. 29 it is clear that the Mo sublattice orders above 80 K and that the Gd moments are polarized due to the Gd-Mo coupling. The ordered moments on both sublattices are significantly smaller than the spin only values of $2.0\mu_B$ and $7.0\mu_B$ for Mo^{4+} and Gd^{3+}, respectively, although the Mo moments are similar to those found for the $A=$Nd phase. Muon spin relaxation data (Apetrei *et al.*, 2007a), which are most sensitive to the Gd spins, indicate that strong spin fluctuations persist below T_c and as low as 6.6 K. This is consistent with the ^{155}Gd Mössbauer data of Hodges *et al.* (2003) and also with the specific heat data of Schnelle and Kremer (2004). The conclusion is that $Gd_2Mo_2O_7$ is perhaps an unconventional ferromagnet with strong spin fluctuations. This maybe analogous to the situation encountered for manganate pyrochlores in Sec. III.A.5. The remarkable properties of this material under applied pressure will be described in Sec. III.E.2.b.

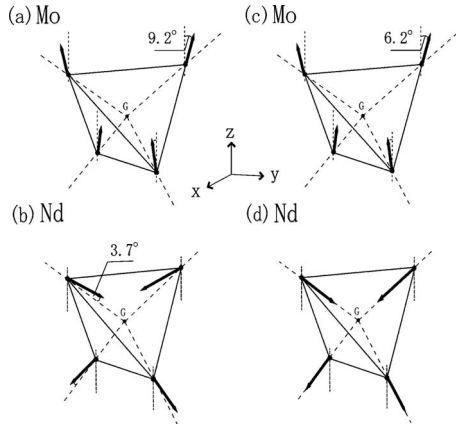

FIG. 30. Proposed spin configurations [(a),(b) and (c),(d)] for the Mo and Nd moments from neutron diffraction on a single crystal of $Nd_2Mo_2O_7$ at 4 K. From Yasui *et al.*, 2001.

b. $Nd_2Mo_2O_7$

Magnetism. It is well established that the $Nd_2Mo_2O_7$ phase is a metallic ferromagnet with $T_c=95$ K for stoichiometric polycrystalline samples. That the ferromagnetism is due to the Mo sublattice was first demonstrated by Greedan *et al.* (1991) from powder neutron diffraction studies. A canted ferromagnetic structure on the Mo sites with an ordered moment of $1.1\mu_B$ was proposed from an analysis of the data at 53 K which are dominated by magnetic scattering from the Mo. Subsequent studies by Yasui *et al.* (2001) using a single crystal with $T_c=93$ K have provided a better defined magnetic structure for both the Nd and Mo sublattices. The magnetic structure at 4 K is shown in Fig. 30. The Mo spins are noncollinear making an angle of 9° with the local z axis which is parallel to a fourfold axis of the crystal. The Mo moment is $1.2\mu_B$, close to that found earlier and slightly greater than half the value expected for a spin only $S=1$ ion. The Nd moments are aligned nearly along the principal threefold rotation axes of the tetrahedra in a two-in, two-out pattern. Nd moments at 4 K are $1.5\mu_B$ and the relative orientations of the Nd and Mo sublattice moment directions are antiferromagnetic.

Anomalous Hall effect. Much attention has been focussed on $Nd_2Mo_2O_7$ since the observation of the unprecedented behavior of the so-called anomalous Hall effect (AHE) independently by Katsufuji *et al.* (2000) and Taguchi *et al.* (2001). In ferromagnets, the transverse or Hall resistivity has two contributions, the "ordinary" Hall coefficient R_o, which is proportional to the applied magnetic field B, and the "anomalous" coefficient R_s, which is proportional to the sample magnetization M as in Eq. (6),

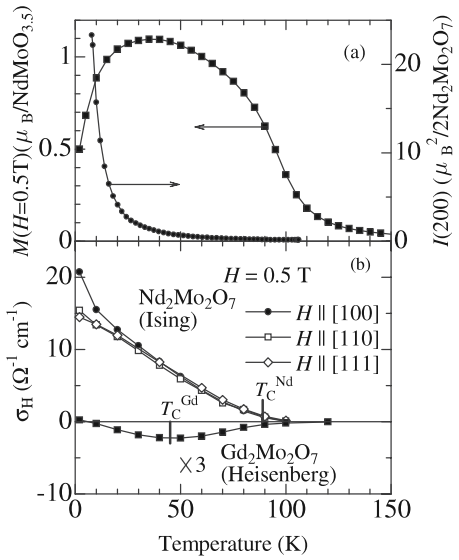

FIG. 31. Magnetic and electric (dc and Hall transport) properties of $Nd_2Mo_2O_7$. (a) Temperature dependence of the bulk magnetic moment and the (200) magnetic reflection which tracks the development of the chiral order on the Nd sites in $Nd_2Mo_2O_7$. (b) Temperature dependence of Hall conductivities for $Nd_2Mo_2O_7$ and $Gd_2Mo_2O_7$. Note the conventional behavior for A=Gd while the conductivity remains large and finite at low temperature for A=Nd. From Taguchi *et al.*, 2004.

$$\rho_H = R_o B + 4\pi R_s M. \tag{6}$$

The usual behavior is for the AHE contribution to vanish at low temperatures in ferromagnetic metals with collinear spin configurations. However, in the case of $Nd_2Mo_2O_7$, the AHE actually increases and remains large and finite at T=0 (see Fig. 31). In one interpretation this behavior has been attributed to the spin chirality (the two-in, two-out state is sixfold degenerate) of the Nd^{3+} moment configuration which acts as an effective magnetic field and effects the carrier dynamics in the same way as a real magnetic field (Taguchi *et al.*, 2001, 2004). A strong point of this argument is the contrast between this AHE and that in the Heisenberg A=Gd phase where spin chirality is not present. For the A=Gd material the AHE vanishes at low temperatures as with a normal ferromagnetic metal. However, this interpretation has been questioned by Kageyama *et al.* (2001) and Yasui, Iikubo, *et al.* (2003) who argued, based on extensive neutron scattering and specific heat studies, that the origins of the AHE for $Nd_2Mo_2O_7$ are much more complex than thought originally and that the spin chirality mechanism alone cannot provide a quantitative explanation and may at best play only a minor role (Kageyama *et al.*, 2001; Yasui, Soda, *et al.*, 2003; Yasui *et al.*, 2006). Kézsmárki *et al.* (2005) interpreted magneto-optical data on both $Nd_2Mo_2O_7$ and $Gd_2Mo_2O_7$ in favor of an important contribution from spin chirality. At present this controversy appears to be unresolved. Further comment on this problem is presented in Sec. III.A.7.d below.

c. $Sm_2Mo_2O_7$

Stoichiometric samples of this material generally show T_c=93 K, although as mentioned in Sec. II.C, for oxygen deficient samples this value can be significantly reduced (see Fig. 9). A crystal of $Sm_2Mo_2O_7$ with a T_c=73 K was reported by Taguchi and Tokura (1999) to also show a finite anomalous Hall Effect coefficient at T=0 K. A giant negative magnetoresistance of 13% near T_c and 18% at 4 K has been reported (Taguchi and Tokura, 2000), but little more is known about $Sm_2Mo_2O_7$.

d. $A_2(MoB)_2O_7$

Studies of B-site substituted compounds are very sparse. Troyanchuk *et al.* (1998) reported the preparation of V-doped $Gd_2Mo_2O_7$ with B site composition $Mo_{1.2}V_{0.8}$. $Gd_2Mo_2O_7$ is a ferromagnetic metal, while the corresponding Gd-V pyrochlore does not exist even under high pressures. Nonetheless, the $A_2V_2O_7$ series members, which include only A=Lu, Yb, and Tm at ambient pressure, are all ferromagnetic semiconductors with T_c in the range of 70–75 K (Bazuev *et al.*, 1976; Shin-ike *et al.*, 1977; Soderholm *et al.*, 1980). At this particular composition, the solid solution is insulating with resistivities in the range of Ω cm but remains ferromagnetic with a slightly enhanced T_c relative to the undoped material and a GMR effect of about 40% seen for the pure material has been destroyed (Troyanchuk *et al.*, 1998).

In another case, the AHE has been studied for $Nd_2Mo_2O_7$ with Ti substitutions for Mo up to the B-site composition $Mo_{1.7}Ti_{0.3}$ (Kageyama *et al.*, 2001). At this doping level the compound is still metallic. This group had shown earlier that the AHE has two contributions, proportional to the magnetizations of Mo and Nd separately, that is (Yoshii *et al.*, 2000; Iikubo *et al.*, 2001)

$$\rho_H = R_o B + 4\pi R_s M(\mathrm{Mo}) + 4\pi R_s' M(\mathrm{Nd}). \tag{7}$$

Of these two components, the doping experiments showed that R_s changes sign from positive to negative with increasing Ti content while R_s' does not. This observation was taken as evidence that the mechanism for AHE in these materials is more complex than the pure chirality model originally advanced (Taguchi *et al.*, 2001).

B. Spin-glass phases

The spin-glass state is one where the combination of randomness and frustration prevents the development of conventional long-range magnetic order characterized by delta-function magnetic Bragg peaks (Binder and Young, 1986). There are a number of experimental pathways to the spin-glass state. The classic case involves dilute concentrations of magnetic atoms in a metallic diamagnetic host such as $Au_{1-x}Fe_x$, where $x \sim 0.05$, as mentioned in Sec. I.A. Here the effective coupling between Fe moments is mediated by the Au conduction electrons, giving rise to an RKKY interaction whose sign depends on the distance between two Fe moments. This

leads to competing random ferromagnetic and antiferromagnetic constraints at each magnetic site. Another approach is to introduce disorder into a magnetically ordered but geometrically frustrated material by dilution of the magnetic sites with diamagnetic ions to levels near the percolation threshold for the particular lattice. An example is $Eu_{1-x}Sr_xS$ where Sr^{2+} dilution of the face-centered-cubic Eu^{2+} sites destroys the ferromagnetic ground state and a spin-glass state emerges near $x=0.5$. Similar to the latter example is $LiHo_xY_{1-x}F_4$, where Ho^{3+} is an effective Ising spin and where the predominant interactions are dipolar. Dipolar interactions are intrinsically frustrated since they can be either ferromagnetic or antiferromagnetic depending on the orientation of the vector $\boldsymbol{r}_j-\boldsymbol{r}_i$ between spins at positions $\boldsymbol{r}_i$ and $\boldsymbol{r}_j$. As a result, substitution of Ho by Y generates random frustration. Indeed, $LiHo_xY_{1-x}F_4$ is an Ising ferromagnet for x down to about $x\sim0.2$. For $x\lesssim0.2$, a dipolar-spin-glass state develops (Reich *et al.*, 1990; Wu *et al.*, 1993), although this conclusion has recently been questioned (Jönsson *et al.*, 2007).

One question that has attracted much attention in the field of spin glasses is whether or not a thermodynamic spin freezing transition occurs at nonzero temperature for physical spatial dimensions. While it was determined some time ago that there is no spin-glass transition in two dimensions, a seemingly definite conclusion for three-dimensional (3D) systems has only recently become available, thanks to the work of Ballesteros *et al.* (2000) who pioneered the use of the scaled correlation length method in finite-size scaling analysis of spin-glass models. A large majority of real magnetic systems are better described by Heisenberg spins rather than Ising spins and it was long believed that the 3D XY and Heisenberg spin-glass models do not have a transition. The explanation for the experimentally observed transition in real systems therefore had to invoke random anisotropy as the mechanism responsible for driving the system into the Ising spin-glass universality class (Binder and Young, 1986). However, recent extensive Monte Carlo simulations on the 3D XY and Heisenberg models employing the method of Ballesteros *et al.* (2000) found some compelling evidence for a phase transition at nonzero temperature in these two systems (Lee and Young, 2003), although the lower-critical dimension for these models for a nonzero transition temperature seems to be very close to 3 (Lee and Young, 2007).

From a theoretical perspective, models with exchange couplings of random signs, such as the so-called Edwards-Anderson model, have attracted by far the most attention. One generally believes that as long as there is a transition at nonzero temperature, the universality class should be the same irrespective of the details of the model, i.e., either continuous or discrete distributions of random bonds or a randomly diluted frustration.

Experimentally, a number of signatures are taken as indicative of the spin-glass state, such as the frequency dependence of χ' in the ac susceptibility, the linear temperature dependence of the low temperature heat capacity, or the μSR line shape, but the definitive approach is measuring the temperature dependence of the nonlinear magnetic susceptibility χ_3 (Binder and Young, 1986). The dc magnetization $M_z(T,B_z)$ can be expanded as a Taylor series of the applied magnetic field B_z as

$$M_z(T,B_z)\approx\chi_1(T)B_z-\chi_3(T)B_z^3, \tag{8}$$

where T is the temperature. At a second order spin glass transition, one expects $\chi_3(T)$ to show a power-law divergence as $\chi_3(T)\sim(T-T_f)^{-\gamma}$, with γ a critical exponent characterizing the spin-glass transition at the freezing temperature T_f (Binder and Young, 1986; Gingras *et al.*, 1997). Other critical exponents can also be determined by measuring the full nonlinear magnetic field dependence of $M_z(B_z,T)$ (Binder and Young, 1986; Gingras *et al.*, 1997).

With this very minimal background material in hand, we can now discuss the spin-glass behaviors observed in some of the pyrochlore oxides.

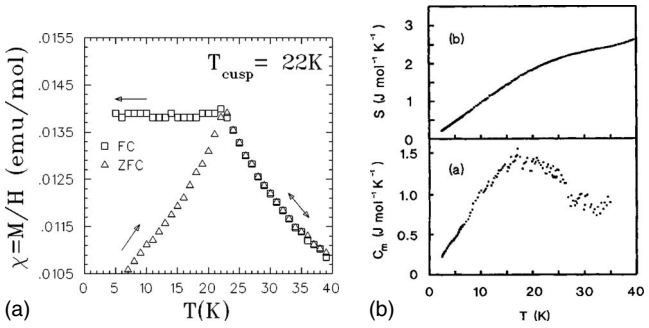

FIG. 32. Susceptibility and heat capacity data for the spin glass, $Y_2Mo_2O_7$. Left: dc magnetic susceptibility for $Y_2Mo_2O_7$ at an applied field of 100 Oe (Gingras *et al.*, 1997). Right: (a) Heat capacity and (b) entropy for $Y_2Mo_2O_7$. Note the broad maximum below 20 K and the linear dependence on temperature below 7 K. From Raju *et al.*, 1992.

1. $Y_2Mo_2O_7$ and $Tb_2Mo_2O_7$

a. $Y_2Mo_2O_7$

The initial report by Greedan *et al.* (1986), showing a canonical spin glass behavior [see Fig. 32(a)], for $Y_2Mo_2O_7$ sparked considerable interest which currently continues. Neutron powder diffraction data, albeit of moderate resolution, could be analyzed in terms of a fully ordered pyrochlore model (Reimers *et al.*, 1988). Specific heat studies by Raju *et al.* (1992) showed only a broad maximum near the apparent $T_f=22$ K and a linear dependence on temperature at low T, another feature typical of spin glasses [see Fig. 32(b)]. ac susceptibility by Miyoshi *et al.* (2000) and thermoremanent magnetization by Dupuis *et al.* (2002) and Ladieu *et al.* (2004) provided more evidence for the canonical spin-glass behavior of this material. The ac susceptibility in nearly zero field shows the classic frequency dependence [see Fig. 33(b)].

The best evidence for the canonical spin-glass character came from measurements of the nonlinear susceptibility χ_3 by Gingras *et al.* (1996, 1997). The nonlinear

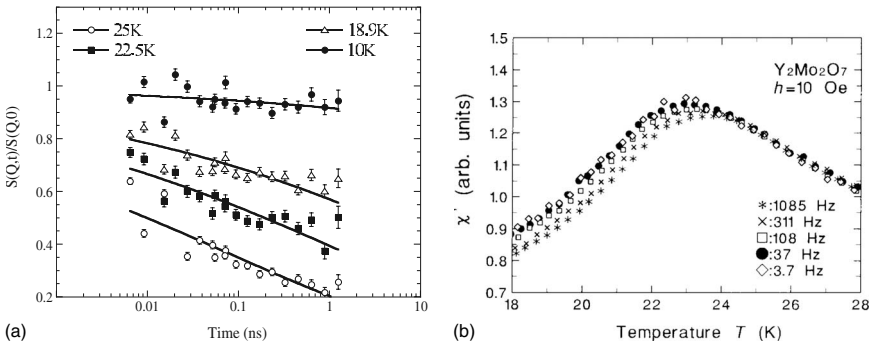

FIG. 33. Spin dynamics in $Y_2Mo_2O_7$. Left: Neutron spin echo results for $Y_2Mo_2O_7$ at temperatures spanning T_f=22.5 K determined from static magnetization data. Note that within this time window spin freezing is not fully established until 10 K. From Gardner, Ehlers, *et al.*, 2001; Gardner, Ehlers, Bramwell, and Gaulin, *et al.*, 2004. Right: Frequency dependent ac susceptibility χ' for $Y_2Mo_2O_7$ showing classical spin-glass behavior. From Miyoshi *et al.*, 2000.

magnetization could be analyzed (see Fig. 34), according to a scaling model for phase transitions, yielding critical exponents γ, β, and δ which satisfied the scaling relationship

$$\delta = 1 + \gamma/\beta, \tag{9}$$

with values T_f=22 K, γ=2.9(5), β=0.8(2), and $\delta \approx 4.7$. These agree well with those found for conventional spin glasses with dilute magnetic centers and positional disorder (Binder and Young, 1986), making $Y_2Mo_2O_7$ indistinguishable from such systems.

Strong evidence for spin freezing also comes from studies of spin dynamics by muon spin relaxation (Dunsiger *et al.*, 1996a). Figure 35 shows $1/T_1$, the muon spin relaxation rate, as a function of temperature. These data show features typical of disordered spin-frozen systems such as a critical slowing down as T_f is approached from above followed by a sharp decrease. A finite $1/T_1$ persists down to the lowest temperatures studied, but this is at the resolution limit of this technique and more needs to be done to conclusively determine if the spins are still dynamic in the mK temperature range.

Neutron scattering experiments (Gardner, Gaulin, *et al.*, 1999) provide more insight into the possible local ordering and the spin dynamics over a wide temperature range. Figure 36 shows the $|\mathbf{Q}|$ dependence of the magnetic elastic scattering at 1.8 K. The obvious feature is a broad peak centered at $|\mathbf{Q}|$=0.44 Å^{-1}. In terms of unit cell dimensions, this value of $|\mathbf{Q}|$ corresponds to $2\pi/d(110)$, which involves the cubic face diagonal. From the half width at half maximum (HWHM) a correlation length can be estimated as ξ=1/HWHM=5 Å. These two observations are consistent with a short-range four-sublattice structure as depicted in the inset of Fig. 36.

Inelastic scattering data give a detailed picture of the evolution of the spin dynamics in terms of four distinct regimes. (1) For T>200 K there are no discernable correlations in either space or time. (2) Between 200 K and $T=2T_f$ spatial correlations build up, peaking at $|\mathbf{Q}|$ =0.44 Å^{-1}, but the energy distribution is broad. (3) Within the interval $T_f < T < 2T_f$, the spatial correlations are no longer evolving but the spin fluctuation rate decreases proportionally to $T-T_f$ in a manner appropriate to the approach to a phase transition. (4) Below T_f the

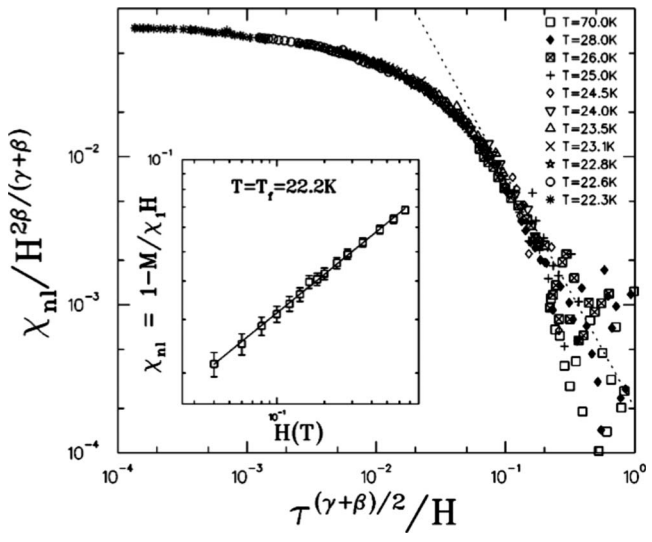

FIG. 34. Nonlinear magnetization analyzed according to a scaling model for T_f=22 K, γ=2.8, and β=0.75. Inset shows a log-log plot which allows determination of the critical parameters with δ=4.73 which follows from the scaling law with the above γ and β values. From Gingras *et al.*, 1997.

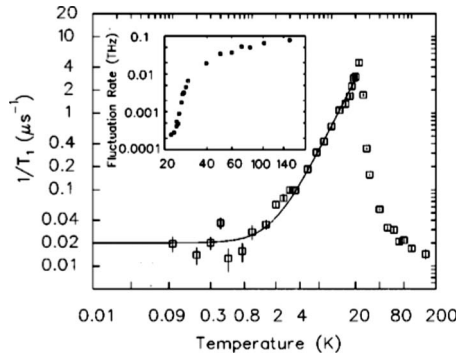

FIG. 35. The muon spin relaxation rate, $1/T_1$, versus temperature. Note the critical slowing down near T_f and the presence of a small but finite relaxation rate persisting to very low temperatures. From Dunsiger *et al.*, 1996a.

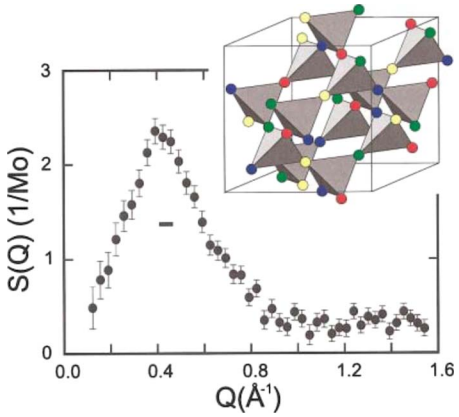

FIG. 36. (Color online) Elastic neutron scattering for $Y_2Mo_2O_7$ shown as the difference between data at 1.8 and 50 K. The broad peak suggests the short-range order model shown in the inset. From Gardner, Gaulin, *et al.*, 1999.

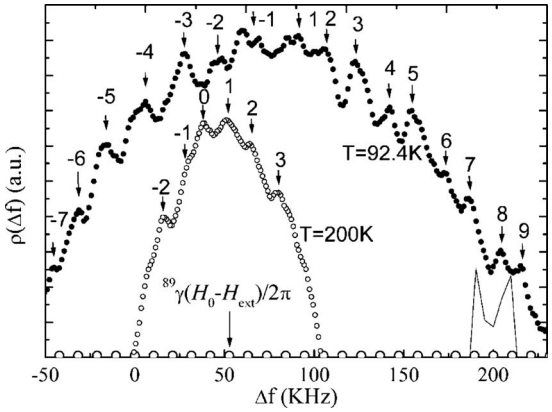

FIG. 37. Y-NMR data for $Y_2Mo_2O_7$ showing multiple peaks arising below 200 K, indicating the presence of multiple Y sites. From Keren and Gardner, 2001.

spin fluctuation rate is small and changes very little, consistent with a highly spin-frozen state.

The neutron spin echo technique provides information on spin dynamics over a shorter time scale than μSR from about 1 to 10^{-2} ns. Within this time window, a different view of the spin dynamics emerges (Gardner, Ehlers, *et al.*, 2001; Gardner, Ehlers, Bramwell, and Gaulin, 2004). The left panel of Fig. 33 shows the time dependence of the normalized intermediate scattering function $S(Q,t)/S(Q,0)$ for temperatures spanning T_f (22.5 K) determined from static magnetization studies. While the data for 10 K show spin-frozen behavior, there are still significant spin dynamics below T_f. Fits to these data indicate that spin relaxation times increase by a factor of 10^7 between 25 and 10 K from 0.07 ns to 8×10^5 ns.

The evidence presented above raises a fundamental question: Why is $Y_2Mo_2O_7$ such a typical spin glass? In general, insulating antiferromagnetic spin glasses involve dilution of the magnetic centers by diamagnetic ions at a concentration below the percolation limit which introduces both positional disorder and frustration simultaneously, two conditions considered necessary for the establishment of the spin-glass ground state. In $Y_2Mo_2O_7$ the magnetic frustration is "already" provided by the magnetic lattice topology, but is there also disorder of some subtle type? While powder neutron diffraction data show that the average structure is well described by the fully ordered pyrochlore model (Reimers *et al.*, 1988; Greedan *et al.*, 2009), local structure probes such as extended x-ray-absorption fine structure (EXAFS) and NMR suggested the presence of disorder at some level in this material. Mo *K* edge EXAFS data were interpreted by Booth *et al.* (2000) to show that the variance in the Mo-Mo nearest-neighbor distance was about ten times larger than that for the Mo-O and Mo-Y distances. From this and a number of assumptions it was estimated that the level of disorder introduced in a pairwise exchange constant would be of the order of 5%. This was judged to be about a factor of 5 too small when compared with predictions from the Sherrington and Southern (1975) mean field theory for spin glasses. Keren and Gardner (2001) carried out ^{89}Y NMR experiments over a limited temperature range. Data obtained above 200 K (the Curie-Weiss temperature) showed a smooth and broad resonance but, at 200 and 92.4 K, a large number of peaks of small amplitude become superimposed on the broad feature (see Fig. 37). This was interpreted in terms of a distribution of ^{89}Y environments due to localized "lattice" distortions and led to speculation that these distortions are frustration driven. A similar experiment was performed using muon spin relaxation by Sagi *et al.* (2005) down to 20 K. The width of the internal field distribution as detected by the muon grows upon cooling at a rate which cannot be explained by the increasing susceptibility alone. Therefore, they concluded that the width of the distribution of coupling constants also grows upon cooling, or, in other words, the lattice and spin degrees of freedom are involved in the freezing process in $Y_2Mo_2O_7$. A model of Heisenberg spins with magnetoelastic coupling was invoked to account for the high freezing temperature. The derivative of the exchange strength relative to bond length was found to be 0.01 eV/Å and the elastic constant to be 0.1 eV/Å^2. In $ZnCr_2O_4$, where magnetoelastic coupling appears to be important, these values are 0.04 and 6.5 eV/Å^2, respectively (Sushkov *et al.*, 2005). Other theoretical studies that have considered classical pyrochlore Heisenberg antiferromagnets with random variations in the exchange couplings include Bellier-Castella *et al.* (2001) and Saunders and Chalker (2007).

Currently the microscopic mechanism behind the spin-glass transition in $Y_2Mo_2O_7$ is unresolved. Ideally, one would like to find a means to reconcile the diffraction studies with the local probe results. One possibility is the application of the neutron pair distribution function method (Proffen *et al.*, 2003; Billinge, 2004). Studies using this approach have recently been reported. It was found that the major source of disorder involves the Y-O1 bonds rather than the Mo-Mo sublattice which is consistent with the ^{89}Y NMR studies but not the analysis

of the EXAFS data. See Greedan *et al.* (2009).

Dunsiger *et al.* (1996b) showed that a 20% dilution of the magnetic Mo^{4+} site with nonmagnetic Ti^{4+} reduces the freezing temperature but increases the residual muon relaxation rate, indicating an increased density of states for magnetic excitations near zero energy. While there are no other published reports on *B*-site substitution in $Y_2Mo_2O_7$, there may be much to learn from such efforts. As noted, the microscopic origin of the spin glass behavior in this material is not understood. What is known suggests that $Y_2Mo_2O_7$ falls into the category of a bond disordered spin glass rather than a site disordered glass such as $Eu_{1-x}Sr_xS$, for example. In the context of a picture in which $Y_2Mo_2O_7$ is an "intrinsic" random bond spin glass, it would be of interest to track T_f as a function of the doping of the Mo site with a nonmagnetic ion such as Ti^{4+}. Interesting physics may emerge at low temperature close to the percolation limit which is 39% of magnetic site occupancy for the pyrochlore lattice.

b. $Tb_2Mo_2O_7$

Although this material has received much less attention than the Y-based pyrochlore, there are strong similarities. $Tb_2Mo_2O_7$ is an inherently more complex system with two geometrically frustrated magnetic sublattices. Also, the A=Tb phase is just on the insulating side of the MI boundary for this series and is not a bulk ferromagnet although the Curie-Weiss temperature is θ_{CW}=+17 K (Sato *et al.*, 1986). Among the few detailed studies of transport properties, the material is shown to exhibit an unusual magnetoresistance (MR) with both positive (10%) and negative (30%) MR at low and high fields, respectively (Troyanchuk and Derkachenko, 1988). This behavior lacks an explanation to date.

Magnetization and neutron scattering studies indicated spin glass like behavior with T_f=25 K and intense diffuse magnetic scattering (Greedan *et al.*, 1990; Gaulin *et al.*, 1992). The diffuse magnetic scattering sets in below 50 K (see Fig. 38), showing two very broad peaks near $|\mathbf{Q}|$=1.0 and 2.0 Å^{-1}. This pattern is quite different from that for $Y_2Mo_2O_7$ (see Sec. III.B.1.a) and indicates that the Tb sublattice scattering is dominant here. Note also the upturn at low Q.

SANS data were also reported over the Q range of 0.019–0.140 Å^{-1}. Subtraction of the 300 K data from low-temperature data shows that nonzero SANS appeared only above $|\mathbf{Q}|$=0.14 Å^{-1}, so it is unlikely that this SANS tail is of ferromagnetic origin (Greedan *et al.*, 1990). However, these results might be in conflict with a recent report from Apetrei *et al.* (2007a) who observed SANS above $|\mathbf{Q}|$=0.25 Å^{-1}. This issue should be clarified. From inelastic neutron scattering, the Tb spins have been shown to be fluctuating at about 0.02 THz above T_f, but spin freezing within the experimental time window was seen below 25 K (Gaulin *et al.*, 1992). Spin relaxation studies were extended into the μSR time window (see Fig. 39). Comparing with Fig. 35, which shows

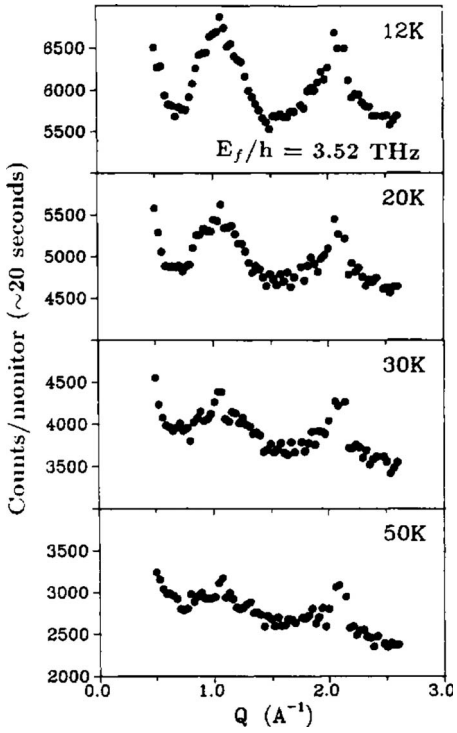

FIG. 38. Diffuse magnetic elastic scattering for $Tb_2Mo_2O_7$ at various temperatures (Gaulin *et al.*, 1992).

corresponding data for $Y_2Mo_2O_7$, one notes some similarities and differences. The data above T_f are similar, indicating a critical slowing down behavior, followed by a clear maximum and a subsequent decrease. Note, however, that the relaxation time below about 1 K remains very large (5 μs) relative to that for A=Y (0.02 μs). This difference is attributed to the larger moment of Tb^{3+} relative to Mo^{4+} being roughly proportional to the ratio of the squares of the moments. These results show that the Tb spins are involved in the freezing and that there exists an appreciable density of states for low-energy magnetic excitations for these materials which are accessible even at very low temperatures.

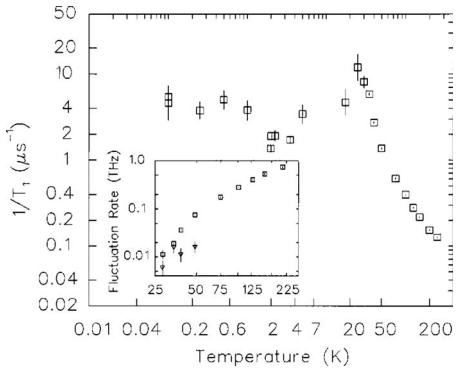

FIG. 39. The muon spin relaxation rate vs temperature for $Tb_2Mo_2O_7$ in an applied field of 5 mT. The inset shows the Tb moment fluctuation rate above the spin freezing point compared with neutron data indicated by the inverted triangles. From Dunsiger *et al.*, 1996a.

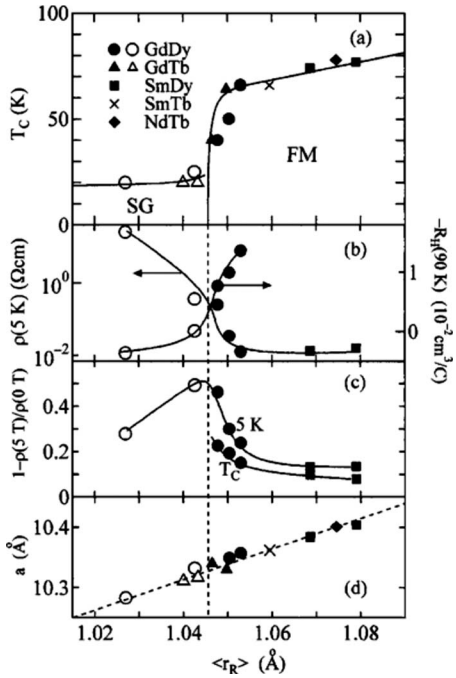

FIG. 40. A phase diagram for $(A_{1-x}A'_x)Mo_2O_7$ pyrochlores. (a) T_c or T_f. (b) Resistivity at 5 K. (c) Magnetoresistance at 5 K and T_c (d) Unit cell constant. From Katsufuji *et al.*, 2000.

c. Other $A_2Mo_2O_7$

In fact, there is relatively little published information on other members of this series for A=Dy, Ho, Er, Tm, Yb, or Lu. Most show dc and ac susceptibility anomalies near T=22 K, as in the A=Y material (Raju and Gougeon, 1995). Miyoshi *et al.* (2000) showed ac susceptibility data for A=Ho and Tb. The A=Yb material has been studied using ^{170}Yb Mössbauer measurements. The major results are that evidence was found for a lower than axial symmetry at the Yb site, suggesting some local disorder and that the local magnetic fields acting on the Yb nucleus show a random distribution, consistent with the bulk spin-glass properties (Hodges *et al.*, 2003).

There have been a few studies involving mixed occupation of the A site. Katsufuji *et al.* (2000) investigated materials of the type $A_{1-x}A'_x$ with A=Nd, Sm, and Gd and A'=Tb and Dy. That is, solid solutions between the ferromagnetic phases A=Nd, Sm, and Gd and the spin-glass materials A'=Tb and Dy. The results are summarized in Fig. 40 where the FM metal to spin-glass insulator transition occurs at an average A-site radius between that for Gd^{3+} (1.053 Å) and that for Tb^{3+} (1.04 Å). This is fully consistent with the results from the pure samples. Two studies have been reported in which the A site is substituted with nonmagnetic ions and the results are markedly different. In early work by Sato and Greedan (1987), solid solutions of the type $A=Y_{1-x}La_x$ were investigated. Compositions were chosen to span the average A site radius from Nd to Y, intending to cover the ferromagnet to spin-glass transition range. Surprisingly, all samples showed only spin-glass behavior with T_f values not far from that for A=Y, $T_f \sim 22$ K. Even the compositions $A=Y_{0.5}La_{0.5}$ and $Y_{0.6}La_{0.4}$, which have an average A-site radius equivalent to Nd and Sm, respectively, showed no ferromagnetic transition, although the Curie temperatures were positive, +41 and +31 K, respectively. Unfortunately, no electrical transport data have been reported.

Hanasaki *et al.* (2007) chose solid solutions with A=Eu (Eu^{3+} is, technically, a nonmagnetic ion as J=0) and A'=Y or La. The pure A=Eu is reported to be metallic and ferromagnetic with T_c=50 K (Kézsmárki *et al.*, 2006). The data are from an image furnace grown crystal and unfortunately no unit cell constant is reported, so some electron doping is likely. Hanasaki *et al.* (2007) reported ferromagnetic behavior for the La-doped materials but with a re-entrant spin-glass transition at 22 K. T_c for the $Eu_{0.85}La_{0.15}$ material appears to be about 65 K. For this A-site composition the average A-site radius is equivalent to that of Sm^{3+} and one might expect a higher value. Perhaps electron doping is playing a role again. The phases with A=(Eu,Y) are spin glasses. These results are quite new and interesting but the system should be investigated further. Finally, the discrepancy between the results of Sato and Greedan (1987) where the A site involves La and Y and those of Hanasaki *et al.* (2007), just described, is difficult to understand. One obvious difference is that the variance of the average radius is of course greater for the A=La,Y combination than for Eu, La or Eu, Y. Thus, the influence of the A-site composition on the magnetic and transport properties is apparently subtle and merits closer investigation.

C. Spin-ice phases

The spin-ice phenomenology in the pyrochlore oxides was discovered in 1997 in $Ho_2Ti_2O_7$ (Harris *et al.*, 1997; Harris, Bramwell, Zeiske, *et al.*, 1998; Bramwell and Gingras, 2001). This system possesses a ferromagnetic Curie-Weiss temperature $\theta_{CW} \sim +2$ K. It was thus quite surprising that this material does not develop long-range order down to 50 mK, with neutron scattering revealing only broad diffuse scattering features for temperatures much lower than θ_{CW}.

In $Ho_2Ti_2O_7$ the strong axial crystal electric field acting on Ho^{3+} gives rise to an almost ideal classical Ising spin. Because of symmetry, the local Ising (quantization) axis is along the local cubic ⟨111⟩ directions, such that on a tetrahedron a spin can only point "in" toward the middle of the opposing triangular face, or oppositely, hence "out" of the tetrahedron. While geometric frustration is generally associated with antiferromagnetic interactions, frustration arises here for ferromagnetic ones. Indeeed, there are six "two-in, two-out" spin configurations that minimize the ferromagnetic exchange energy on an individual tetrahedron and thus six ground states. There is an infinity of such ground states for a macroscopically large sample, and there is therefore an extensive ground state entropy. This entropy, S_0, can be estimated by borrowing the argument used by Pauling for estimating the residual proton configuration disorder

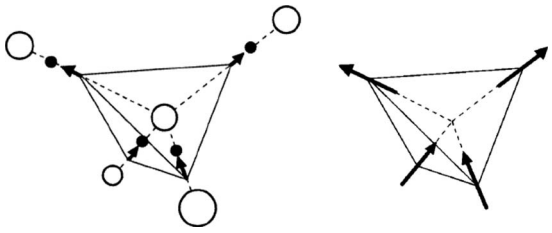

FIG. 41. Illustration of the equivalence of the water ice rule "two protons near, two protons far" and the spin-ice rule "two spins in, two spins out." The diagram (left) illustrates a water molecule in the tetrahedral coordination of the ice structure with proton positions located by displacement vectors that occupy a lattice of linked tetrahedra. In spin ice (right) the displacement vectors are replaced by rare-earth moments ("spins") occupying the pyrochlore lattice, which is the dual lattice (i.e., the lattice formed by the midpoints of the bonds) of the oxide lattice in cubic ice.

in common hexagonal water ice (Pauling, 1935). The main point is to consider the difference between the number of constraints necessary to determine a ground state and the number of degrees of freedom that the system possesses. Consider Anderson's Ising pyrochlore antiferromagnet, onto which the local ⟨111⟩ pyrochlore Ising model maps, as discussed in Sec. I.C (Anderson, 1956). The ground state condition is "underconstrained," demanding only that the total magnetization of the four Ising spins on each tetrahedron be zero. Six of the $2^4=16$ possible spin configurations satisfy this condition. Counting 2^4 configurations for each tetrahedron gives, for a system of N spins and $N/2$ tetrahedra, a total number of microstates, $\tilde{\Omega}=(2^4)^{N/2}=4^N$. This number drastically overestimates the exact total, $\Omega=2^N$. The reason is that each spin is shared between two tetrahedra; hence the above 16 configurations on each tetrahedron are not independent. Following Pauling's argument, we allocate $2^2=4$ states per tetrahedron and, assuming that 6/16 of them satisfy the constraint, this leads to a ground state degeneracy $\Omega_0=\{2^2(6/16)\}^{N/2}=(3/2)^{N/2}$. The corresponding entropy, $S_0=k_B\log(\Omega_0)=(Nk_B/2)\ln(3/2)$, is of course just Pauling's original result.

Not only is the residual entropy of ferromagnetic ⟨111⟩ spins on the pyrochlore lattice the same as Pauling's entropy for water ice but, as shown in Fig. 41, there is also a rather direct connection between the spin configurations in the pyrochlore problem and that of the proton positions in water ice. For this reason, the term *spin ice* was coined (Harris *et al.*, 1997). In anticipation of the forthcoming discussion of the physics at play in $Tb_2Ti_2O_7$, it is worthwhile to comment on a case where the nearest-neighbor exchange interactions are antiferromagnetic for a situation with local ⟨111⟩ spins. In that case, the ground state consists of all spins pointing in or out of a reference tetrahedron. Hence, there are in that case only two ground states related by a global spin inversion symmetry, and a second order transition in the universality class of the (unfrustrated) three-dimensional Ising model is expected. Earlier, Anderson had noticed the connection between the statistical mechanics of antiferromagnetically coupled Ising spins on the pyrochlore lattice and Pauling's model of proton disorder in water ice. However, in Anderson's model, the Ising spins share a common (global) z-axis direction, and frustration arises as usual for antiferromagnetic interactions with spins on triangular or tetrahedral units. However, since the pyrochlore lattice has cubic symmetry, the x, y, and z directions are equivalent, and this renders Anderson's global antiferromagnetic Ising model unrealistic. It is the local nature of the quantization direction that is crucial and which is the origin of the frustration for ferromagnetic interactions and for the "elimination" of the frustration for antiferromagnetic exchange. To see this, consider the following toy-model Hamiltonian,

$$H=-J\sum_{\langle i,j\rangle}\boldsymbol{S}_i\cdot\boldsymbol{S}_j-\Delta\sum_i(\hat{z}_i\cdot\boldsymbol{S}_i)^2, \tag{10}$$

with classical Heisenberg spins $\boldsymbol{S}_i$ on the sites i of the pyrochlore lattice, interacting via nearest-neighbor exchange coupling J. The second term is a single-ion anisotropy interaction with Δ the anisotropy parameter and $\hat{z}_i$ a unit vector in the local ⟨111⟩ direction at site i. For $J=0$ and $\Delta>0$, the energy is lower if $\boldsymbol{S}_i$ points along $\hat{z}_i$, and one refers to this as an Ising anisotropy. The case $\Delta<0$ would be referred to as an XY model (Bramwell *et al.*, 1994; Champion and Holdsworth, 2004). However, as discussed in Sec. II.A.2, the real microscopic crystal-field Hamiltonian is more complicated than that considered by Bramwell *et al.* (1994) and Champion and Holdsworth (2004) where the limit $\Delta\to-\infty$ was taken.

Hence, we assume an extreme Ising limit, $\Delta/J\to\infty$. $\boldsymbol{S}_i$ is then confined to be either parallel or antiparallel to $\hat{z}_i$. To implement this energetic single-ion constraint, we write $\boldsymbol{S}_i=\sigma_i^{z_i}\hat{z}_i$. Injecting this back into H above, we obtain

$$H=-J\sum_{\langle i,j\rangle}(\hat{z}_i\cdot\hat{z}_j)\sigma_i^{z_i}\sigma_j^{z_j}=+(J/3)\sum_{\langle i,j\rangle}\sigma_i^{z_i}\sigma_j^{z_j}, \tag{11}$$

where $\hat{z}_i\cdot\hat{z}_j=-1/3$ for two distinct cubic ⟨111⟩ directions. One sees that for ferromagnetic J ($J>0$), the now "global" $\sigma_i^{z_i}$ Ising variables map onto an equivalent Ising antiferromagnet [Anderson's model (Anderson, 1956)] with coupling $J/3$ and is therefore frustrated. Conversely, for antiferromagnetic J ($J<0$), the minimum energy state consists of all spins pointing in (say $\sigma_i^{z_i}=-1\ \ \forall i$) or all out ($\sigma_i^{z_i}=+1\ \ \forall i$).

As discussed in Sec. III.C.1, $Dy_2Ti_2O_7$ is also identified as a spin-ice material. It turns out that both Ho^{3+} and Dy^{3+} carry a sizable magnetic moment μ of $\sim10\mu_B$ in the crystal-field ground states of $Ho_2Ti_2O_7$ and $Dy_2Ti_2O_7$. Thus, these systems have a magnetostatic dipole-dipole interaction $D=\mu_0\mu^2/4\pi r_{nn}^3$ of $D\sim1.4$ K at the nearest-neighbor distance r_{nn}. Since D is approximately the same as θ_{CW}, it is surprising that the long-range and complex natures of the dipolar interactions do not lift the spin-ice degeneracy and drive the system to long-range order at a critical temperature $T_c\sim D$. In

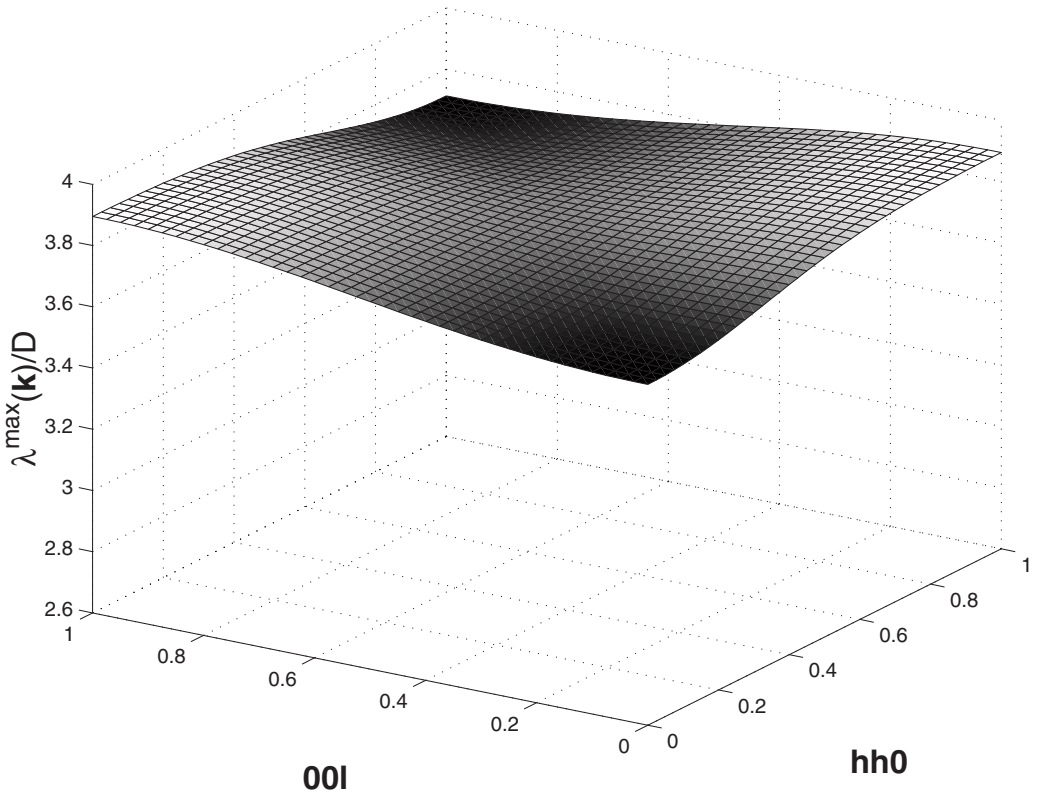

FIG. 42. Dipolar- spin-ice model: the scaled maximum eigenvalues $\lambda^{max}(\mathbf{k})/D$ in the (hhl) plane. The dipole-dipole interactions are treated with the Ewald approach. Here the exchange coupling J in Eq. (1) was set to zero. While the spectrum is very flat, suggesting a weak propensity toward long-range order, a maximum at a unique ordering wave vector $\mathbf{k}_{ord}=001$. From Gingras and den Hertog, 2001.

fact, numerical and theoretical studies have compellingly demonstrated that it is precisely the mathematical form of the dipole-dipole interactions that is at the origin of the spin-ice phenomenology in rare-earth pyrochlores. In particular, it is the ferromagnetic character of the dipolar interactions at the nearest-neighbor distance and not a ferromagnetic nearest-neighbor exchange (which turns out to be antiferromagnetic as analysis of experimental data on $Ho_2Ti_2O_7$ and $Dy_2Ti_2O_7$ has revealed) that is primarily the source of frustration. Indeed, as discussed above, if it were not for the dipolar interactions, the nearest-neighbor antiferromagnetic interactions alone in $Ho_2Ti_2O_7$ and $Dy_2Ti_2O_7$ would drive the system into a long-range ordered phase.

The minimal model, called the dipolar- spin-ice model (DSM), that is needed to investigate these questions includes nearest-neighbor exchange (first term) and long-range magnetic dipole interactions (second term) in

$$H = -J\sum_{\langle ij\rangle} \boldsymbol{S}_i^{\hat{z}_i}\cdot\boldsymbol{S}_j^{\hat{z}_j} + Dr_{\rm nn}^3\sum_{i>j}\frac{\boldsymbol{S}_i^{\hat{z}_i}\cdot\boldsymbol{S}_j^{\hat{z}_j}}{|\boldsymbol{r}_{ij}|^3} - \frac{3(\boldsymbol{S}_i^{\hat{z}_i}\cdot\boldsymbol{r}_{ij})(\boldsymbol{S}_j^{\hat{z}_j}\cdot\boldsymbol{r}_{ij})}{|\boldsymbol{r}_{ij}|^5}. \quad (12)$$

For the open pyrochlore lattice structure, we expect further neighbor exchange to be small, so these can be neglected as a first approximation. Results from Monte Carlo simulations compared with experiments seem to confirm this expectation (Ruff *et al.*, 2005; Yavors'kii *et al.*, 2008). Here the spin vector $\boldsymbol{S}_i^{\hat{z}_i}$ labels the Ising moment of magnitude $|\boldsymbol{S}_i^{\hat{z}_i}|=1$ at lattice site i, oriented along the local Ising $\langle 111\rangle$ axis $\hat{z}_i$. The distance $|\boldsymbol{r}_{ij}|$ is measured in units of the nearest-neighbor distance $r_{\rm nn}$. J represents the exchange energy and $D=\mu_0\mu^2/4\pi r_{\rm nn}^3$. Because of the local Ising axes, the effective nearest-neighbor energy scale is $J_{\rm eff}=J_{\rm nn}+D_{\rm nn}$, where $J_{\rm nn}\equiv J/3$ and $D_{\rm nn}\equiv 5D/3$, since $\hat{z}_i\cdot\hat{z}_j=-1/3$ and $(\hat{z}_i\cdot\mathbf{r}_{ij})(\mathbf{r}_{ij}\cdot\hat{z}_j)=-2/3$. If $D_{\rm nn}=0$ and $J>0$, one obtains the spin-ice model originally proposed by Harris *et al.* (1997) and Harris, Bramwell, Holdsworth, and Champion (1998) henceforth referred to as the "nearest-neighbor spin-ice model."

The condition $J_{\rm eff}>0$ is a simple criterion to assess whether a system displays a spin-ice state. Mean field theory (Gingras and den Hertog, 2001) and Monte Carlo simulations (Melko and Gingras, 2004) find a critical value for the transition between "all-in, all-out" Néel order and spin ice at $J_{\rm nn}/D_{\rm nn}\approx -0.905$, hence quite close to the naive nearest-neighbor estimate $J_{\rm nn}/D_{\rm nn}=-1$. The dipolar interactions beyond nearest neighbors provide a weak extra stabilization of the $\mathbf{k}_{ord}=0$ all-in, all-out Néel phase over the true zero temperature long-range ordered spin-ice state with $\mathbf{k}_{ord}=001$ (see Fig. 42).

The success of the nearest-neighbor criterion in assessing whether a system should display spin-ice phenomenology or not indicate that, to a large extent, dipo-

lar interactions beyond nearest neighbors are *self-screened*, as originally suggested by a mean field calculation (Gingras and den Hertog, 2001), Fig. 42, and Monte Carlo simulations (den Hertog and Gingras, 2000). The reason why dipolar-spin-ice systems obey the ice rules is not immediately apparent. Isakov *et al.* (2005) proposed that the ice rules result from the fact that the dipolar interactions are, up to a perturbatively small and rapidly decaying function, a real-space projector onto the manifold of ice-rule obeying states. A possibly simpler explanation has been proposed which involves separating each point dipole into its constituent magnetic (monopole) charges and requiring that each tetrahedron is, magnetic-charge-wise, neutral, which automatically leads to the conclusion that all ice-rule obeying states are, again up to a small correction, ground states of the dipolar interactions (Castelnovo *et al.*, 2008). Such a real-space argument is possibly not unrelated to the Ewald energy calculations in which the dipolar lattice sums are regularized by effective Gaussian charges either in reciprocal space (Enjalran and Gingras, 2003) or in direct space (Melko and Gingras, 2004).

1. $Dy_2Ti_2O_7$ and $Ho_2Ti_2O_7$

The Dy^{3+} ion in $Dy_2Ti_2O_7$ was first identified as having strongly anisotropic properties from the maximum in the dc susceptibility (Blöte *et al.*, 1969) at $T\sim0.9$ K followed by a precipitous drop to essentially 0 at $T\sim0.4$ K. This suggested a strongly anisotropic effective g tensor with a $g_\perp\approx0$ component perpendicular to the local $\langle111\rangle$ axis, making Dy^{3+} in effect a $\langle111\rangle$ Ising model. This was confirmed by Flood (1974) from direct measurement of the magnetic moment and from analysis of inelastic neutron scattering data by Rosenkranz (Rosenkranz *et al.*, 2000). Calculations from crystal-field theory, complemented by fitting crystal-field parameters (CFPs) to susceptibility data, also confirmed the strong Ising nature of Dy^{3+} in $Dy_2Ti_2O_7$ (Jana *et al.*, 2002). Specifically, the single-ion electronic ground state of Dy^{3+} is a Kramers doublet of almost pure $|J=15/2,\ m_J=\pm15/2\rangle$ separated from the first excited state by a gap $\Delta\approx33$ meV (~380 K) using the rescaled CFPs of Rosenkranz *et al.* (2000) while Jana *et al.* (2002) find a much smaller excitation gap $\Delta\approx100$ cm^{-1} (~140 K).

Blöte *et al.* (1969) measured the specific heat $C(T)$ of $Dy_2Ti_2O_7$ between 0.37 and 1.3 K and found only a broad maximum around 1.2 K and no sign of a sharp specific heat feature indicating a phase transition to long-range magnetic order. Most interestingly, a total magnetic entropy of only approximately $\frac{3}{4}R\ln(2)$ was found. Hence, a noticeable fraction of $R\ln(2)$ expected for a Kramers ground doublet was missing.

Soon after the proposal of spin ice in $Ho_2Ti_2O_7$ (Harris *et al.*, 1997; Harris, Bramwell, Zeiske, *et al.*, 1998); Ramirez *et al.* (1999) showed that the missing entropy in $Dy_2Ti_2O_7$ could be determined rather precisely by a measurement of the magnetic specific heat $C(T)$ between 0.4 and 12 K. Figure 43(a) shows the temperature dependence of $C(T)/T$. The magnetic entropy change $\Delta S_{1,2}$ between temperatures T_1 and T_2 can be found by integrating $C(T)/T$ between these two temperatures,

$$\Delta S_{1,2}\equiv S(T_2)-S(T_1)=\int_{T_1}^{T_2}\frac{C(T)}{T}dT. \tag{13}$$

Figure 43(b) shows that the magnetic entropy recovered is 3.9 J mol^{-1} K^{-1}, a value that falls considerably short of $R\ln(2)\approx5.76$ J mol^{-1} K^{-1}. The difference, 1.86 J mol^{-1} K^{-1}, is close to Pauling's estimate for the residual extensive entropy of water ice, $(R/2)\ln(3/2)\approx1.68$ J mol^{-1} K^{-1}, thus providing compelling thermodynamic evidence for the existence of an ice rules obeying state in $Dy_2Ti_2O_7$.

As mentioned above, the large $10\mu_B$ moments of both Dy^{3+} and Ho^{3+} lead to a critical role for magnetic dipole-dipole interactions in spin ices. The energy $D_{\rm nn}$ at nearest-neighbor distances can be estimated from the effective Curie constant or from the single-ion crystal-field doublet wave functions. The earlier theoretical studies (Siddharthan *et al.*, 1999; den Hertog and Gingras, 2000) of the DSM estimated

$$D_{\rm nn}=\frac{5}{3}\left(\frac{\mu_0}{4\pi}\right)\frac{\mu^2}{r_{\rm nn}^3}\approx+2.35\ \text{K} \tag{14}$$

for both $Ho_2Ti_2O_7$ and $Dy_2Ti_2O_7$. Here $r_{\rm nn}=(a_0/4)\sqrt{2}$ is the nearest-neighbor distance and a_0 is the size of the conventional cubic unit cell. As discussed above, the factor 5/3 originates from the orientation of the Ising quantization axes relative to the vector direction $\boldsymbol{r}_{\rm nn}$ that connects nearest-neighbor magnetic moments. As discussed below, the current estimate on $D_{\rm nn}$ for $Dy_2Ti_2O_7$ is probably accurate to within 10%. Hence, the nearest-neighbor exchange $J_{\rm nn}$ is the main unknown. It can be estimated from the high-temperature (paramagnetic) regime of the magnetic susceptibility χ (Siddharthan *et al.*, 1999), or of the specific heat $C(T)$ (Jana *et al.*, 2002) data. A different approach, followed by den Hertog and Gingras (2000) and Bramwell *et al.* (2001), has been to determine $J_{\rm nn}$ by fitting either the height of the specific heat C_p peaks near 1 K or the temperature at which the peak occurs, T_p, against Monte Carlo simulations of the DSM. Interestingly, fits of T_p or C_p allow for a consistent determination of $J_{\rm nn}\approx-1.24$ K for $Dy_2Ti_2O_7$. Figures 43(a) and 43(b) show good agreement between Monte Carlo results and experimental data on $Dy_2Ti_2O_7$ (den Hertog and Gingras, 2000). Note here that the parameter $D_{\rm nn}$ sets the scale for the dipolar interactions at $D_{\rm nn}=(5/3)\mu_0\mu^2/4\pi r_{\rm nn}^3$; the simulations themselves use true long-range dipole-dipole interactions implemented via the Ewald method (Melko and Gingras, 2004). These results show convincingly the spin-ice phenomenology in $Dy_2Ti_2O_7$ and also in $Ho_2Ti_2O_7$, as we now discuss.

While $Ho_2Ti_2O_7$ was the first compound to be proposed as a spin ice, specific heat measurements proved initially less straightforward to interpret than in $Dy_2Ti_2O_7$, and this led to some confusion. Specifically, the rapid increase in the specific heat below 1 K was originally interpreted as an indication of a phase transi-

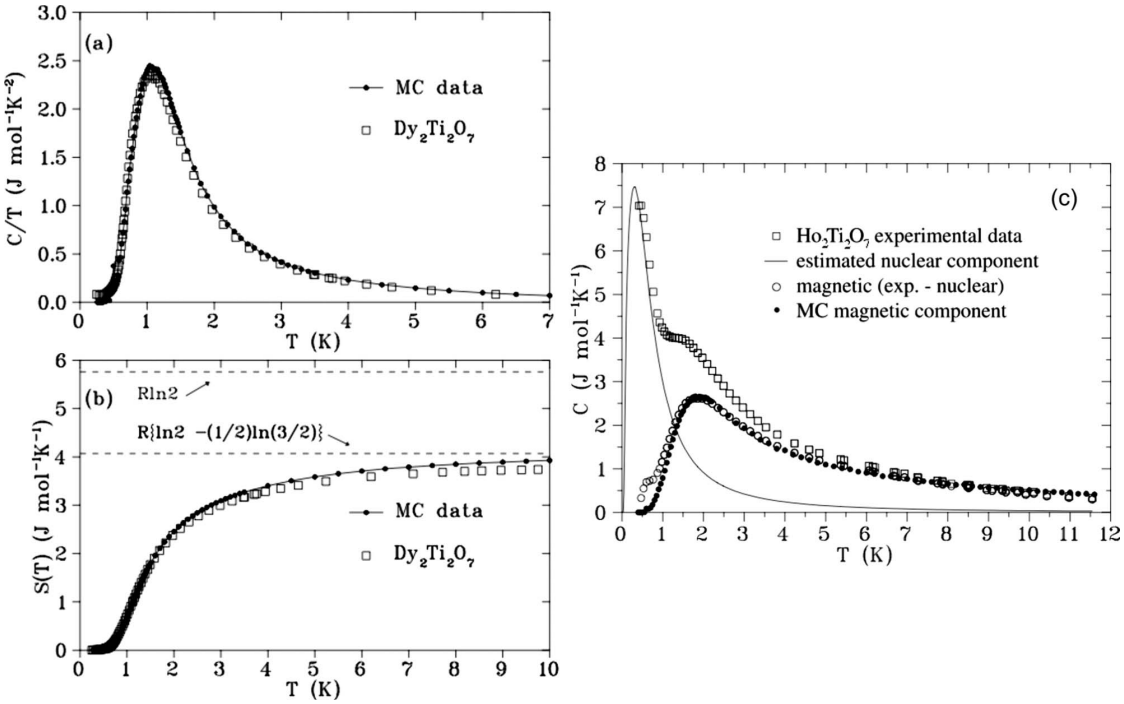

FIG. 43. $Dy_2Ti_2O_7$: (a) Specific heat and (b) entropy vs temperature measured by Ramirez *et al.* (1999). The recovered entropy at 10 K agrees reasonably well with Pauling's entropy, $R/2\ln(3/2)$. The data are compared to that calculated by Monte Carlo simulations of den Hertog and Gingras (2000) for the dipolar- spin-ice model with exchange $J_{nn}=-1.24$ K and dipolar coupling $D_{nn}=2.35$ K. (c) $Ho_2Ti_2O_7$: The total specific heat is shown by the empty squares and the expected nuclear contribution by the solid line. The electronic contribution has been estimated by subtracting these two curves (open circles). Near to 0.7 K, this subtraction is prone to a large error (see text). Dipolar- spin-ice simulation results are indicated by the filled circles. From Bramwell *et al.*, 2001.

tion to a partially ordered state around a temperature of 0.6 K (Siddharthan *et al.*, 1999). Instead, it turns out that the anomalous low-temperature behavior of the specific heat in $Ho_2Ti_2O_7$ is of nuclear origin. An anomalously large hyperfine interaction between the electronic and nuclear spins for Ho commonly leads to a nuclear specific heat Schottky anomaly at approximately 0.3 K. A subtraction of the nuclear contribution from the total low-temperature specific heat reveals the purely electronic specific heat, $C(T)$ (Bramwell *et al.*, 2001), see Fig. 43(c). The integration of $C(T)/T$ from 300 mK up to 10 K gave a magnetic entropy deficit of an amount close to Pauling's $R/2\ln(3/2)$ zero-point entropy, hence confirming, thermodynamically, that $Ho_2Ti_2O_7$ is indeed a spin ice (Cornelius and Gardner, 2001). Following the same procedure as the one used for $Dy_2Ti_2O_7$ (den Hertog and Gingras, 2000), a comparison of $C(T)$ with Monte Carlo simulations [see Fig. 43(c)] allows one to estimate the exchange constant in $Ho_2Ti_2O_7$ as $J_{nn}\sim-0.55$ K, an antiferromagnetic value (Bramwell *et al.*, 2001).

While specific heat measurements on $Ho_2Ti_2O_7$ are problematic, this is emphatically not so for neutron scattering experiments. Unlike dysprosium, holmium has only one stable isotope whose neutron absorption cross section is negligible. Comparison of the experimental neutron scattering intensity with that calculated from Monte Carlo simulations of the dipolar spin-ice model with an exchange constant $J_{nn}\sim-0.55$ K determined as above shows excellent agreement (Bramwell *et al.*, 2001). Interestingly, both the experiment and Monte Carlo data differ substantially from that calculated for the nearest-neighbor spin-ice model (see Fig. 44). This shows that nontrivial spin correlations develop in the material as it progressively freezes within the low-temperature spin-ice regime. Indeed, those correlations are the precursors of those that would ultimately lead to long-range order (see Fig. 42) if not precluded by spin freezing (Melko *et al.*, 2001; Melko and Gingras, 2004).

A puzzling question raised by the good agreement between Monte Carlo simulations of the DSM and the experimental results illustrated in Fig. 43 is the following: Why the dipolar interactions do not drive a transition to long-range order at a critical temperature $T_c\sim D_{nn}\sim 2$ K? A partial answer can be found in the mean field theory calculations of Gingras and den Hertog (2001). They found that the $\mathbf{k}$ dependence of the softest branch of critical modes in the dipolar- spin-ice model is weakly dispersive, reaching a global maximum eigenvalue $\lambda^{max}(\mathbf{k}_{ord})$ at $\mathbf{k}_{ord}=001$. At the mean field level, this indicates that a transition to long-range order should occur at a critical temperature $T_c=\lambda(\mathbf{k}_{ord})$, with the development of delta-function Bragg peaks below T_c.

First of all, this transition does not occur at $T_c\sim D_{nn}$ because the soft (critical) mode at $\mathbf{k}_{ord}$ is in "entropic" competition with the other quasisoft modes at $\mathbf{k}\neq\mathbf{k}_{ord}$.

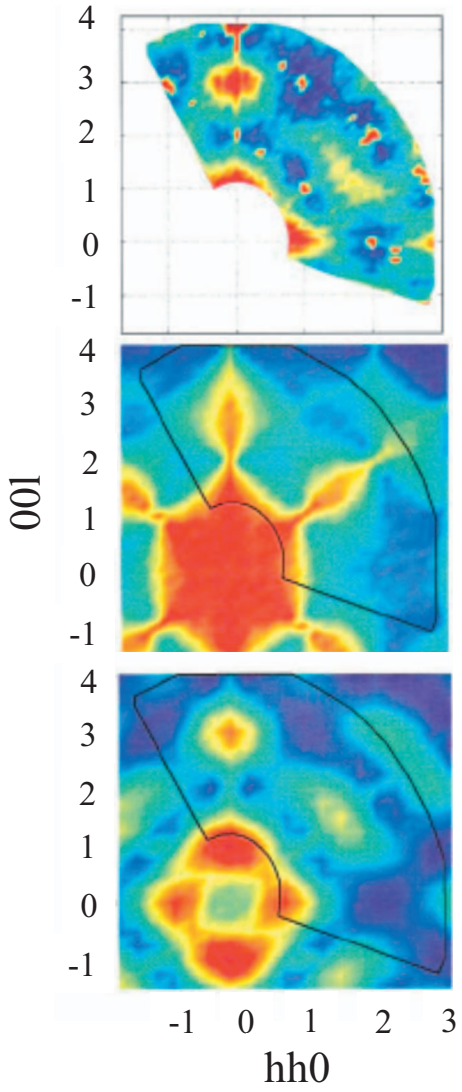

FIG. 44. (Color) $Ho_2Ti_2O_7$: Neutron scattering in the *hhl* plane showing experimental data (upper panel; the sharp spots are nuclear Bragg scattering with no magnetic component) compared with Monte Carlo simulations of the near neighbor spin-ice model (middle panel) and the dipolar spin ice model (lower panel) (Bramwell *et al.*, 2001). Blue indicates the weakest intensity and red-brown the strongest intensity.

The correlated spin ice regime, also called a "collective paramagnet" in Villain's sense (Villain, 1979), albeit with utterly sluggish spin dynamics for $T \lesssim 1$ K in $Dy_2Ti_2O_7$, has so much entropic disorder that it is not energetically favorable to localize the system in phase space to a long-range ordered state. In the standard single spin-flip Monte Carlo simulations (den Hertog and Gingras, 2000), this transition is not observed because the probability to flip a spin once the system enters a state where each tetrahedron obeys on average the two-in, two-out ice rule is very small and decreases exponentially fast with decreasing temperature (Melko and Gingras, 2004). The low-energy excitations deep in the spin-ice state correspond to nonlocal closed loops of spins flipping from in to out and vice versa so that the system, as it experiences those excitations, remains in a spin-ice state

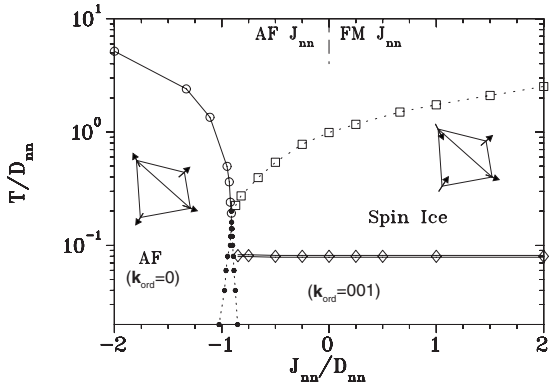

FIG. 45. Dipolar spin-ice model: the phase diagram. The antiferromagnetic ground state is an all-spin-in or all-spin-out configuration for each tetrahedron. The spin-ice configuration, which includes the $\mathbf{k}_{ord}=001$ ground state, is a two-spin-in–two-spin-out configuration for each tetrahedron. The region encompassed between the quasivertical dotted lines displays hysteresis in the long-range ordered state selected ($\mathbf{k}_{ord}=000$ vs $\mathbf{k}_{ord}=001$) as J_{nn}/D_{nn} is varied at fixed temperature T. From Melko and Gingras, 2004.

(Barkema and Newman, 1998). Using such loop excitations, Monte Carlo simulations (Melko *et al.*, 2001; Melko and Gingras, 2004) found a transition to the long-range order predicted by mean field theory (Gingras and den Hertog, 2001), see Fig. 45. In Monte Carlo simulations of the DSM, a strongly first order transition occurs at a critical temperature $T_c \sim 0.07 D_{nn}$ where the residual Pauling entropy is recovered through the pretransitional buildup of correlations and mostly via a large latent heat (Melko *et al.*, 2001; Melko and Gingras, 2004). For $D_{nn} \sim 2.35$ K believed appropriate for $Dy_2Ti_2O_7$ (and $Ho_2Ti_2O_7$), this T_c value amounts to 160 mK. However, to date no experimental work has observed a transition to long-range order in spin-ice materials down to 60 mK [see, e.g., Fukazawa *et al.* (2002)]. A common explanation for this absence of a transition in real spin-ice materials is that equilibration is lost in the spin-ice state (e.g., $T \lesssim 0.4$ K in $Dy_2Ti_2O_7$ and $T \lesssim 0.6$ K in $Ho_2Ti_2O_7$), with the real materials not "benefitting" from nonlocal dynamics as employed in the simulations (Melko *et al.*, 2001; Melko and Gingras, 2004). However, this explanation is certainly somewhat incomplete since, as discussed below, a number of experiments report spin dynamics down to 20 mK. However, before discussing experiments investigating the dynamics of spin ices, we comment on the spin-spin correlations in the spin-ice regime of $Dy_2Ti_2O_7$.

Since the work of Ramirez *et al.* (1999), other measurements of the magnetic specific heat data of $Dy_2Ti_2O_7$ have been reported (Higashinaka *et al.*, 2002, 2003a; Hiroi, Matsuhira, Takagi, *et al.*, 2003; Ke *et al.*, 2007). Measurements of the magnetic specific heat of magnetic insulators are difficult experiments owing to the poor sample thermal conductivity. It is perhaps for this reason that specific heat data of $Dy_2Ti_2O_7$ from different measurements show some disparity. For example,

the height of the magnetic specific heat at its maximum C_p for a powder sample (Ramirez *et al.*, 1999) differs by as much as 10% compared to that reported in Higashinaka *et al.* (2003) for a single crystal. Ultimately, precise measurements of $C(T)$ are needed if one wants to make an accurate determination of the residual entropy in the system (Ke *et al.*, 2007).

The Monte Carlo prediction of long-range order developing at low temperature in the dipolar spin-ice model and the experimentally observed collapse of the magnetic specific heat below 0.4 in $Dy_2Ti_2O_7$ raise the question of low-temperature spin dynamics in spin-ice materials. In fact, experimental studies of this question have led to the observation of a much richer phenomenology than that which would have been naively expected.

Measurements of the ac magnetic susceptibility $\chi(\omega)$ of $Dy_2Ti_2O_7$ down to 60 mK (Fukazawa *et al.*, 2002) and 100 mK (Matsuhira *et al.*, 2001) found that the real part of χ, χ' drops precipitously below a temperature of roughly 1 K for a frequency of the order of 10 Hz (see Fig. 46). At the same time, the imaginary part χ'' shows a rounded maximum. Both χ' and χ'' remain essentially zero below 0.5 K down to the lowest temperature considered, hence signaling an essentially complete spin freezing of the system. Thus, no signature of the transition to long-range order predicted by numerical simulations (Melko *et al.*, 2001; Melko and Gingras, 2004) is observed.

The behavior of χ' and χ'' near 1 K signals a spin freezing process analogous to what is observed in spin glasses. Indeed, measurements of the magnetization of $Dy_2Ti_2O_7$ show irreversibilities between zero field cooling and field cooling below 0.7 K (Matsuhira *et al.*, 2001; Snyder, Ueland, Slusky, *et al.*, 2004). Similar FC-ZFC irreversibilities occur in the $Ho_2Sn_2O_7$ spin ice (Matsuhira *et al.*, 2000). An analysis of the temperature dependence of the frequency f_m at which χ'' displays a peak reveals a sort of thermally activated freezing behavior which was originally parametrized by an Arrhenius form with an activation energy of approximately 10 K. However, Snyder, Ueland, Slusky, *et al.* (2004) questioned the application of the Arrhenius law to these data. Monte Carlo simulations that employ a standard single spin-flip Metropolis algorithm found that the fraction of accepted spin flips decreases with decreasing temperature according to a Vogel-Fulcher form $\exp[-A/(T-T^*)]$, with $T^* \sim 0.3$ K (Melko and Gingras, 2004). The dynamical freezing behavior seen in $Dy_2Ti_2O_7$ differs from the critical slowing down observed in conventional disordered spin-glass materials (Binder and Young, 1986). Interestingly, for the lowest temperature considered, χ'' is cut off on the low-frequency regime (Snyder, Ueland, Slusky, *et al.*, 2004), reminding one of what is observed in the $LiHo_xY_{1-x}F_4$ Ising system—a phenomenon that has been referred to as "antiglass" behavior (Reich *et al.*, 1987; Ghosh *et al.*, 2002). Another difference between the spin freezing in $Dy_2Ti_2O_7$ and that in conventional disordered spin glasses is the magnetic field dependence

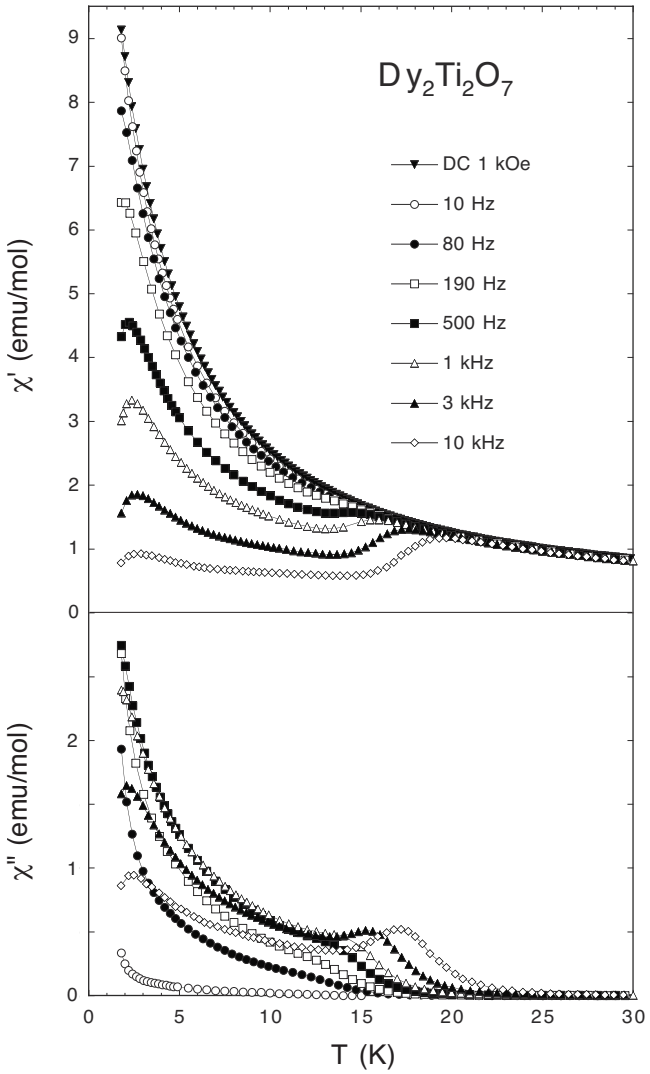

FIG. 46. $Dy_2Ti_2O_7$: ac susceptibility (upper panel: χ'; lower panel; χ'') as a function of temperature at several frequencies, illustrating the "15 K peak." From Matsuhira *et al.*, 2001.

of T_f. In spin glasses, T_f decreases with increasing magnetic field strength, while in $Dy_2Ti_2O_7$, the opposite is seen for applied magnetic fields up to 5 kOe (Snyder, Ueland, Slusky, *et al.*, 2004). Measurements on single crystals (Shi *et al.*, 2007) find that the spin freezing has a stronger frequency and magnetic field dependence for a field along the [111] axis compared to [100], and the starting freezing frequency of the single crystal is higher than that of the powder sample (Snyder *et al.*, 2001). While a quantitative understanding does not exists, the behavior at $T \lesssim 4$ K is qualitatively interpreted as a signature of the collective freezing as the system enters the low-temperature state where the two-in, two-out ice rules become fulfilled.

In addition to the low-temperature freezing in the ice-rule obeying state, two experimental studies coincidentally reported results from ac susceptibility $\chi(\omega)$ measurements in $Dy_2Ti_2O_7$ above 4 K (Matsuhira *et al.*, 2001; Snyder *et al.*, 2001), finding another freezing process in a temperature range around 15 K, referred to

below as the "15 K feature." The signature of this freezing is only seen in the ac susceptibility at finite frequency and not in the dc susceptibility data (see Fig. 46). The maximum in the imaginary part χ'' is at 12 K for a frequency of 10 Hz increasing to 17 K for a frequency of 10 kHz. While the raw data of Matsuhira *et al.* (2001) and Snyder *et al.* (2001) are similar, they were analyzed somewhat differently. Snyder *et al.* (2001) characterized the freezing via a single exponential relaxation, while Matsuhira *et al.* (2001) characterized the ac susceptibility using the so-called Davidson-Cole framework based on an underlying distribution of time scales. Notwithstanding these differences, both analyses agreed that there exists a typical time scale $\tau(T)$ for this freezing phenomenon that is parametrized by an Arrhenius form, $\tau \sim \exp(E_a/T)$ with an activation barrier energy E_a of the order of 200 K. A recent μSR study also finds that the relaxation rate of the muon spin polarization in a temperature range of 70–280 K can be described by a typical relaxation rate $\lambda(T) \sim \exp(-E_a/T)$, with $E_a \sim 220$ K (Lago *et al.*, 2007). The $\exp(E_a/T)$ dependence of the typical time scale characterizing the dynamics around 15 K and the energy scale $E_a \sim 220$ K indicates that the relaxation involves transitions to and from the first excited doublet which constitutes the main contribution to the spin dynamics in the temperature range above 20 K or so. While this freezing phenomenon and energy scales characterizing it suggest an Orbach process (Finn *et al.*, 1961; Orbach, 1961) that involves both the lattice degrees of freedom and the excited crystal-field states, a concrete microscopic calculation has not yet been done.

One interesting aspect of the 15 K feature is its behavior when Dy^{3+} is substituted by diamagnetic Y^{3+} in $Dy_{2-x}Y_xTi_2O_7$. In particular, initial studies found that the 15 K peak in $\chi''(\omega)$ disappears by $x=0.4$ (Snyder *et al.*, 2002). This was originally interpreted as a sign that the 15 K feature is of collective origin. However, in a subsequent study (Snyder, Ueland, Mizel, *et al.*, 2004) it was found to reemerge as x is further increased and is almost as strong for $x=1.98$, as it is for $x=0$, but interestingly repositioned at a higher temperature of 22 K for a frequency of 1 kHz. This high-temperature freezing feature is essentially a single-ion phenomenon akin to superparamagnetic spin blocking. While this is not seen in ac measurements on $Ho_2Ti_2O_7$, it can be revealed by the application of a magnetic field (Ehlers *et al.*, 2003). Neutron spin echo experiments on the same material confirm the single-ion nature of the 15 K feature (Ehlers *et al.*, 2003, 2004).

Another noteworthy aspect of the spin dynamics in $Dy_2Ti_2O_7$ is the temperature independence of the relaxation time τ between 5 and 10 K (Snyder *et al.*, 2003). Below 5 K, the relaxation time becomes again sharply dependent on temperature upon approaching the spin-ice freezing discussed above. This temperature independence of τ has been interpreted as a quantum tunneling effect between the up and down Ising spin states. This was first observed in $Ho_2Ti_2O_7$ using neutron spin echo (Ehlers *et al.*, 2003). Such temperature-independent relaxation in $Dy_2Ti_2O_7$ has also been seen in muon spin relaxation (μSR) (Lago *et al.*, 2007). However, there are three orders of magnitude difference between the relaxation rate measured in μSR and ac susceptibility. Perhaps this is because μSR relies on a local measurement that probes all wave vectors of the spin susceptibility. Currently this discrepancy is unresolved.

A further important topic pertaining to the dynamics of spin-ice materials is that of the low-temperature spin dynamics deep in the frozen spin-ice state. As discussed above, there is evidence that the electron spin-flip dynamics are exponentially frozen out below 1 K in $Dy_2Ti_2O_7$ as well as in other spin-ice materials. There is, however, some indication of residual spin dynamics in these systems that survives down to the lowest temperatures. For example, μSR experiments find a relaxation rate of 0.2 μs^{-1} of the muon spin polarization at a temperature of 20 mK (Lago *et al.*, 2007). This relaxation has been ascribed to hyperfine coupling of the electronic and nuclear spins which induce a "wobble" around the local $\langle 111 \rangle$ Ising directions. Other work has suggested that the absence of a low-temperature nuclear specific heat anomaly in $Dy_2Ti_2O_7$ may indicate that the electron spin dynamics persist to the lowest temperature (Bertin *et al.*, 2002). This argument would suggest that $Ho_2Ti_2O_7$, which has a fully developed nuclear specific heat (Bramwell *et al.*, 2001), is completely static. More experimental and theoretical work is required to fully understand the low-temperature dynamics of the spin ices.

Above we touched on what role magnetic dilution plays on the spin dynamics and freezing phenomenon in $Dy_2Ti_2O_7$. A recent magnetocaloric study of $Dy_2Ti_2O_7$ has found a crossover at a temperature of about 0.3 K to a low-temperature regime characterized by extremely slow relaxation (Orendác *et al.*, 2007). In addition, a dilution of Dy by 50% of nonmagnetic Y, giving $DyYTi_2O_7$, leads to an increase in the relaxation time compared to pure $Dy_2Ti_2O_7$. This is in contrast with the behavior seen above in the formation of the ice state, say above 2 K, where a nontrivial dependence of the relaxation time as a function of Dy concentration is observed. In particular, a level of magnetic dilution less than 12% was found to accelerate the relaxation rate, while a dilution level higher than 12% was found to slow it down again, such that the relaxation rates are nearly the same for $DyYTi_2O_7$ and $Dy_2Ti_2O_7$ (Snyder, Ueland, Mizel, *et al.*, 2004).

This discussion illustrates that the nature of the dynamics in spin ices and the role magnetic dilution is still poorly understood. In the context of magnetic dilution, we note that a recent paper reports a nonmonotonic dependence of the residual entropy in $Dy_{2-x}Y_xTi_2O_7$ and $Ho_{2-x}Y_xTi_2O_7$. The data are qualitatively explained by a generalization of Pauling's theory for the entropy of ice that incorporates site dilution (Ke *et al.*, 2007). The topic of residual entropy in spin ice when the magnetic species are diluted is an interesting problem. One would naively expect that the extensive degeneracy would ulti-

mately be lifted by disorder (Villain, 1979). There are two obvious ways that one can envisage this happening. Perhaps the most interesting is where dilution would lead to conventional long-range order. For example, in water ice KOH doping (which effectively removes protons) leads to a long-range ordered phase of ice called ice XI. The proton vacancies created in the proton structure enhance the dynamics so that the system can develop long-range order. Studies of diluted spin ice, such as $Dy_{2-x}Y_xTi_2O_7$ (Ke *et al.*, 2007) and $Ho_{2-x}Y_xTi_2O_7$ (Ehlers *et al.*, 2006), have so far not reported any signs that diamagnetic dilution leads to long-range order. Most likely, the extensive degeneracy is lifted at high x with the system leaving the ice regime to become a dipolar Ising spin glass akin to $LiHo_xY_{1-x}F_4$ (Reich *et al.*, 1987). Indeed, the systematic study of the development of dipolar-spin glass in both $Dy_{2-x}Y_xTi_2O_7$ and $Ho_{2-x}Y_xTi_2O_7$ might help shed light on the paradoxical antiglass phenomenon in $LiHo_xY_{1-x}F_4$ (Reich *et al.*, 1987; Ghosh *et al.*, 2002) or even the possible absence of a spin-glass phase altogether in that material (Jönsson *et al.*, 2007).

On the theoretical front, the DSM of Eq. (12) with nearest-neighbor exchange and long-range dipole-dipole interactions has been fairly successful in describing semiquantitatively the thermodynamic properties of $Dy_2Ti_2O_7$ both in zero (den Hertog and Gingras, 2000; Fennell *et al.*, 2004) and in nonzero (Fukazawa *et al.*, 2002; Ruff *et al.*, 2005; Tabata *et al.*, 2006) magnetic fields. A detailed comparison between experimental results from measurements and Monte Carlo simulations (Ruff *et al.*, 2005) for a field along the [112] direction provides strong evidence that exchange interactions beyond nearest neighbors are required to describe quantitatively the experimental data [see also Tabata *et al.* (2006)]. This may come as a surprise given the already good agreement that was first reported between Monte Carlo simulations of the DSM (den Hertog and Gingras, 2000) and the specific heat measurements of Ramirez *et al.* (1999). However, since that work, several other zero field specific heat data sets have been reported (Higashinaka *et al.*, 2002, 2003a; Hiroi, Matsuhira, Takagi, *et al.*, 2003; Ke *et al.*, 2007) and these are no longer so well described by the original DSM. A systematic study of more recent specific heat measurements in zero and nonzero fields and magnetization measurements for [110] and [111] fields have estimated first (J_1), second (J_2), and third (J_3) nearest-neighbor exchange parameters in $Dy_2Ti_2O_7$ (Yavors'kii *et al.*, 2008). Perhaps most interestingly, such a refinement of the spin Hamiltonian seemingly allows one to explain from a microscopic basis the diffuse scattering on the Brillouin zone boundary (Fennell *et al.*, 2004) akin to the highly structured inelastic features found in the $ZnCr_2O_4$ spinel (Lee *et al.*, 2002).

2. $A_2Sn_2O_7$ (A=Pr, Dy, and Ho)

Other pyrochlore oxides with similar properties include $Ho_2Sn_2O_7$, $Dy_2Sn_2O_7$, and $Pr_2Sn_2O_7$ (Matsuhira *et al.*, 2000, 2004; Matsuhira, Hinatsu, *et al.*, 2002). These have not been studied in single crystal form, as far as we know, but bulk magnetic properties would suggest they are ferromagnetic with large Ising anisotropy and very slow dynamics.

Of these three compounds, only $Ho_2Sn_2O_7$ has been investigated using neutron scattering techniques on powder samples (Kadowaki *et al.*, 2002). In the inelastic spectrum they found very slow dynamics below 40 K and crystal-field levels at 22 and 26 meV, suggesting the local Ho environment is very similar to that of $Ho_2Ti_2O_7$. Analysis of the diffuse magnetic scattering also led to the conclusion that $Ho_2Sn_2O_7$ is a dipolar spin-ice material.

3. $Ho_{2+x}Ti_{2-x}O_{7-\delta}$: Stuffed spin ice

Besides thermodynamic variables such as temperature and magnetic field, the chemical composition of the systems may be altered to study the relationship of structural and magnetic properties. To this end, "stuffed" spin ices with general formula $A_{2+x}B_{2-x}O_{7-\delta}$ have recently been synthesized (Lau, Freitas, *et al.*, 2006; Ueland *et al.*, 2008), in which additional magnetic ions replace the nonmagnetic Ti^{4+} ions ($\delta>0$ as the oxygen content needs to be adjusted for charge balance). The entire rare-earth series of titanates have been formed (Lau, Muegge, *et al.*, 2006), but to date the only published data are on the stuffed spin-ice (SSI) compounds. Lau *et al.* (2007) reported phase separation in these compounds, however, the magnetic properties are very similar between samples. Single crystals have been produced by Zhou *et al.* (2007).

The additional magnetic exchange pathways represent a major disturbance of the system, introducing positional disorder and, naively, an increased level of energetic constraints to the formation of the spin-ice manifold. Surprisingly, it has been found that the stuffed spin-ice systems do not freeze, have short-range correlations down to the lowest temperatures, and have the same entropy per spin at low temperature as the "unstuffed" spin ice (Lau, Freitas, *et al.*, 2006; Zhou *et al.*, 2007). The origins of this residual entropy per spin in these systems are still debatable.

Another interesting feature of the residual entropy in the stuffed spin-ice materials is its robustness to an applied field. As shown in Fig. 47 the entropy per spin with $x=0.67$ in 1 T and zero field are identical. This robust residual entropy in a very disordered sample such as $Ho_{2.67}Ti_{1.33}O_{6.67}$ ($x=0.67$) needs further investigation.

Inelastic and quasielastic neutron scattering on polycrystalline and single crystalline $Ho_{2.3}Ti_{1.7}O_{7-\delta}$ have revealed subtle changes vis-à-vis the parent compound. Diffuse scattering is centered at 0.9 $Å^{-1}$, but it is broader than the diffuse scattering seen in $Ho_2Ti_2O_7$. Also, as shown in Fig. 48, the quasielastic scattering at temperatures above 10 K opens a gap resulting in a low lying excitation centered at 0.8 meV (Zhou *et al.*, 2007).

More research is currently being done by several groups on stuffed spin ice. It appears that the stuffed Dy

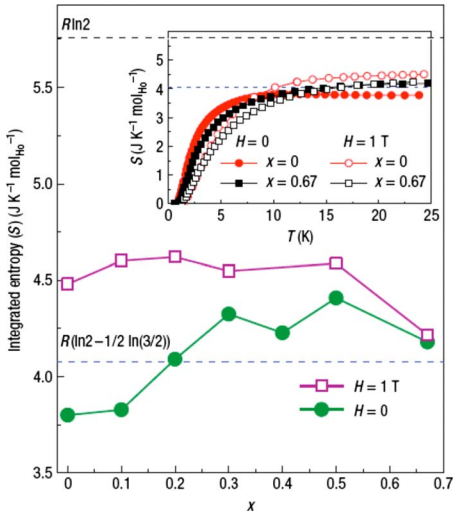

FIG. 47. (Color online) The magnetic entropy for $Ho_{2+x}Ti_{2-x}O_{7-\delta}$ (integrated from below $T \approx 1-22$ K) as a function of stuffing at $H=0$ and 1 T. The dashed lines represent the predicted ice entropy and total spin entropy values. Inset: The temperature dependence of the integrated entropy for few compositions at $H=0$ and 1 T. From Lau, Freitas, *et al.*, 2006.

spin ices do not have a residual entropy (Ueland *et al.*, 2008).

D. Spin-liquid phases

Having discussed so far the ordered, glassy, and icy phases that pyrochlore oxides exhibit, we now move to the least ordered and most dynamic spin liquid phases. Given that theory for both Heisenberg spins in either the classical (Moessner and Chalker, 1998a, 1998b; Moessner, 2001) or quantum (Canals and Lacroix, 1998, 2000) limit and Ising spins (Anderson, 1956) on a pyrochlore lattice with AF nearest neighbor exchange predicts a disordered, highly degenerate ground state at finite temperatures, one would expect the spin liquid state to be rather common. In fact only a few candidate pyrochlore materials have been identified, namely, $Tb_2Ti_2O_7$, $Yb_2Ti_2O_7$, $Er_2Sn_2O_2$, and $Pr_2Ir_2O_7$. In the following, each case is examined in some detail.

1. $Tb_2Ti_2O_7$

$Tb_2Ti_2O_7$ is a well-studied system where Tb^{3+} ions are magnetic and Ti^{4+} ions are nonmagnetic. The tem-

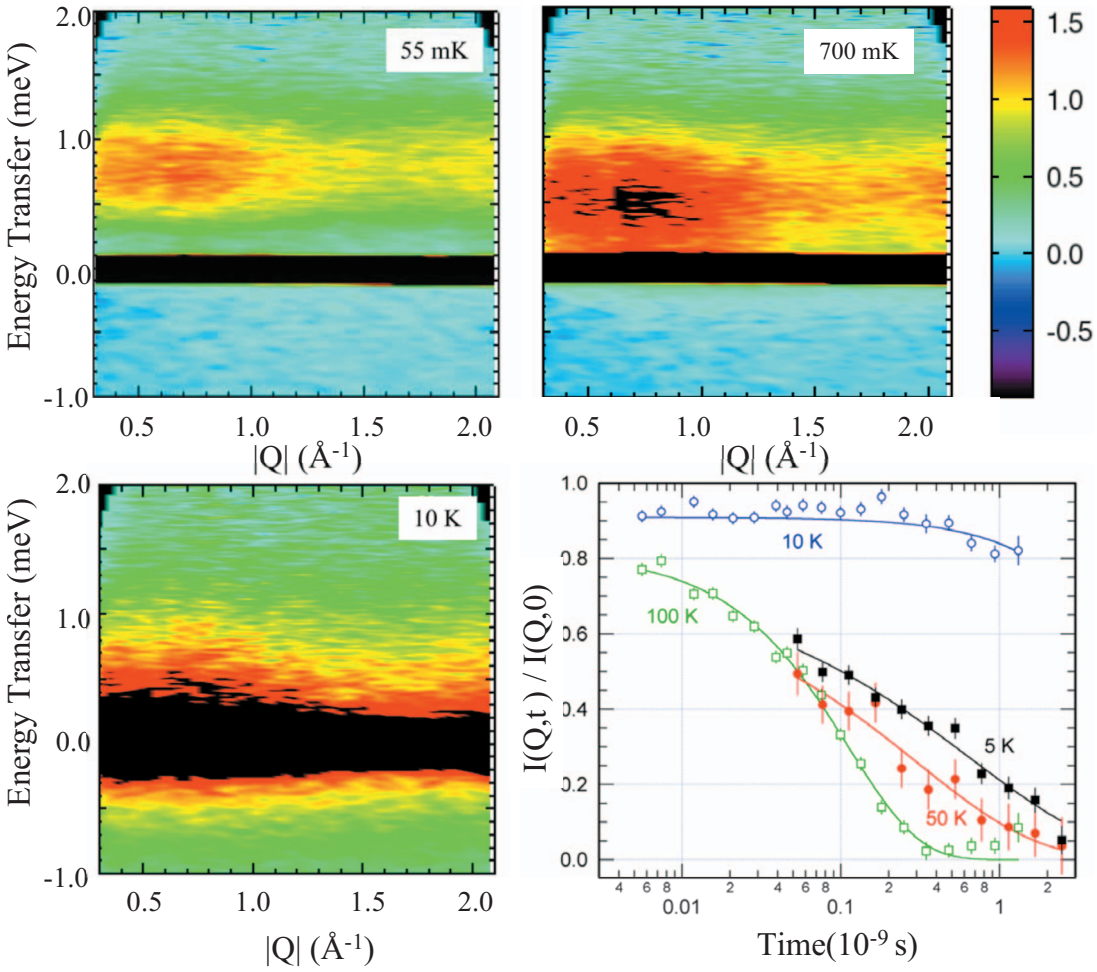

FIG. 48. (Color) Inelastic neutron scattering from $Ho_{2.3}Ti_{1.7}O_{7-\delta}$ (Zhou *et al.*, 2007). Data at 55 mK, 700 mK, and 10 K, noting the appearance of a gapped spin excitation at low temperatures. Neutron spin echo results on stuffed (open symbols) and unstuffed (closed symbols) spin ice are depicted in the bottom right panel. Within the neutron time window, the spin ice appears static by 10 K (90% of the spin are static), but the stuffed spin ice has persistent dynamics.

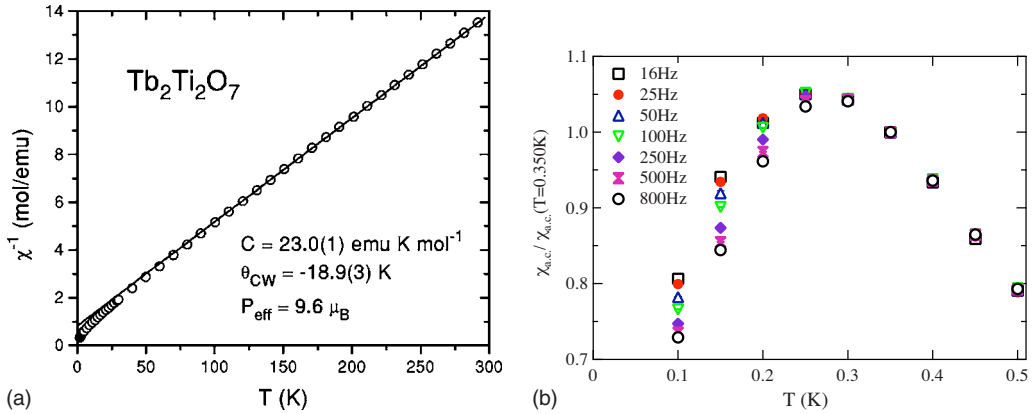

FIG. 49. (Color online) dc and ac susceptibility for $Tb_2Ti_2O_7$. Left: The temperature dependence on the inverse molar susceptibility and the resulting fit to the Curie-Weiss law at high temperature ($T>250$ K). From Gingras *et al.*, 2000. Right: The low-temperature ($T<0.5$K) dependence of the magnetic susceptibility as a function of frequency. From Gardner *et al.*, 2003.

perature dependence of the magnetic susceptibility of $Tb_2Ti_2O_7$ is described well by the Curie-Weiss law down to 50 K with $\theta_{CW}=-19$ K and $9.6\mu_B$/Tb ion. This effective moment is appropriate for the $^7F_6$ Tb^{3+} ion. By studying a magnetically dilute sample, $(Tb_{0.02}Y_{0.98})_2Ti_2O_7$, a value of −6 K was established as the crystal-field contribution to θ_{CW}. Assuming a maximum of −2 K for the dipolar interactions, ≈ -11 K was proposed as a good estimate for the contribution of the exchange interactions to θ_{CW}. Figure 49 (left) shows the temperature dependence of the bulk susceptibility down to 0.5 K.

Han *et al.* (2004) found, using neutron powder diffraction and x-ray absorption fine structure, that the chemical structure of $Tb_2Ti_2O_7$ is well ordered with no structural transitions between 4.5 and 600 K. More recently, however, Ruff *et al.* (2007) found a broadening of structural peaks in a high-resolution, single crystal, x-ray diffraction experiment below 20 K, as expected just above a cubic-to-tetragonal transition; however, this transition never fully develops even at 300 mK.

Powder neutron diffraction measurements on $Tb_2Ti_2O_7$ clearly revealed two contributions to the scattering at 2.5 K (Gardner, Dunsiger, *et al.*, 1999). One of these consists of sharp nuclear Bragg peaks due to the crystalline order in the material and results in a cubic lattice parameter of 10.133 Å. A second diffuse, liquid-like, background is also present and was attributed to magnetic short-range correlations. Gardner, Dunsiger, *et al.* (1999) used an *isotropic* spin model, correlated over nearest spins only, to describe this scattering which captured the minimum in the forward direction, $|\mathbf{Q}| \sim 0$ Å^{-1}, as well as the approximate location of the peaks and valleys in the data.

Inelastic scattering experiments were also carried out on polycrystalline $Tb_2Ti_2O_7$ (Gardner, Gaulin, *et al.*, 2001) and a typical scan at $|\mathbf{Q}|=2$ Å^{-1} is shown in Fig. 50. Three bands of excitations are clearly observed near 0.37, 2.53, and 3.50 THz and these were shown to be dispersionless above 30 K, a characteristic of a single-ion effect associated with the rare-earth site. A weak but interesting dispersion develops in the lowest energy band at temperatures below ~20 K, which we discuss later.

A crystalline electric field (CEF) level scheme appropriate to the $^7F_6$ configuration of Tb^{3+} in the A-site environment of $Tb_2Ti_2O_7$ was determined on the basis of these neutron and other bulk property data (Gingras *et al.*, 2000). The ground state and first excited states are both doublets, with two singlets at much higher energies, as shown schematically in Fig. 50. The J^z eigenstates $|\pm 4\rangle$ and $|\pm 5\rangle$ are believed to make up most of the weight of the ground state doublet and of the first excited state, respectively. Such a CEF scheme means the moment can be considered extremely Ising in nature and pointing in the local $\langle 111\rangle$ directions at temperatures $T \lesssim 20$ K. More recently Mirebeau *et al.* (2007) reported a series of neutron scattering measurements that "refined" the CEF scheme of $Tb_2Ti_2O_7$ and compared it to $Tb_2Sn_2O_7$, which orders just below 1 K and which was discussed in Sec. III.A.3.

Large single crystals of $Tb_2Ti_2O_7$ were first grown using floating zone image furnace techniques by Gardner *et al.* (1998). The resulting single crystals enabled a series of experiments which could probe the four-dimensional dynamic structure factor $S(\mathbf{Q},\hbar\omega)$. Figure 51 shows

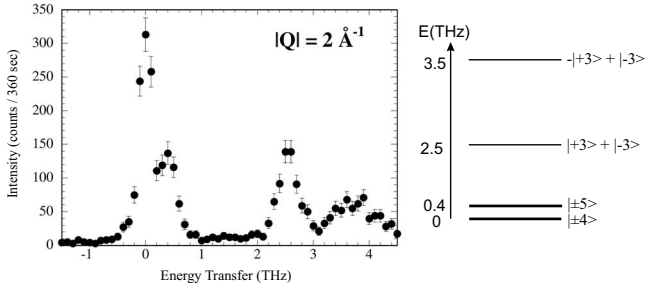

FIG. 50. Crystal field levels in $Tb_2Ti_2O_7$ derived from inelastic neutron scattering data. Left: A typical constant $|\mathbf{Q}|$ scan at 2 Å^{-1} revealing low-energy inelastic modes at 12 K on a powder sample of $Tb_2Ti_2O_7$. Right: Schematic of the crystalline electric field levels. From Gingras *et al.*, 2000.

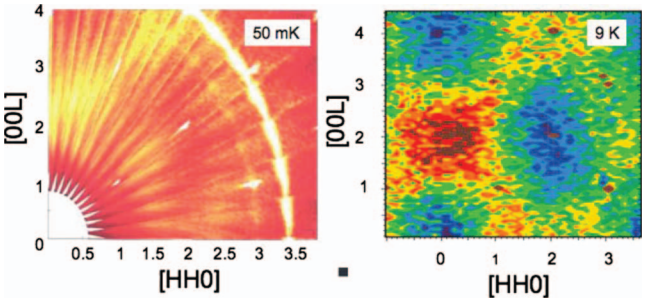

FIG. 51. (Color) Diffuse scattering from a single crystal of $Tb_2Ti_2O_7$ at 50 mK (left) and 9 K (right) (Gardner, Gaulin, *et al.*, 2001; Gardner *et al.*, 2003). Sharp Bragg peaks can be seen at the appropriate reciprocal lattice positions in the 50 mK data set, but at 9 K these have been subtracted out using a high-temperature (100 K) data set.

$S(\mathbf{Q})=\int S(\mathbf{Q},\hbar\omega)d\omega$ measured at $T=50$ mK and at 9 K within the (hhl) plane. Bragg peaks are clearly seen at the allowed positions for the $Fd\bar{3}m$ space group, that is, (hhl) being all even or all odd integers. One clearly observes a "checkerboard" pattern to the magnetic diffuse scattering. This covers the entire Brillouin zone indicating the spins are correlated on a length scale much smaller than the unit cell ~10.1 Å. However, the single-crystal data are clearly not isotropic in reciprocal space, explaining the quantitative failure of the simple isotropic model used to analyze the earlier powder data (Gardner, Gaulin, *et al.*, 2001). Also the scattering does not conform to that expected for an Ising model with local ⟨111⟩ spin directions. Specifically, an Ising model with local ⟨111⟩ spins cannot simultaneously produce a large amount of scattering around 002 and null scattering at 000 (Enjalran and Gingras, 2004).

Single crystals also allow the study of the low-lying excitations as a function of $\mathbf{Q}$ (Gardner, Gaulin, *et al.*, 2001; Gardner *et al.*, 2003) as opposed to the modulus $|\mathbf{Q}|$ derived from powder samples. As was observed in powders (Gardner, Dunsiger, *et al.*, 1999), the dispersion develops below ~25 K. This low-temperature dispersion is plotted along the three high-symmetry directions within the (hhl) plane in Fig. 52, on which there are overlaid cuts of $S(\mathbf{Q})$ along [001] (top), [hh0] (middle), and [hhh] (bottom). The diffuse scattering is well described by simple near-neighbor antiferromagnetic spin correlations on the pyrochlore lattice, as shown by the solid lines in Fig. 52. We also see that the minima in the dispersion of this low-lying magnetic mode (closed symbols) correspond exactly with peaks in $S(\mathbf{Q})$ even though $S(\mathbf{Q})$ is anisotropic in $\mathbf{Q}$. Gardner *et al.* (2003) showed the gap between the first excited state and the ground state drops from 0.37 THz at 30 K to ~0.25 THz at 100 mK but does not soften further as the temperature is further decreased.

Neutron spin echo (Gardner *et al.*, 2003; Gardner, Ehlers, Bramwell, and Gaulin, 2004) and μSR (Gardner, Dunsiger, *et al.*, 1999; Keren *et al.*, 2004) measurements have also been carried out at mK temperatures to

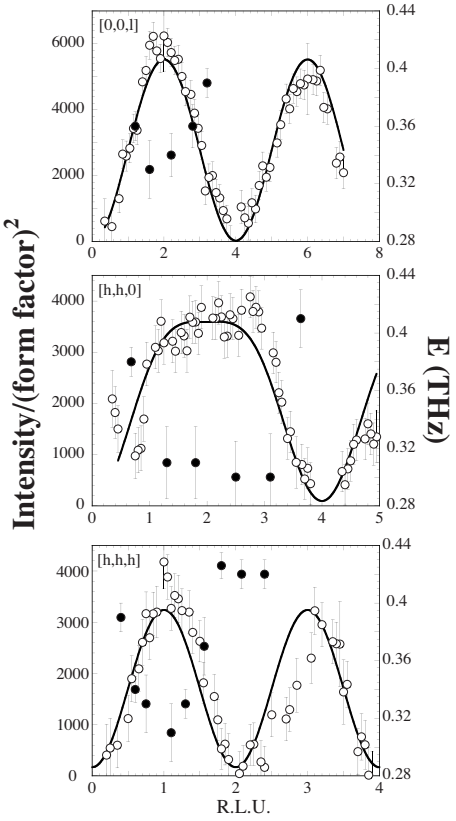

FIG. 52. Cuts through the checkerboard board pattern of diffuse magnetic scattering (open symbols) along high-symmetry directions of the cubic lattice. To complement these data, the dispersion of the lowest-lying magnetic excitation, at 4 K, is also plotted (closed symbols). Fits to the diffuse scattering are shown and discussed in the text. From Gardner, Gaulin, *et al.*, 2001.

probe the dynamics of the magnetic moments. Both show large fluctuating moments down to at least 70 mK (Gardner, Dunsiger, *et al.*, 1999), as expected for a cooperative paramagnet. However, below $T\approx 0.3$ K the $S(\mathbf{Q},t)/S(\mathbf{Q},0)$ baseline is no longer zero indicating a proportion ($\approx 20\%$) of the magnetic moments is frozen in the neutron spin echo time window. This is consistent with the frequency dependence of the ac susceptibility shown in Fig. 49 (right) (Luo *et al.*, 2001; Gardner *et al.*, 2003). This partial spin freezing has been attributed to a small subset of magnetic moments distributed near a small number of defects (Gardner *et al.*, 2003). Evidence for spin freezing was also found independently in neutron scattering experiments performed on other single-crystal samples (Yasui *et al.*, 2002). In this case, hysteresis is observed in the scattering near 002 at temperatures $\lesssim$1.7 K, but again most of the scattering remains diffuse in nature even below 1.7 K.

Dilution studies by Keren *et al.* (2004) perturbed the lattice through the percolation threshold but found that fluctuating moments prevail at all magnetic concentration as shown by the muon relaxation rate in Fig. 53. They also noted that the magnetic coverage of the lattice was important to the cooperative phenomenon but the

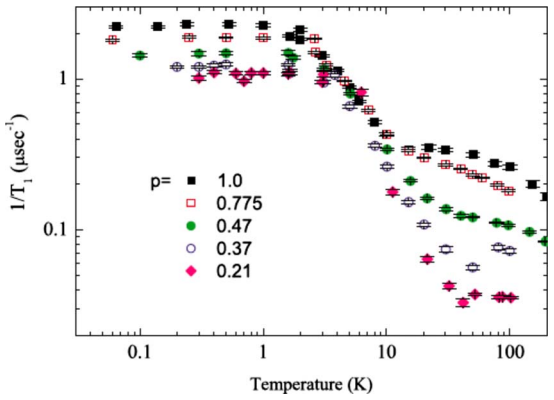

FIG. 53. (Color online) Temperature dependence of the muon relaxation rate in a field of $(Tb_pY_{1-p})_2Ti_2O_7$. From Keren *et al.*, 2004.

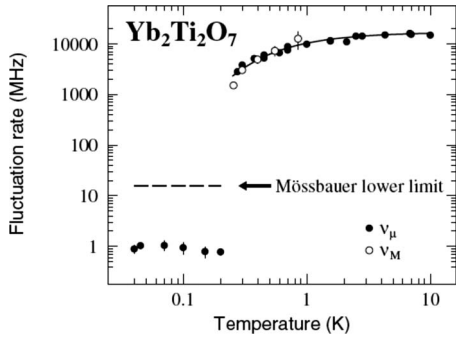

FIG. 54. Estimate fluctuation rate of the Yb^{3+} moment derived from muon (filled circles) and Mössbauer (open circles) spectroscopies. Note the constant nonzero rate below 200 mK. From Hodges *et al.*, 2002.

percolation threshold played no critical role.

At first sight, it would be tempting to ascribe the failure of $Tb_2Ti_2O_7$ to develop long-range order down to such a low temperature compared to θ_{CW} to the collective paramagnetic behavior of the classical pyrochlore Heisenberg antiferromagnet (Villain, 1979; Moessner and Chalker, 1998). However, consideration of the single-ion crystal-field ground state doublet of Tb^{3+} in $Tb_2Ti_2O_7$ strongly suggests that, in absence of exchange and dipolar interactions, bare Tb^{3+} should be considered as an effective Ising spin (Gingras *et al.*, 2000; Rosenkranz *et al.*, 2000).

Considering only nearest-neighbor exchange and long-range dipolar interactions, the DSM of Eq. (12) would be the appropriate Hamiltonian to describe $Tb_2Ti_2O_7$ as an Ising system. On the basis of the estimated value of the nearest-neighbor exchange and dipolar coupling, $Tb_2Ti_2O_7$ would be predicted to develop a $\mathbf{k}_{ord}=000$ four-sublattice long-range Néel order at a critical temperature $T_c \approx 1$ K (den Hertog and Gingras, 2000) in dramatic contradition with experimental results. Furthermore, the paramagnetic neutron scattering of such a classical Ising model is inconsistent with that observed in $Tb_2Ti_2O_7$ at 9 K shown in Fig. 51. Indeed, mean field theory calculations on a Heisenberg model with dipolar and exchange interactions and with a simple single-ion anistropy (Enjalran and Gingras, 2004) as well as a random phase approximation (RPA) calculation (Kao *et al.*, 2003) that considers a semirealistic description of the crystal-field levels of Tb^{3+} show that the strong scattering intensity around 002 should be extremely weak for Ising spins. Rather, the intensity is caused by the finite amount of fluctuations perpendicular to the local ⟨111⟩ directions (Enjalran and Gingras, 2004). In the RPA calculations (Kao *et al.*, 2003), the scattering intensity near 002 originates from the contribution of the excited crystal-field levels at an energy ~18 K to the susceptibility, which is made dispersive via the exchange and dipolar interactions. The experimental observation that the diffuse scattering intensity is largely unaltered down to a temperature of 50 mK, as shown in Fig. 51, suggests that the "restored" effective isotropicity of the spins is an intrinsic part of the effective low-energy theory that describes $Tb_2Ti_2O_7$. In that context, Molavian *et al.* (2007) argued, on the basis of a calculation that considers noninteracting tetrahedra, that virtual fluctuations between the ground state and excited crystal-field levels lead to renormalization of the coupling constants entering the effective low-energy theory. In particular, Molavian *et al.* (2007) proposed that, for the simple model considered, the system is pushed to the spin-ice side of the phase diagram by those virtual crystal field fluctuations. In other words, within that description $Tb_2Ti_2O_7$ is a sort of quantum spin-ice system where the spin-ice-like correlations remain hidden down to $T \lesssim 500$ mK.

In this discussion of the lack of order in $Tb_2Ti_2O_7$, it is not clear what is the role of the structural or lattice fluctuations reported by Ruff *et al.* (2007). Currently there is really no robust theoretical understanding of the physics at play in $Tb_2Ti_2O_7$ and more theoretical and experimental studies are required.

2. $Yb_2Ti_2O_7$

Ytterbium titanate is an insulator with lattice parameter $a_0=10.026(1)$ Å at room temperature (Brixner, 1964). Early work suggested an ordered magnetic state just below 0.2 K (Blöte *et al.*, 1969), where a sharp anomaly in the specific heat was observed. In a detailed magnetization study, Bramwell *et al.* (2000) found a Curie-Weiss temperature of 0.59(1) K, indicative of weak ferromagnetic coupling and a free ion moment of $3.34(1)\mu_B$. Hodges *et al.* (2001) used Mössbauer spectroscopy to investigate the crystal-field scheme and determined that the ground state Kramers doublet was separated by 620 K from the first excited state producing an easy-plane anisotropy, like in $Er_2Ti_2O_7$. They also found the effective paramagnetic moment to be $3.05(8)\mu_B$.

Hodges *et al.* (2002) extended their study of $Yb_2Ti_2O_7$ and found an abrupt change in the fluctuation rate of the Yb^{3+} spin at 0.24 K (see Fig. 54), but not a frozen ground state as expected from the earlier studies (Blöte *et al.*, 1969). Using muon spin relaxation and Mössbauer spectroscopies, they concluded that the Yb^{3+} spin fluctua-

tions slow down by more than three orders of magnitude to several megahertz, without freezing completely (see Fig. 54). This was confirmed in their neutron powder diffraction, where no extra Bragg intensity was reported below 0.24 K. Single-crystal neutron diffraction by Yasui, Soda, *et al.* (2003) has revealed extra Bragg scattering below 0.24 K from a static ferromagnetic state, albeit with a reduced moment of $1.1\mu_B$. The latter study motivated a polarized neutron scattering study by Gardner, Ehlers, Rosov, *et al.* (2004). That work conclusively ruled out a frozen ferromagnetic state and confirmed that the majority of the spin system continues to fluctuate below the 240 mK transition while a small amount of magnetic scattering was observed at the 111 Bragg position at 90 mK. To this day, essentially nothing is understood about the transition at 0.24 K and the type of order(s) that may exist below that temperature in $Yb_2Ti_2O_7$.

3. $Er_2Sn_2O_7$

$Er_2Sn_2O_7$ and $Er_2Ti_2O_7$ are thought to constitute experimental realizations of the highly frustrated XY antiferromagnet on the pyrochlore lattice. Little is known about $Er_2Sn_2O_7$ compared to the isostructural $Er_2Ti_2O_7$ compound which develops a noncollinear Néel state at 1.1 K possibly via an order-by-disorder transition [see Sec. III.A.2, Champion *et al.* (2003)]. Bondah-Jagalu and Bramwell (2001) reported a pronounced field cooled–zero field cooled divergence in the susceptibility of $Er_2Sn_2O_7$ at 3.4 K. The temperature and field dependence of the bulk magnetization of $Er_2Sn_2O_7$ was published by Matsuhira, Hinatsu, *et al.* (2002). At high temperatures $1/\chi(T)$ is linear and a fit to the Curie-Weiss law results in a ground state moment of $9.59\mu_B$ appropriate for the $^4I_{15/2}$ ion (see Fig. 55, top). It also gives a Curie-Weiss temperature $\theta_{CW}\approx -14$ K suggestive of antiferromagnetic correlations. At 10 K, $1/\chi(T)$ starts bending downward presumably due to crystal-field effects. However, no anomaly indicative of a freezing into either a long- or short-range ordered system was seen down to 0.13 K, suggesting that geometrical frustration plays a large role in determining the magnetic ground state. μSR studies by Lago *et al.* (2005) revealed persistent spin dynamics at 20 mK in both Er based samples (see Fig. 55, bottom). While the temperature dependence of the muon relaxation rate is similar, the depolarization curve for $Er_2Sn_2O_7$ remains exponential down to the lowest temperatures suggesting the system fails to enter an ordered state, while the titanate takes on a Gaussian relaxation at early times.

Neutron diffraction results by Bramwell *et al.* (2004) and Shirai and Bramwell (2007a, 2007b) suggested that $Er_2Sn_2O_7$ enters a state with long-range order at $\approx$0.1 K. This ordered ground state is different than that of $Er_2Ti_2O_7$, which appears to be stable in the $Er_2(Sn,Ti)_2O_7$ solid solution until 90% substitution of Ti for Sn.

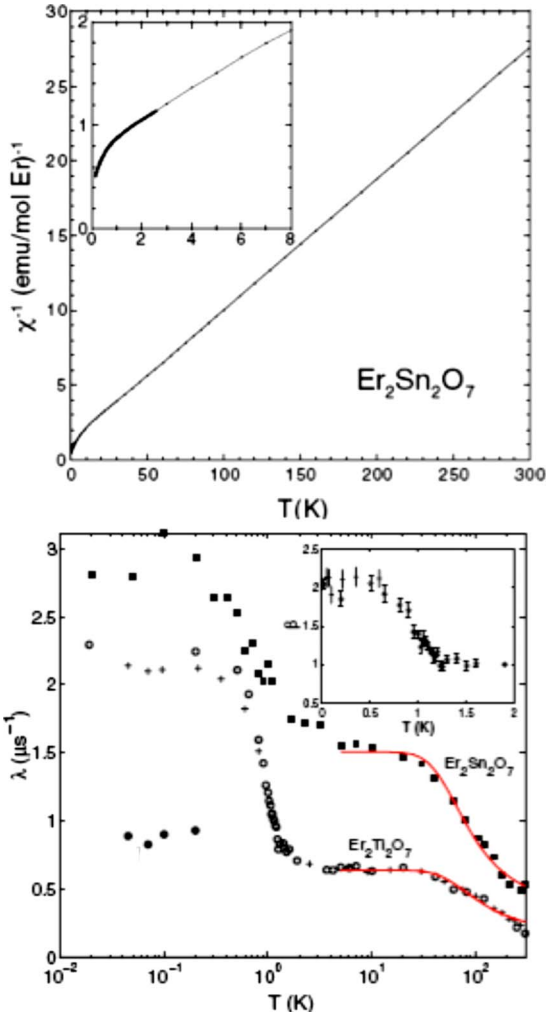

FIG. 55. (Color online) Magnetic susceptibility and μSR relaxation times for $Er_2Sn_2O_7$. Top: The temperature dependence of the inverse magnetic susceptibility from a powder sample of $Er_2Sn_2O_7$. The inset shows the temperature dependence of the stretch exponential exponent β for $Er_2Ti_2O_7$ showing the evolution from exponential ($\beta\sim1$) to Gaussian ($\beta\sim2$) curve shape across T_N. For $Er_2Sn_2O_7$, the relaxation is exponential ($\beta\sim1$) for the entire temperature range. From Lago *et al.*, 2005.

4. $Pr_2Ir_2O_7$

Recently, much attention has been devoted to the metallic material $Pr_2Ir_2O_7$ which is reported to remain paramagnetic down to 0.3 K by Machida *et al.* (2005). From magnetization, specific heat, and inelastic neutron scattering studies the Pr ground state was determined to be a well isolated doublet with Ising-like moments oriented along the local $\langle 111\rangle$ axes. The antiferromagnetically coupled spins have an energy scale of $\approx$20 K and no freezing was observed. Subsequent studies carried out on crystals grown from a KF flux showed remarkably complex behavior, including a Kondo-like effect and partial spin freezing below 120 mK (see Fig. 56) (Nakatsuji *et al.*, 2006; Millican *et al.*, 2007). It was concluded that a spin-liquid state exists for the Pr moments but no studies of spin dynamics have yet been presented to support this claim.

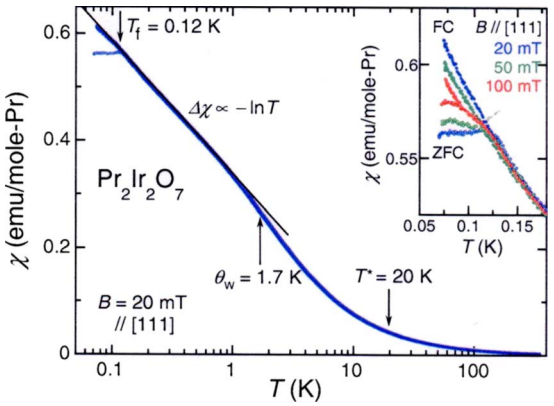

FIG. 56. (Color online) dc susceptibility at a field of 20 mT applied along [111] for $Pr_2Ir_2O_7$. Note the ln(T) dependence expected for the Kondo effect and (inset) evidence for spin freezing. From Nakatsuji *et al.*, 2006.

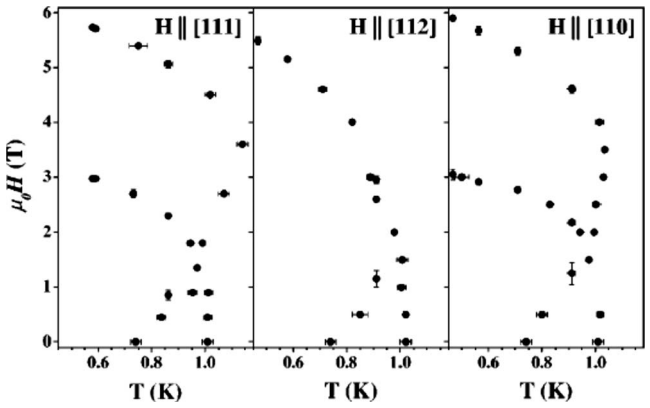

FIG. 57. Magnetic phase diagrams of the $Gd_2Ti_2O_7$ for three different orientations of an applied magnetic field. These phase boundaries roughly approximate those seen by Ramirez *et al.* (2002) on a powder sample. From Petrenko *et al.*, 2004.

Finally, a report of an unconventional anomalous Hall effect by Machida *et al.* (2007) has recently appeared and a chirality mechanism, similar to that proposed for $Nd_2Mo_2O_7$ (Taguchi *et al.*, 2001, 2004), has been invoked.

E. External perturbations

Many studies have been performed on geometrically frustrated magnets where an external pertubation (apart from nonzero temperature) has been applied to the system. These perturbations can take the form of common variables such as magnetic field and the chemical composition of the systems. Less common perturbations include applied pressure and irradiation damage and the effects of these too have been investigated on pyrochlore oxides. To date, no magnetic studies of irradiation damaged pyrochlores have been published, though several have studied the structural properties of pyrochlores after being bombarded with radiation (Sickafus *et al.*, 2000; Ewing *et al.*, 2004). Where appropriate, the results from changes in temperature or chemical composition have been mentioned and we restrict ourselves here to those studies where profound changes to the magnetic nature of the behavior or state of the pertinent magnetic pyrochlore oxide have been observed.

1. Magnetic field

Most magnetic pyrochlore oxides have been subject to an applied field and their behavior monitored. In some cases, drastic effects have been observed. Indeed, one must remember that these systems are delicately balanced between several competing energy scales and a magnetic field, even small fields, can alter the system significantly. For example, in the spin ices, $Ho_2Ti_2O_7$ and $Dy_2Ti_2O_7$, in a field as small as 100 Oe applied along [001] or [110], many ground states are favored creating metastable states, magnetization plateaus, and slow spin dynamics (Fennell *et al.*, 2005). In a few cases, the application of a field can drive the system into a new ground state. These facts must be remembered when probing frustrated systems possibly even in the remanent field of a magnet.

a. $Gd_2Ti_2O_7$

The magnetic field versus temperature phase diagram for the Heisenberg pyrochlore magnet $Gd_2Ti_2O_7$ was first determined on polycrystalline samples using specific heat and ac susceptibility (Ramirez *et al.*, 2002), and a mean field model was used to justify the five phases found below 1 K and in fields up to 8 T. Petrenko *et al.* (2004) later reproduced these field induced transitions by measuring the specific heat along three different crystallographic directions on a single crystal (see Fig. 57).

To determine the magnetic structure in these phases, neutron powder diffraction measurements have been performed. Although significant differences can be seen in the diffraction patterns in every phase, only the zero field structures have been modeled successfully (Stewart, Ehlers, Wills, *et al.*, 2004; Shirai and Bramwell, 2007).

With the recent knowledge that $Gd_2Sn_2O_7$ is a better representation of a Heisenberg pyrochlore magnet with dipolar interactions and near neighbor exchange (Wills *et al.*, 2006; Del Maestro and Gingras, 2007) (see Sec. III.A.1), one would want to study it in single-crystalline form and in a magnetic field.

b. Spin ice

By applying a magnetic field along the [111] direction of single crystals of $Dy_2Ti_2O_7$ or $Ho_2Ti_2O_7$ one can induce a new microscopically degenerate phase, known as kagome ice. In this state the two-in, two-out spin configuration, known as the ice-rules state, is still found; however, one spin is pinned by the field and the number of possible ground states is lowered (Moessner and Sondhi, 2003). As shown in Fig. 4, the pyrochlore structure as observed along the [111] is comprised of stacked alternating kagome and triangular planes. When the applied field exceeds 0.3 kOe the kagome ice phase is

stable and exhibits a residual entropy of ≈40% of that seen in zero field spin ice.

Matsuhira, Hiroi, *et al.* (2002) performed magnetization and specific heat experiments on $Dy_2Ti_2O_7$, proving the existence of this phase. Since then, several pieces of work have been done, mainly on $Dy_2Ti_2O_7$, with probes like ac susceptibility and specific heat (Higashinaka *et al.*, 2004; Sakakibara *et al.*, 2004; Tabata *et al.*, 2006). Fennell *et al.* (2007) performed neutron diffraction measurements on $Ho_2Ti_2O_7$ in the kagome ice phase and speculated that a Kasteleyn transition takes place. Wills *et al.* (2002) investigated via analytical and Monte Carlo calculations an icelike state in a kagome lattice with local Ising anisotropy before one was experimentally realized. While the physics of kagome ice emerging from a spin-ice single crystal subject to a [111] field is interesting, the behavior of spin ice subject to a magnetic field along one of the [110], [112], and [100] directions is also worthy of a comment.

The pyrochlore lattice can be viewed as two sets of orthogonal chains of spins. One set is parallel to the [110] direction and the other along $[1\bar{1}0]$. These two sets are referred to as α and β chains, respectively. The application of a field parallel to [110] and of strength slightly larger than 1 T leads to a pinning of the spins on the α chain, effectively freezing those spins. Both the net exchange and net dipolar field produced by the frozen spins on the α chains vanish by symmetry for the spins on the β chains. Since the β chains are perpendicular to the field along [110], the spins along those β chains are free to interact only among themselves. Just as a [111] field leads to a decomposition of the pyrochlore lattice into weakly coupled kagome planes with their normal along [111], a field along [110] induces a "magnetic break up" of an otherwise cubic pyrochlore system into a set of quasi-one-dimensional β chains predominantly weakly coupled by dipolar interactions. On the basis of Monte Carlo simulations (Yoshida *et al.*, 2004; Ruff *et al.*, 2005) and chain mean field theory (Ruff *et al.*, 2005), one expects that dipolar spin ice would have a transition to a long-range ordered state, referred to as $\mathbf{q}=X$ order (Harris *et al.*, 1997). However, while neutron scattering experiments on $Ho_2Ti_2O_7$ and $Dy_2Ti_2O_7$ (Fennell *et al.*, 2005) and specific heat measurements (Hiroi, Matsuhira, and Ogata, 2003) on $Dy_2Ti_2O_7$ find some evidence for a transition with a field along [110], the transition is not sharp. It is not known whether the apparent failure of the system to develop full long-range $\mathbf{k}=X$ order is due to either an imperfect alignment of the field along [110] or the inability of the system to properly equilibrate upon approaching the putative transition.

The [100] field problem was probably the first one studied theoretically (Harris, Bramwell, Holdsworth, and Champion, 1998). It was predicted on the basis of Monte Carlo simulations on the nearest-neighbor spin-ice model that the system should exhibit a field-driven transition between a gaslike weakly magnetized ice-rule obeying state and a strongly polarized state. It was originally argued that this transition is first order and terminates at a critical point similarly to the gas-liquid critical point (Harris, Bramwell, Holdsworth, and Champion, 1998). However, recent work that combines numerical and analytical calculations argued for a more exotic topological Kastelyn transition driven by the proliferation of defects in the ice state as the temperature or the field strength is varied (Jaubert *et al.*, 2008). The same work speculates that there exists preliminary evidence for such a rounded Kastelyn transition in the neutron scattering data on $Ho_2Ti_2O_7$ subject to a [100] field (Fennell *et al.*, 2005). While the Monte Carlo data of Harris *et al.* (1998) find a sharp and a broad feature in the specific heat as a function of temperature for sufficiently low (but nonzero) [100] field, specific heat measurements (Higashinaka *et al.*, 2003b) on $Dy_2Ti_2O_7$ only find one peak down to a temperature of 0.35 K. Perhaps long-range dipolar interactions are of some relevance to the phenomenology at play for the case of a [100] field. Indeed, long-range dipole-dipole interactions are definitely crucial to the qualitative physics at play for fields along [110] and near [112] (Ruff *et al.*, 2005). Clearly more experimental and theoretical work on the problem of spin ice in a [100] magnetic field is needed.

c. $Tb_2Ti_2O_7$

Neutron diffraction and susceptibility data been collected on the cooperative paramagnet $Tb_2Ti_2O_7$ in high magnetic fields (Rule *et al.*, 2006; Ueland *et al.*, 2006). In the ac susceptibility work by Ueland *et al.* (2006) unusual cooperative effects and slow spin dynamics were induced by applying fields as high as 9 T at temperatures above 1 K.

Rule *et al.* (2006) performed single-crystal neutron scattering on $Tb_2Ti_2O_7$. They showed that the short-range spin-spin correlations, discussed in Sec. III.D (Gardner, Gaulin, *et al.*, 2001; Gardner *et al.*, 2003), are dynamic in origin and that they become of longer range as a field is applied. Applying a small field of 1000 Oe, at 400 mK, causes the magnetic diffuse scattering to condense into peaks, with characteristics similar to a polarized paramagnet. Figure 58 shows similar data at 1 K. In zero field, Bragg peaks are seen at 113 and 222 from the underlying nuclear structure and broad diffuse scattering, magnetic in origin is centered at 002. In a field up to 2 T (not shown) the diffuse scattering sharpens into a 002 peak and in higher fields ($\mu_0 H > 2$ T) a magnetically ordered phase is induced, with the development of true long-range order accompanied by spin waves.

2. High pressure

The study of pressure on samples in polycrystalline and single crystal form has become more common in recent years, with a paper on the pressure effect on the magnetoresistive material $Tl_2Mn_2O_7$ being among the earliest (Sushko *et al.*, 1996) in pyrochlore physics. More recently, studies have been performed on the transport, structural and magnetic properties of other pyrochlores (Mirebeau *et al.*, 2002; Saha *et al.*, 2006; Zhang *et al.*, 2006, 2007).

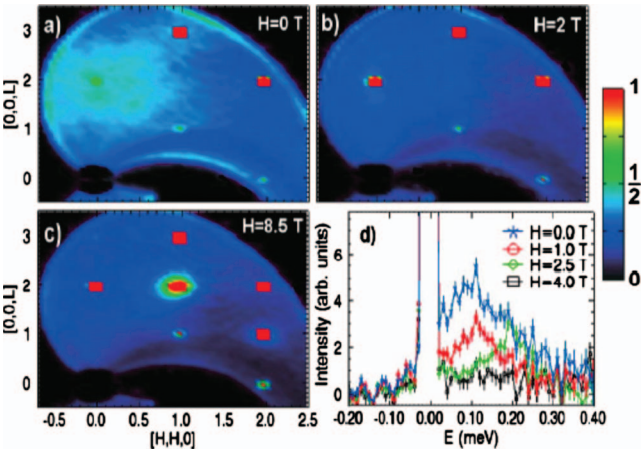

FIG. 58. (Color) Neutron scattering with $\Delta E = \pm 0.5$ meV from $Tb_2Ti_2O_7$ at 1 K. (a) Zero field, (b) 2 T, and (c) 8.5 T. (d) Constant Q scans at 0.1 K indicating that the low-lying magnetic scattering (slow spin dynamics) is quenched as the field increases. From Rule *et al.*, 2006.

$Sm_2Zr_2O_7$ undergoes a pressure-induced structural distortion at low pressures. However, the distortion is not observed between 13.5 and 18 GPa. Above 18 GPa, the pyrochlore structure is unstable and a distorted fluorite structure, in which the cations and anion vacancies are disordered, is observed (Zhang *et al.*, 2007). Similar things occur to $Cd_2Nb_2O_7$ at 12 GPa (Samara *et al.*, 2006; Zhang *et al.*, 2006). $Gd_2Ti_2O_7$ undergoes a subtle distortion of the lattice at 9 GPa at room temperature (Saha *et al.*, 2006). Neutron diffraction at 1.4 K on $Ho_2Ti_2O_7$ at pressures up to 6 GPa saw no change in the spatial correlations of this spin-ice compound (Mirebeau and Goncharenko, 2004), but a recent study of $Dy_2Ti_2O_7$ observed a small change in the magnetization at 1.3 GPa (Mito *et al.*, 2007).

a. $Tb_2Ti_2O_7$

The $Tb_2Ti_2O_7$ cooperative paramagnet has been studied by means of single-crystal and polycrystalline neutron diffraction for an unprecedented range of thermodynamical parameters combining high pressures, magnetic fields, and low temperatures (Mirebeau *et al.*, 2002, 2004). Mirebeau *et al.* (2002) found a long-range magnetically ordered state near 2 K for a hydrostatic pressure exceeding ~1.5 GPa. Powder neutron diffraction data as a function of pressure are shown in Fig. 59. Weak magnetic Bragg peaks occur at positions not associated with nuclear reflections although indexable to the $Fd\bar{3}m$ space group. Two weak reflections attributed to a long-range modulation of the main structure are also observed.

To investigate the transition further, Mirebeau *et al.* (2004) studied single crystals where the ordered magnetic moment may be tuned by means of the direction of the anisotropic pressure component. It was shown that an anisotropic pressure component is needed to suppress the spin-liquid state, but an anisotropic pressure

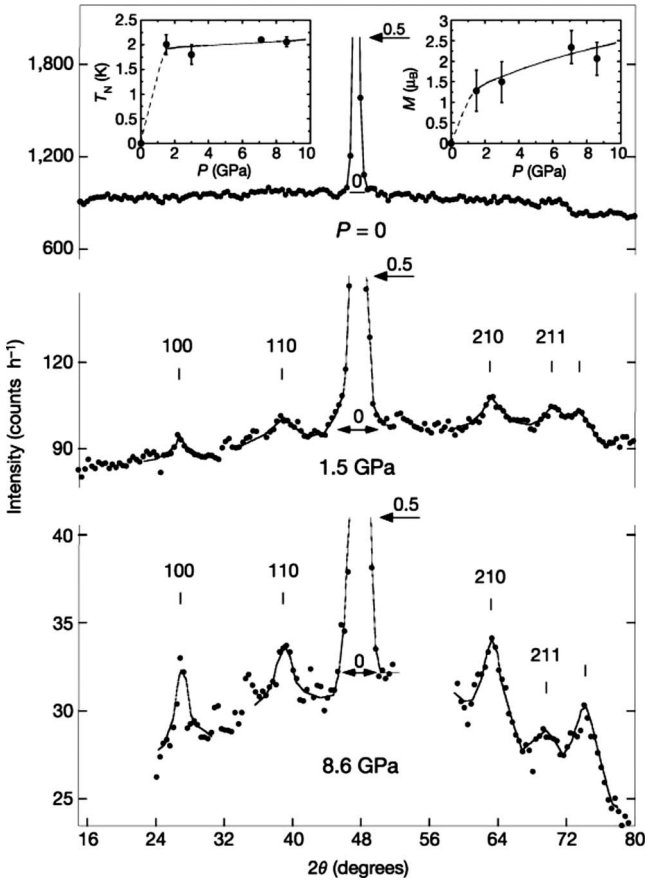

FIG. 59. Pressure induced magnetic Bragg scattering from polycrystalline $Tb_2Ti_2O_7$ at <2 K. The data show the pressure evolution of static correlations in the cooperative paramagnet. Insets: the Néel temperature, T_N (left), and ordered magnetic moment at 1.4 K, M (right), versus pressure. From Mirebeau *et al.*, 2002.

alone with no hydrostatice component produced no effect at 1.4 K. When an ordered phase was induced, the direction of the anisotropic pressure was important with a factor of 30 difference seen in the strength of the magnetic scattering between different directions (Mirebeau *et al.*, 2004). One wonders if the rich behavior of $Tb_2Ti_2O_7$ under pressure is related to the recent observations of seemingly dynamical lattice effects in zero applied pressure (Ruff *et al.*, 2007).

b. $A_2Mo_2O_7$ (A = Gd and Tb)

The properties of $Gd_2Mo_2O_{7-x}$ change remarkably with pressure. Kim *et al.* (2005) applied moderate pressures of 1.6 GPa and found a significant decrease in the saturation moment at 4 K with increased hysteresis. Mirebeau, Apetrei, Goncharenko, Andreica, *et al.* (2006) and Miyoshi *et al.* (2006) extended the pressure range and were able to drive the system into a glassy state at 2.7 GPa. Mirebeau, Apetrei, Goncharenko, Andreica, *et al.* (2006) monitored the melting of the magnetic structure by neutron diffraction (see Fig. 60). Thus, the application of pressure can change the sign of the Mo-Mo exchange interaction from ferromagnetic to antiferro-

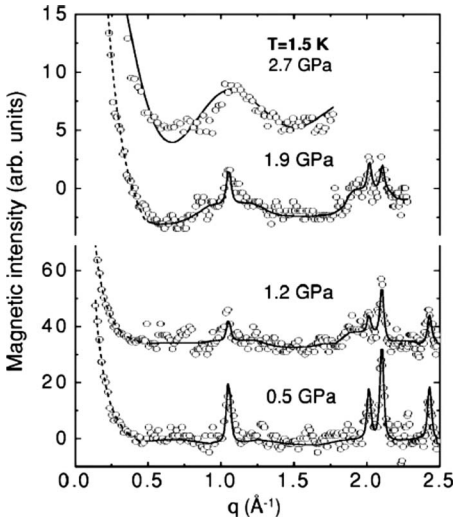

FIG. 60. Pressure dependence on the magnetic scattering from $Gd_2Mo_2O_7$. Note the broadening of the reflection near $q = 1$ Å^{-1} which is complete by 2.7 GPa. From Mirebeau, Apetrei, Goncharenko, Andreica, *et al.*, 2006.

magnetic. In addition, a compound with mixed Tb/La substitution on the A site, namely, $(La_{0.2}Tb_{0.8})_2Mo_2O_7$, was studied by Apetrei *et al.* (2007b). This material, which has nearly the same unit cell constant as $Gd_2Mo_2O_{7-x}$ [10.3787(8) Å], shows ferromagnetism with $T_c = 58$ K but with a different magnetic structure in which the Tb moments form the familiar two-in, two-out Ising structure, but there is still ferromagnetic coupling between the A and B magnetic sublattices. It is also noted that the ordered moments are reduced significantly from the free ion values by 50% for Tb, 30% for Gd, and 70% for Mo. The case for Tb is not surprising and can be ascribed to crystal-field effects, while results for Mo are consistent with earlier results (Greedan *et al.*, 1991; Gaulin *et al.*, 1992; Yasui *et al.*, 2001).

IV. CONCLUSIONS

We have highlighted most of the advances made over the past 20 years in classifying the magnetic ground state in many geometrically frustrated magnets with the pyrochlore lattice. An extensive review on other frustrated magnetic systems such as the spinels and kagome lattice magnets would be most welcomed. Although significant advances have been made in the understanding and characterization of these pyrochlore magnets, much more work can be done. As the systems get more complicated (i.e., through dilution of the magnetic sublattice or mixing of magnetic species) we hope and expect to see more new and exciting physics, but experimentalists will have to be more diligent in their characterization of their samples since it is now clear that the magnetic ground state is highly sensitive to small perturbations. Understanding the role local disorder and spin-lattice interactions play in these materials, as well as the origin of the persistent spin dynamics seen well below apparent ordering temperatures, usually by a local probe, such as μSR, is crucial in advancing this field. Another area that researchers should invest some time studying is the transport properties at metal-insulator or superconducting transitions. Finally, while the models, created for understanding geometrically frustrated systems have become increasingly sophisticated, there persist many outstanding questions. What is the origin of the 15 K anomaly in the ac susceptibility of the titanate spin ices? Why does $Tb_2Ti_2O_7$ remain dynamic and what is the true nature of the Tb^{3+} moments? What is the ground state for $Yb_2Ti_2O_7$? Is the ground state of $Er_2Ti_2O_7$ truly selected by quantum order by disorder? These must be addressed in the near future. We hope that our review proves useful to researchers in the field and motivates further investigation of the collective behavior of magnetic pyrochlore oxides.

ACKNOWLEDGMENTS

We acknowledge all our past and immediate collaborators, postdocs, and students, too numerous to list individually, and with whom we have enjoyed working over the years. Their contributions to this field are clear from the large number of citations of their work in the bibliography which follows. We also thank our many colleagues for hundreds of useful discussions and electronic mail correspondences. We acknowledge the generous financial support of the NSERC of Canada, the Canada Research Chair program (M.J.P.G., Tier 1), the Research Corporation, the Canadian Institute for Advanced Research, Materials and Manufacturing Ontario, the Ontario Innovation Trust, and the Canada Foundation for Innovation.

REFERENCES

Aharony, A., and E. Pytte, 1983, Phys. Rev. B **27**, 5872.
Ali N., M. P. Hill, S. Labroo, and J. E. Greedan, 1989, J. Solid State Chem. **83**, 178.
Alonso, J. A., M. J. Martinez-Lope, M. T. Casais, and J. L. Martinez, 2000, Chem. Mater. **12**, 1127.
Anderson, P. W., 1956, Phys. Rev. **102**, 1008.
Anderson, P. W., 1973, Mater. Res. Bull. **8**, 153.
Anderson, P. W., 1987, Science **235**, 1196.
Apetrei, A., I. Mirebeau, I. Goncharenko, D. Andreica, and P. Bonville, 2007a, J. Phys.: Condens. Matter **19**, 145214.
Apetrei, A., I. Mirebeau, I. Goncharenko, D. Andreica, and P. Bonville, 2007b, Phys. Rev. Lett. **97**, 206401.
Arai, M., Y. Ishikawa, N. Saito, and H. Takei, 1985, J. Phys. Soc. Jpn. **54**, 781.
Balakrishnan, G., O. A. Petrenko, M. R. Lees, and D. McK. Paul, 1998, J. Phys.: Condens. Matter **10**, L723.
Ballesteros, H. G., A. Cruz, L. A. Fernández, V. Martín-Mayor, J. Pech, J. J. Ruiz-Lorenzo, A. Tarancón, P. Téllez, C. L. Ullod, and C. Ungil, 2000, Phys. Rev. B **62**, 14237.
Ballou, R., 2001, Can. J. Phys. **79**, 1475.
Bansal, C., K. Hirofumi, B. Hiroshi, and N. Yoshikazu, 2003, Physica B **329**, 1034.
Bansal, C., H. Kawanaka, H. Bando, and Y. Nishihara, 2002, Phys. Rev. B **66**, 052406.
Barkema, G. T., and M. E. J. Newman, 1998, Phys. Rev. E **57**,

1155.
Barton, W. A., and J. Cashion, 1979, J. Phys. C **12**, 2897.
Bazuev, G. V., O. V. Makarova, V. Z. Oboldin, and G. P. Shveikin, 1976, Dokl. Akad. Nauk SSSR **230**, 869.
Bellier-Castella, L., M. J. P. Gingras, P. C. W. Holdsworth, and R. Moessner, 2001, Can. J. Phys. **79**, 1365.
Berg, E., E. Altman, and A. Auerbach, 2003, Phys. Rev. Lett. **90**, 147204.
Bergman, D. L., R. Shindou, G. A. Fiete, and L. Balents, 2006, Phys. Rev. B **74**, 134409.
Bert, F., P. Mendels, A. Olariu, N. Blanchard, G. Collin, A. Amato, C. Baines, and A. D. Hillier, 2006, Phys. Rev. Lett. **97**, 117203.
Bertaut, E. F., F. Forrat, and M. C. Montmory, 1959, Compt. Rend. **249c**, 276.
Bertin, E., P. Bonville, J.-P. Bouchaud, J. A. Hodges, J. P. Sanchez, and P. Vulliet, 2002, Eur. Phys. J. B **27**, 347.
Billinge, S. J. L., 2004, Z. Kristallogr. **219**, 117.
Binder, K., and A. P. Young, 1986, Rev. Mod. Phys. **58**, 801.
Blacklock, K., and H. W. White, 1980, J. Chem. Phys. **72**, 2191.
Blöte, H. W. J., R. F. Wielinga, and W. J. Huiskamp, 1969, Physica (Amsterdam) **43**, 549.
Bondah-Jagalu, V., and S. T. Bramwell, 2001, Can. J. Phys. **79**, 1381.
Bonville, P., J. A. Hodges, E. Bertin, J.-Ph. Bouchaud, M. Ocio, P. Dalmas de Réotier, L.-P. Regnault, H. M. Rønnow, J. P. Sanchez, S. Sosin, A. Yaouanc, M. Rams, and K. Królas, 2003, e-print arXiv:cond-mat/0306470.
Bonville, P., J. A. Hodges, M. Ocio, J. P. Sanchez, P. Vulliet, S. Sosin, and D. Braithwaite, 2003, J. Phys.: Condens. Matter **15**, 7777.
Booth, C. H., J. S. Gardner, G. H. Kwei, R. H. Heffner, F. Bridges, and M. A. Subramanian, 2000, Phys. Rev. B **62**, R755.
Bramwell, S. T., M. N. Field, M. J. Harris, and I. P. Perkin, 2000, J. Phys.: Condens. Matter **12**, 483.
Bramwell, S. T., and M. J. P. Gingras, 2001, Science **294**, 1495.
Bramwell, S. T., M. J. P. Gingras, and J. N. Reimers, 1994, J. Appl. Phys. **75**, 5523.
Bramwell, S. T., M. J. Harris, B. C. den Hertog, M. J. P. Gingras, J. S. Gardner, D. F. McMorrow, A. R. Wildes, A. L. Cornelius, J. D. M. Champion, R. G. Melko, and T. Fennell, 2001, Phys. Rev. Lett. **87**, 047205.
Bramwell, S. T., M. Shirai, and C. Ritter, 2004, Institut Laue-Langevin Experimental Report No. 5-31-1496.
Brixner, L. H., 1964, Inorg. Chem. **3**, 1065.
Canals, B., and C. Lacroix, 1998, Phys. Rev. Lett. **80**, 2933.
Canals, B., and C. Lacroix, 2000, Phys. Rev. B **61**, 1149.
Cannella, V., and J. A. Mydosh, 1972, Phys. Rev. B **6**, 4220.
Cao, N., T. Timusk, N. P. Raju, J. E. Greedan, and P. Gougeon, 1995, J. Phys.: Condens. Matter **7**, 2489.
Carcia, P. F., A. Ferretti, and A. Suna, 1982, J. Appl. Phys. **53**, 5282.
Castelnovo, C., R. Moessner, and S. L. Sondhi, 2008, Nature (London) **451**, 42.
Cépas, O., and B. S. Shastry, 2004, Phys. Rev. B **69**, 184402.
Cépas, O., A. P. Young, and B. S. Shastry, 2005, Phys. Rev. B **72**, 184408.
Chalker, J. T., P. C. W. Holdsworth, and E. F. Shender, 1992, Phys. Rev. Lett. **68**, 855.
Champion, J. D. M., M. J. Harris, P. C. W. Holdsworth, A. S. Wills, G. Balakrishnan, S. T. Bramwell, E. Čižmár, T. Fennell, J. S. Gardner, J. Lago, D. F. McMorrow, M. Orendáč, A. Orendáčová, D. McK. Paul, R. I. Smith, M. T. F. Telling, and A. Wildes, 2003, Phys. Rev. B **68**, 020401.
Champion, J. D. M., and P. C. W. Holdsworth, 2004, J. Phys.: Condens. Matter **16**, S665.
Champion, J. D. M., A. S. Wills, T. Fennell, S. T. Bramwell, J. S. Gardner, and M. A. Green, 2001, Phys. Rev. B **64**, 140407(R).
Chandra, P., and P. Coleman, 1995, in *Strongly Interacting Fermions and High Temperature Superconductivity*, edited by B. Douçot and J. Zinn-Justin (North-Holland, Amsterdam), p. 495.
Chapuis, Y., A. Yaouanc, P. Dalmas de Réotier, S. Pouget, P. Fouquet, A. Cervellino, and A. Forget, 2007, J. Phys.: Condens. Matter **19**, 446206.
Chen, D., and R. Xu, 1998, Mater. Res. Bull. **33**, 409.
Cheong, S.-W., H. Y. Hwang, B. Batlogg, and L. W. Rupp, Jr., 1996, Solid State Commun. **98**, 163.
Coey, J. M. D., 1987, Can. J. Phys. **65**, 1210.
Cornelius, A. L., and J. S. Gardner, 2001, Phys. Rev. B **64**, 060406.
Corruccini, L. R., and S. J. White, 1993, Phys. Rev. B **47**, 773.
Dalmas de Réotier, P., A. Yaouanc, P. C. M. Gubbens, C. T. Kaiser, C. Baines, and P. J. C. King, 2003, Phys. Rev. Lett. **91**, 167201.
Dalmas de Réotier, P., A. Yaouanc, L. Keller, A. Cervellino, B. Roessli, C. Baines, A. Forget, C. Vaju, P. C. M. Gubbens, A. Amato, and P. J. C. King, 2006, Phys. Rev. Lett. **96**, 127202.
Del Maestro, A. G., and M. J. P. Gingras, 2004, J. Phys.: Condens. Matter **16**, 3339.
Del Maestro, A. G., and M. J. P. Gingras, 2007, Phys. Rev. B **76**, 064418.
den Hertog B. C., and M. J. P. Gingras, 2000, Phys. Rev. Lett. **84**, 3430.
Diep, H. T., 1994, Ed., *Magnetic Systems with Competing Interactions (Frustrated Spin Systems)* (World Scientific, Singapore).
Diep, H. T., 2004, Ed., *Frustrated Spin Systems* (World Scientific, Singapore).
Dunsiger S. R., J. S. Gardner, J. A. Chakhalian, A. L. Cornelius, J. Jaime, R. F. Kiefl, R. Movshovich, W. A. MacFarlane, R. I. Miller, J. E. Sonier, and B. D. Gaulin, 2000, Phys. Rev. Lett. **85**, 3504.
Dunsiger, S. R., R. F. Kiefl, J. A. Chakhalian, J. E. Greedan, W. A. MacFarlane, R. I. Miller, G. D. Morris, A. N. Price, N. P. Raju, and J. E. Sonier, 2006, Phys. Rev. B **73**, 172418.
Dunsiger, S. R., R. F. Kiefl, K. H. Chow, B. D. Gaulin, M. J. P. Gingras, J. E. Greedan, A. Keren, K. Kojima, G. M. Luke, W. A. MacFarlane, N. P. Raju, J. E. Sonier, Y. Uemura, and W. D. Wu, 1996a, Phys. Rev. B **54**, 9019.
Dunsiger, S. R., R. F. Kiefl, K. H. Chow, B. D. Gaulin, M. J. P. Gingras, J. E. Greedan, A. Keren, K. Kojima, G. M. Luke, W. A. MacFarlane, N. P. Raju, J. E. Sonier, Y. Uemura, and W. D. Wu, 1996b, J. Appl. Phys. **79**, 6636.
Dupuis, V., E. Vincent, J. Hammann, J. E. Greedan, and A. S. Wills, 2002, J. Appl. Phys. **91**, 8384.
Ehlers, G., 2006, J. Phys.: Condens. Matter **18**, R231.
Ehlers, G., A. L. Cornelius, T. Fennell, M. Koza, S. T. Bramwell, and J. S. Gardner, 2004, J. Phys.: Condens. Matter **16**, S635.
Ehlers, G., A. L. Cornelius, M. Orendác, M. Kajnaková, T. Fennell, S. T. Bramwell, and J. S. Gardner, 2003, J. Phys.: Condens. Matter **15**, L9.
Ehlers, G., J. S. Gardner, C. H. Booth, M. Daniel, K. C. Kam,

A. K. Cheetham, D. Antonio, H. E. Brooks, A. L. Cornelius, S. T. Bramwell, J. Lago, W. Haussler, and N. Rosov, 2006, Phys. Rev. B **73**, 174429.
Elhajal, M., B. Canals, R. Sunyer, and C. Lacroix, 2005, Phys. Rev. B **71**, 094420.
Enjalran, M., and M. J. P. Gingras, 2003, e-print arXiv:cond-mat/0307152.
Enjalran, M., and M. J. P. Gingras, 2004, Phys. Rev. B **70**, 174426.
Erwing, R. C., W. J. Weber, and J. Lian, 2004, J. Appl. Phys. **95**, 5949.
Fazekas, P., and P. W. Anderson, 1974, Philos. Mag. **30**, 432.
Fennell, T., S. T. Bramwell, D. F. McMorrow, P. Manuel, and A. R. Wildes, 2007, Nat. Phys. **3**, 566.
Fennell, T., O. A. Petrenko, B. Fåk, S. T. Bramwell, M. Enjalran, T. Yavors'kii, M. J. P. Gingras, R. G. Melko, and G. Balakrishnan, 2004, Phys. Rev. B **70**, 134408.
Fennell, T., O. A. Petrenko, B. Fåk, J. S. Gardner, S. T. Bramwell, and B. Ouladdiaf, 2005, Phys. Rev. B **72**, 224411.
Finn, C. P. B., R. Orbach, and W. P. Wolf, 1961, Proc. Phys. Soc. London **77**, 261.
Flood, D. J., 1974, J. Appl. Phys. **45**, 4041.
Fujinaka, H., N. Kinomura, M. Koizumi, Y. Miyamoto, and S. Kume, 1979, Mater. Res. Bull. **14**, 1133.
Fukazawa, H., and Y. Maeno, 2002, J. Phys. Soc. Jpn. **71**, 2578.
Fukazawa, H., R. G. Melko, R. Higashinaka, Y. Maeno, and M. J. P. Gingras, 2002, Phys. Rev. B **65**, 054410.
Gardner, J. S., A. L. Cornelius, L. J. Chang, M. Prager, Th. Brükel, and G. Ehlers, 2005, J. Phys.: Condens. Matter **17**, 7089.
Gardner, J. S., S. R. Dunsiger, B. D. Gaulin, M. J. P. Gingras, J. E. Greedan, R. F. Kiefl, M. D. Lumsden, W. A. MacFarlane, N. P. Raju, J. E. Sonier, I. Swainson, and Z. Tun, 1999, Phys. Rev. Lett. **82**, 1012.
Gardner, J. S., G. Ehlers, S. T. Bramwell, and B. D. Gaulin, 2004, J. Phys.: Condens. Matter **16**, S643.
Gardner, J. S., G. Ehlers, R. H. Heffner, and F. Mezei, 2001, J. Magn. Magn. Mater. **226-230**, 460.
Gardner, J. S., G. Ehlers, N. Rosov, R. W. Erwin, and C. Petrovic, 2004, Phys. Rev. B **70**, 180404(R).
Gardner, J. S., B. D. Gaulin, A. J. Berlinsky, P. Waldron, S. R. Dunsiger, N. P. Raju, and J. E. Greedan, 2001, Phys. Rev. B **64**, 224416.
Gardner, J. S., B. D. Gaulin, S.-H. Lee, C. Broholm, N. P. Raju, and J. E. Greedan, 1999, Phys. Rev. Lett. **83**, 211.
Gardner, J. S., B. D. Gaulin, and D. McK. Paul, 1998, J. Cryst. Growth **191**, 740.
Gardner, J. S., A. Keren, G. Ehlers, C. Stock, E. Segal, J. M. Roper, B. Fåk, P. R. Hammar, M. B. Stone, D. H. Reich, and B. D. Gaulin, 2003, Phys. Rev. B **68**, 180401.
Garton, G., and B. Wanklyn, 1968, J. Mater. Sci. **3**, 395.
Gaulin, B. D., 1994, Hyperfine Interact. **85**, 159.
Gaulin, B. D., J. N. Reimers, T. E. Mason, J. E. Greedan, and Z. Tun, 1992, Phys. Rev. Lett. **69**, 3244.
Ghosh, S., R. Parthasarathy, T. F. Rosenbaum, and G. Aeppli, 2002, Science **296**, 2195.
Gingras M. J. P., and B. C. den Hertog, 2001, Can. J. Phys. **79**, 1339.
Gingras, M. J. P., B. C. den Hertog, M. Faucher, J. S. Gardner, S. R. Dunsiger, L. J. Chang, B. D. Gaulin, N. P. Raju, and J. E. Greedan, 2000, Phys. Rev. B **62**, 6496.
Gingras, M. J. P., C. V. Stager, B. D. Gaulin, N. P. Raju, and J. E. Greedan, 1996, J. Appl. Phys. **79**, 6170.
Gingras, M. J. P., C. V. Stager, N. P. Raju, B. D. Gaulin, and J. E. Greedan, 1997, Phys. Rev. Lett. **78**, 947.
Greedan, J. E., 1992, in *Magnetic Properties of Nonmetallic Compounds Based on Transition Elements*, edited by H. P. J. Wijn, Landolt-Börnstein, New Series, Vol. 27 (Springer-Verlag, Berlin), p. 100.
Greedan, J. E., 2001, J. Mater. Chem. **11**, 37.
Greedan, J. E., 2006, J. Alloys Compd. **408-412**, 444.
Greedan, J. E., J. Avelar, and M. A. Subramanian, 1992, Solid State Commun. **82**, 797.
Greedan, J. E., D. Gout, A. D. Lozano-Gorrin, S. Derahkshan, Th. Proffen, H.-J. Kim, T. Božin, and S. J. L. Billinge, 2009, Phys. Rev. B **79**, 014427.
Greedan, J. E., N. P. Raju, A. Maignan, C. Simon, J. S. Pedersen, A. M. Niraimathi, E. Gmelin, and M. A. Subramanian, 1996, Phys. Rev. B **54**, 7189.
Greedan, J. E., N. P. Raju, and M. A. Subramanian, 1996, Solid State Commun. **99**, 399.
Greedan, J. E., J. N. Reimers, S. L. Penny, and C. V. Stager, 1990, J. Appl. Phys. **67**, 5967.
Greedan, J. E., J. N. Reimers, C. V. Stager, and S. L. Penny, 1991, Phys. Rev. B **43**, 5682.
Greedan, J. E., M. Sato, N. Ali, and W. R. Datars, 1987, J. Solid State Chem. **68**, 300.
Greedan, J. E., M. Sato, X. Yan, and F. S. Razavi, 1986, Solid State Commun. **59**, 895.
Gurgul, J., M. Rams, Z. Świątkowska, R. Kmieć, and K. Tomala, 2007, Phys. Rev. B **75**, 064426.
Haldane, F. D. M., 1983, Phys. Rev. Lett. **50**, 1153.
Han, S.-W., J. S. Gardner, and C. H. Booth, 2004, Phys. Rev. B **69**, 024416.
Hanasaki, N., M. Kinuhara, I. Kézmárki, S. Iguchi, S. Miyasaka, N. Takeshita, C. Terakura, H. Takagi, and Y. Tokura, 2006, Phys. Rev. Lett. **96**, 116403.
Hanasaki, N., K. Watanabe, T. Ohtsuka, I. Kezmarki, S. Iguchi, S. Miyasaka, and Y. Tokura, 2007, Phys. Rev. Lett. **99**, 086401.
Hanawa, M., Y. Muraoka, T. Sakakibara, T. Yamaura, and Z. Hiroi, 2001, Phys. Rev. Lett. **87**, 187001.
Harris, A. B., A. J. Berlinsky, and C. Bruder, 1991, J. Appl. Phys. **69**, 5200.
Harris, M. J., S. T. Bramwell, P. C. W. Holdsworth, and J. D. Champion, 1998, Phys. Rev. Lett. **81**, 4496.
Harris, M. J., S. T. Bramwell, D. F. McMorrow, T. Zeiske, and K. W. Godfrey, 1997, Phys. Rev. Lett. **79**, 2554.
Harris, M. J., S. T. Bramwell, T. Zeiske, D. F. McMorrow, and P. J. C. King, 1998, J. Magn. Magn. Mater. **177-181**, 757.
Harrison, A., 2004, J. Phys.: Condens. Matter **16**, S553.
Hassan, A. K., L. P. Levy, C. Darie, and P. Strobel, 2003, Phys. Rev. B **67**, 214432.
He, J., R. Jin, B. C. Chakoumakos, J. S. Gardner, D. Mandrus, and T. M. Tritt, 2007, J. Electron. Mater. **36**, 740.
Higashinaka, R., H. Fukazawa, K. Deguchi, and Y. Maeno, 2004, J. Phys.: Condens. Matter **16**, S679.
Higashinaka, R., H. Fukazawa, and Y. Maeno, 2003a, Phys. Rev. B **68**, 014415.
Higashinaka, R., H. Fukazawa, and Y. Maeno, 2003b, Physica B **329-333**, 1040.
Higashinaka, R., H. Fukazawa, D. Yanagishima, and Y. Maeno, 2002, J. Phys. Chem. Solids **63**, 1043.
Hiroi, Z., K. Matsuhira, and M. Ogata, 2003, J. Phys. Soc. Jpn. **72**, 3045.
Hiroi, Z., K. Matsuhira, S. Takagi, T. Tayama, and T. Sakakibara, 2003, J. Phys. Soc. Jpn. **72**, 411.

Hizi, U., and C. L. Henley, 2007, J. Phys.: Condens. Matter **19**, 145268.
Hodges, J. A., P. Bonville, A. Forget, M. Rams, K. Królas, and G. Dhalenne, 2001, J. Phys.: Condens. Matter **13**, 9301.
Hodges, J. A., P. Bonville, A. Forget, J. P. Sanchez, P. Vulliet, M. Rams, and K. Królas, 2003, Eur. Phys. J. B **33**, 173.
Hodges, J. A., P. Bonville, A. Forget, A. Yaouanc, P. Dalmas de Réotier, G. André, M. Rams, K. Królas, C. Ritter, P. C. M. Gubbens, C. T. Kaiser, P. C. King, and C. Baines, 2002, Phys. Rev. Lett. **88**, 077204.
Hoekstra, H. R., and F. Gallagher, 1968, Inorg. Chem. **7**, 2553.
Horowitz, H. S., J. M. Longo, and H. H. Horowitz, 1983, J. Electrochem. Soc. **130**, 1851.
Houtappel, R. M. F., 1950, Physica (Utrecht) **16**, 425.
Hubert, P. H., 1974, Bull. Chim. Soc. Fr. **11**, 2385.
Hüfner, S., 1978, *Optical Spectra of Transparent Rare Earth Compounds* (Academic, New York), p. 38.
Iikubo, S., S. Yoshii, T. Kageyama, K. Oda, Y. Kondo, K. Murata, and M. Sato, 2001, J. Phys. Soc. Jpn. **70**, 212.
Isakov, S. V., R. Moessner, and S. L. Sondhi, 2005, Phys. Rev. Lett. **95**, 217201.
Ito, M., Y. Yasui, M. Kanada, H. Harashina, S. Yoshii, K. Murata, M. Sato, H. Okumura, and K. Kakurai, 2001, J. Phys. Chem. Solids **62**, 337.
Jana, Y. M., A. Sengupta, and D. Ghosh, 2002, J. Magn. Magn. Mater. **248**, 7.
Jaubert, L., J. T. Chalker, P. C. W., Holdsworth, and R. Moessner, 2008, Phys. Rev. Lett. **100**, 067207.
Jönsson, P. E., R. Mathieu, W. Wernsdorfer, A. M. Tkachuk, and B. Barbara, 2007, Phys. Rev. Lett. **98**, 256403.
Kadowaki, H., Y. Ishii, K. Matsuhira, and Y. Hinatsu, 2002, Phys. Rev. B **65**, 144421.
Kageyama, T., S. Iikubo, S. Yoshii, Y. Kondo, M. Sato, and Y. Iye, 2001, J. Phys. Soc. Jpn. **70**, 3006.
Kao, Y.-J., M. Enjalran, A. G. Del Maestro, H. R. Molavian, and M. J. P. Gingras, 2003, Phys. Rev. B **68**, 172407.
Katsufuji, T., H. Y. Hwang, and S.-W. Cheong, 2000, Phys. Rev. Lett. **84**, 1998.
Kawamura, H., 1988, Phys. Rev. B **38**, 4916.
Ke, X., R. S. Freitas, B. G. Ueland, G. C. Lau, M. L. Dahlberg, R. J. Cava, R. Moessner, and P. Schiffer, 2007, Phys. Rev. Lett. **99**, 137203.
Keren, A., and J. S. Gardner, 2001, Phys. Rev. Lett. **87**, 177201.
Keren, A., J. S. Gardner, G. Ehlers, A. Fukaya, E. Segal, and Y. J. Uemura, 2004, Phys. Rev. Lett. **92**, 107204.
Kézsmárki, I., N. Hanasaki, D. Hashimoto, S. Iguchi, Y. Taguchi, S. Miyasaka, and Y. Tokura, 2004, Phys. Rev. Lett. **93**, 266401.
Kézsmárki, I., N. Hanasaki, K. Watanabe, S. Iguchi, Y. Taguchi, S. Miyasaka, and Y. Tokura, 2006, Phys. Rev. B **73**, 125122.
Kézsmárki, I., S. Onoda, Y. Taguchi, T. Ogasawara, M. Matsubara, S. Iguchi, N. Hanasaki, N. Nagaosa, and Y. Tokura, 2005, Phys. Rev. B **72**, 094427.
Kido, H., S. Komarneni, and R. Roy, 1991, J. Am. Ceram. Soc. **74**, 422.
Kim, H. C., Y. Jo, J. G. Park, S. W. Cheong, M. Ulharz, C. Pfleiderer, and H. V. Lohneysen, 2005, Physica B **359-361**, 1246.
Kmieć, R., Z. Światkowska, J. Gurgul, M. Rams, A. Zarzycki, and K. Tomala, 2006, Phys. Rev. B **74**, 104425.
Kwei, G. H., C. H. Booth, F. Bridges, and M. A. Subramanian, 1997, Phys. Rev. B **55**, R688.
Lacroix, C., P. Mendels, and F. Mila, 2010, Eds., *Highly Frustrated Magnetism* (Springer, Berlin).
Ladieu, F., F. Bert, V. Dupuis, E. Vincent, and J. Hammann, 2004, J. Phys.: Condens. Matter **16**, S735.
Lago, J., S. J. Blundell, and C. Baines, 2007, J. Phys.: Condens. Matter **19**, 326210.
Lago, J., T. Lancaster, S. J. Blundell, S. T. Bramwell, F. L. Pratt, M. Shirai, and C. Baines, 2005, J. Phys.: Condens. Matter **17**, 979.
Läuchli, A., S. Dommange, B. Normand, and F. Mila, 2007, Phys. Rev. B **76**, 144413.
Lau, G. C., R. S. Freitas, B. G. Ueland, M. L. Dahlberg, Q. Huang, H. W. Zandbergen, P. Schiffer, and R. J. Cava, 2007, Phys. Rev. B **76**, 054430.
Lau, G. C., R. S. Freitas, B. G. Ueland, B. D. Muegge, E. L. Duncan, P. Schiffer, and R. J. Cava, 2006, Nat. Phys. **2**, 249.
Lau, G. C., B. D. Muegge, T. M. McQueen, E. L. Duncan, and R. J. Cava, 2006, J. Solid State Chem. **179**, 3126.
Lazarev, V. B., and V. B. Shaplygin, 1978, Mater. Res. Bull. **13**, 229.
Lecheminant, P., P. Bernu, C. Lhuillier, L. Pierre, and P. Sindzingre, 1997, Phys. Rev. B **56**, 2521.
Lee, L. W., and A. P. Young, 2003, Phys. Rev. Lett. **90**, 227203.
Lee, L. W., and A. P. Young, 2007, Phys. Rev. B **76**, 024405.
Lee, S., J.-G. Park, D. T. Adroja, D. Khomskii, S. Streltsov, K. A. McEwen, H. Sakai, K. Yoshimura, V. I. Anisimov, D. Mori, R. Kanno, and R. I. Ibberson, 2006, Nature Mater. **5**, 471.
Lee, S. H., C. Broholm, T. H. Kim, W. Ratcliff, and S.-W. Cheong, 2000, Phys. Rev. Lett. **84**, 3718.
Lee, S. H., C. Broholm, W. Ratcliff, G. Gasparovic, Q. Huang, T. H. Kim, and S.-W. Cheong, 2002, Nature (London) **418**, 856.
Luo, G., S. T. Hess, and L. R. Corruccini, 2001, Phys. Lett. A **291**, 306.
Lynn, J. W., L. Vasiliu-Doloc, and M. A. Subramanian, 1998, Phys. Rev. Lett. **80**, 4582.
Machida, Y., S. Nakatsuji, Y. Maeno, T. Yamada, T. Tayama, and T. Sakakibara, 2007, J. Magn. Magn. Mater. **310**, 1079.
Machida, Y., S. Nakatsuji, H. Tonomura, T. Tayama, T. Sakakibara, J. van Duijn, C. Broholm, and Y. Maeno, 2005, J. Phys. Chem. Solids **66**, 1435.
Mailhot, A., and M. L. Plumer, 1993, Phys. Rev. B **48**, 9881.
Mandiram, A., and A. Gopalakrishnan, 1980, Indian J. Chem., Sect A: Inorg., Phys., Theor. Anal. **19A**, 1042.
Mandrus, D., J. R. Thompson, R. Gaal, L. Forro, J. C. Bryan, B. C. Chakoumakos, L. M. Woods, B. C. Sales, R. S. Fishman, and V. Keppens, 2001, Phys. Rev. B **63**, 195104.
Matsuda, M., H. Ueda, A. Kikkawa, Y. Tanaka, K. Katsumata, Y. Narumi, T. Inami, Y. Ueda, and S.-H. Lee, 2007, Nat. Phys. **3**, 397.
Matsuhira, K., Y. Hinatsu, and T. Sakakibara, 2001, J. Phys.: Condens. Matter **13**, L737.
Matsuhira, K., Y. Hinatsu, K. Tenya, H. Amitsuka, and T. Sakakibara, 2002, J. Phys. Soc. Jpn. **71**, 1576.
Matsuhira, K., Y. Hinatsu, K. Tenya, and T. Sakakibara, 2000, J. Phys.: Condens. Matter **12**, L649.
Matsuhira, K., Z. Hiroi, T. Tayama, S. Takagi, and T. Sakakibara, 2002, J. Phys.: Condens. Matter **14**, L559.
Matsuhira, K., C. Sekine, C. Paulsen, and Y. Hinatsu, 2004, J. Magn. Magn. Mater. **272-276**, E981.
Matsuhira, K., M. Wakeshima, R. Nakanishi, T. Yamada, W. Kawano, S. Tagaki, and Y. Hinatsu, 2007, J. Phys. Soc. Jpn.

76, 043706.
McCarthy, G. J., 1971, Mater. Res. Bull. **6**, 31.
Melko, R. G., B. C. den Hertog, and M. J. P. Gingras, 2001, Phys. Rev. Lett. **87**, 067203.
Melko, R. G., and M. J. P. Gingras, 2004, J. Phys.: Condens. Matter **16**, R1277.
Millican, J. N., R. T. Macaluso, S. Nakatsuji, Y. Machida, Y. Maeno, and J. Y. Chan, 2007, Mater. Res. Bull. **42**, 928.
Minervini, L., R. W. Grimes, Y. Tabira, R. L. Withers, and K. E. Sickafus, 2002, Philos. Mag. A **82**, 123.
Mirebeau, I., A. Apetrei, I. Goncharenko, D. Andreica, P. Bonville, J. P. Sanchez, A. Amato, E. Suard, W. A. Crichton, A. Forget, and D. Colson, 2006, Phys. Rev. B **74**, 174414.
Mirebeau, I., A. Apetrei, I. N. Goncharenko, and R. Moessner, 2006, Physica B **385-386**, 307.
Mirebeau, I., A. Apetrei, J. Rodrígues-Carvajal, P. Bonville, A. Forget, D. Colson, V. Glazkov, J. P. Sanchez, O. Isnard, and E. Suard, 2005, Phys. Rev. Lett. **94**, 246402.
Mirebeau, I., P. Bonville, and M. Hennion, 2007, Phys. Rev. B **76**, 184436.
Mirebeau, I., and I. N. Goncharenko, 2004, Physica B **350**, 250.
Mirebeau, I., I. N. Goncharenko, P. Cadavez-Peres, S. T. Bramwell, M. J. P. Gingras, and J. S. Gardner, 2002, Nature (London) **420**, 54.
Mirebeau, I., I. N. Goncharenko, D. Dhalenne, and A. Revcolevschi, 2004, Phys. Rev. Lett. **93**, 187204.
Mito, M., S. Kuwabara, K. Matsuhira, H. Deguchi, S. Takagi, and Z. Hiroi, 2007, J. Magn. Magn. Mater. **310**, e432.
Miyoshi, K., Y. Nishimura, K. Honda, K. Fujiwara, and J. Takeuchi, 2000, J. Phys. Soc. Jpn. **69**, 3517.
Miyoshi, K., Y. Takamatsu, and J. Takeuchi, 2006, J. Phys. Soc. Jpn. **75**, 065001.
Miyoshi, K., T. Yamashita, K. Fujiwara, and J. Takeuchi, 2002, Physica B **312-313**, 706.
Moessner, R., 2001, Can. J. Phys. **79**, 1283.
Moessner, R., and J. T. Chalker, 1998a, Phys. Rev. B **58**, 12049.
Moessner, R., and J. T. Chalker, 1998b, Phys. Rev. Lett. **80**, 2929.
Moessner, R., and S. L. Sondhi, 2003, Phys. Rev. B **68**, 064411.
Moessner, R., S. L. Sondhi, and M. O. Goerbig, 2006, Phys. Rev. B **73**, 094430.
Molavian H. R., M. J. P. Gingras, and B. Canals, 2007, Phys. Rev. Lett. **98**, 157204.
Moritomo, Y., Sh. Xu, A. Machida, T. Katsufuji, E. Nishibori, M. Takata, S. Sakata, and S.-W. Cheong, 2001, Phys. Rev. B **63**, 144425.
Munenaka, T., and H. Sato, 2006, J. Phys. Soc. Jpn. **75**, 103801.
Nakatsuji, S., Y. Machida, Y. Maeno, T. Tayama, T. Sakakibara, J. van Duijn, L. Balicas, J. N. Millican, R. T. Macaluso, and J. Y. Chan, 2006, Phys. Rev. Lett. **96**, 087204.
Néel, L., 1948, Ann. Phys. **3**, 137.
Nussinov, Z., C. D. Batista, B. Normand, and S. A. Trugman, 2007, Phys. Rev. B **75**, 094411.
Obradors, X., A. Labarta, A. Isalgue, J. Tejada, J. Rodriguez, and M. Pernet, 1988, Solid State Commun. **65**, 189.
Okamoto, Y., M. Nohara, H. Aruga-Katori, and H. Takagi, 2007, Phys. Rev. Lett. **99**, 137207.
Orbach R., 1961, Proc. Phys. Soc. London **77**, 821.
Orendác, M., J. Hanko, E. Čižmár, A. Orendáčová, J. Shirai, and S. T. Bramwell, 2007, Phys. Rev. B **75**, 104425.
Palmer, S. E., and J. T. Chalker, 2000, Phys. Rev. B **62**, 488.
Park, J. G., Y. Jo, J. Park, H. C. Kim, H. C. Ri, S. Xu, Y. Moritomo, and S. W. Cheong, 2003, Physica B **328**, 90.
Pauling, L., 1935, J. Am. Chem. Soc. **57**, 2680.
Penc, K., N. Shannon, and H. Shiba, 2004, Phys. Rev. Lett. **93**, 197203.
Petrenko, O. A., M. R. Lees, G. Balakrishnan, and D. McK Paul, 2004, Phys. Rev. B **70**, 012402.
Petrenko, O. A., C. Ritter, M. Yethiraj, and D. M. Paul, 1998, Phys. Rev. Lett. **80**, 4570.
Pike, G. E., and C. H. Seager, 1977, J. Appl. Phys. **48**, 5152.
Pinettes, C., B. Canals, and C. Lacroix, 2002, Phys. Rev. B **66**, 024422.
Poole, A., A. S. Wills, and E. Lelièvre-Berna, 2007, J. Phys.: Condens. Matter **19**, 452201.
Proffen, Th., S. J. L. Billinge, T. Egami, and D. Louca, 2003, Z. Kristallogr. **218**, 132.
Quilliam, J. A., K. A. Ross, A. G. Del Maestro, M. J. P. Gingras, L. R. Corruccini, and J. B. Kycia, 2007, Phys. Rev. Lett. **99**, 097201.
Raju, N. P., M. Dion, M. J. P. Gingras, T. E. Mason, and J. E. Greedan, 1999, Phys. Rev. B **59**, 14489.
Raju, N. P., E. Gmelin, and R. Kremer, 1992, Phys. Rev. B **46**, 5405.
Raju, N. P., and P. Gougeon, 1995, unpublished.
Raju, N. P., J. E. Greedan, and M. A. Subramanian, 1994, Phys. Rev. B **49**, 1086.
Ramirez, A. P., 1994, Annu. Rev. Mater. Sci. **24**, 453.
Ramirez, A. P., A. Hayashi, R. J. Cava, R. Siddharthan, and B. S. Shastry, 1999, Nature (London) **399**, 333.
Ramirez, A. P., B. S. Shastry, A. Hayashi, J. J. Krajewski, D. A. Huse, and R. J. Cava, 2002, Phys. Rev. Lett. **89**, 067202.
Ramirez, A. P., and M. A. Subramanian, 1997, Science **277**, 546.
Ranganathan, R., G. Rangarajan, R. Srinivasan, M. A. Subramanian, and G. V. Subba Rao, 1983, J. Low Temp. Phys. **52**, 481.
Reich, D. H., B. Ellman, Y. Yang, T. F. Rosenbaum, G. Aeppli, and D. P. Belanger, 1990, Phys. Rev. B **42**, 4631.
Reich, D. H., T. F. Rosenbaum, and G. Aeppli, 1987, Phys. Rev. Lett. **59**, 1969.
Reimers, J. N., 1992, Phys. Rev. B **45**, 7287.
Reimers, J. N., and A. J. Berlinsky, 1993, Phys. Rev. B **48**, 9539.
Reimers, J. N., A. J. Berlinsky, and A.-C. Shi, 1991, Phys. Rev. B **43**, 865.
Reimers, J. N., J. E. Greedan, and M. Björgvinsson, 1992, Phys. Rev. B **45**, 7295.
Reimers, J. N., J. E. Greedan, R. K. Kremer, E. Gmelin, and M. A. Subramanian, 1991, Phys. Rev. B **43**, 3387.
Reimers, J. N., J. E. Greedan, and M. Sato, 1988, J. Solid State Chem. **72**, 390.
Rhyne, J. J., 1985, IEEE Trans. Magn. **21**, 1990.
Rhyne, J. J., and G. E. Fish, 1985, J. Appl. Phys. **57**, 3407.
Rosenfeld, H. D., and M. A. Subramanian, 1996, J. Solid State Chem. **125**, 278.
Rosenkranz, S., A. P. Ramirez, A. Hayashi, R. J. Cava, R. Siddharthan, and B. S. Shastry, 2000, J. Appl. Phys. **87**, 5914.
Roth, R. S., 1956, J. Res. Natl. Bur. Stand. **56**, 17.
Ruff, J. P. C., B. D. Gaulin, J. P. Castellan, K. C. Rule, J. P. Clancy, J. Rodrigues, and H. A. Dabkowska, 2007, Phys. Rev. Lett. **99**, 237202.
Ruff, J. P. C., R. G. Melko, and M. J. P. Gingras, 2005, Phys. Rev. Lett. **95**, 097202.
Rule, K. C., J. P. C. Ruff, B. D. Gaulin, S. R. Dunsiger, J. S. Gardner, J. P. Clancy, M. J. Lewis, H. A. Dabkowska, I. Mire-

beau, P. Manuel, Y. Qiu, and J. R. D. Copley, 2006, Phys. Rev. Lett. **96**, 177201.
Rushbrooke, G. S., and P. J. Wood, 1958, Mol. Phys. **1**, 257.
Sagi, E., O. Ofer, A. Keren, and J. S. Gardner, 2005, Phys. Rev. Lett. **94**, 237202.
Saha, S., D. V. S. Muthu, C. Pascanut, N. Dragoe, R. Suryanarayanan, G. Dhalenne, A. Revcolevschi, S. M. Karmakar, S. Sharma, and A. K. Sood, 2006, Phys. Rev. B **74**, 064109.
Sakai, H., K. Yoshimura, H. Ohno, H. Kato, S. Kambe, R. E. Walstedt, T. D. Matsuda, and Y. Haga, 2001, J. Phys.: Condens. Matter **13**, L785.
Sakakibara, T., T. Tayama, K. Matsuhira, S. Takagi, and Z. Hiroi, 2004, J. Magn. Magn. Mater. **272-276**, 1312.
Samara, G. A., E. L. Venturini, and L. A. Boatner, 2006, J. Appl. Phys. **100**, 074112.
Sato, M., and J. E. Greedan, 1987, J. Solid State Chem. **67**, 248.
Sato, M., X. Yan, and J. E. Greedan, 1986, Z. Anorg. Allg. Chem. **540**, 177.
Saunders, T. E., and J. T. Chalker, 2007, Phys. Rev. Lett. **98**, 157201.
Schiffer, P., and A. P. Ramirez, 1996, Comments Condens. Matter Phys. **18**, 21.
Schiffer, P., A. P. Ramirez, W. Bao, and S.-W. Cheong, 1995, Phys. Rev. Lett. **75**, 3336.
Schiffer, P., A. P. Ramirez, D. H. Huse, P. L. Gammel, U. Yaron, D. J. Bishop, and A. J. Valentino, 1995, Phys. Rev. Lett. **74**, 2379.
Schiffer, P., A. P. Ramirez, D. A. Huse, and A. J. Valentino, 1994, Phys. Rev. Lett. **73**, 2500.
Schnelle, W., and R. K. Kremer, 2004, J. Phys.: Condens. Matter **16**, S685.
Shender, E. F., V. P. Cherepanov, P. C. W. Holdsworth, and A. J. Berlinsky, 1993, Phys. Rev. Lett. **70**, 3812.
Sherrington, D., and B. W. Southern, 1975, J. Phys. F: Met. Phys. **5**, L49.
Shi, J., Z. Tang, B. P. Zhu, P. Huang, D. Yin, C. Z. Li, Y. Wang, and H. Wen, 2007, J. Magn. Magn. Mater. **310**, 1322.
Shiga, M., K. Fujisawa, and H. Wada, 1993, J. Phys. Soc. Jpn. **62**, 1329.
Shimakawa, Y., Y. Kubo, N. Hamada, J. D. Jorgensen, Z. Hu, S. Short, M. Nohara, and H. Takagi, 1999, Phys. Rev. B **59**, 1249.
Shimakawa, Y., Y. Kubo, and T. Manako, 1996, Nature (London) **379**, 53.
Shin-ike, T., G. Adachi, and J. Shiokawa, 1977, Mater. Res. Bull. **12**, 1149.
Shirai, M., and S. T. Bramwell, 2007a, Ph.D. thesis, UCL.
Shirai, M., and S. T. Bramwell, 2007b, private communication.
Sickafus, K. E., L. Minervini, R. W. Grimes, J. A. Valdez, M. Ishimaru, F. Li, K. J. McClellan, and T. Hartmann, 2000, Science **289**, 748.
Siddharthan, R., B. S. Shastry, A. P. Ramirez, A. Hayashi, R. J. Cava, and S. Rosenkranz, 1999, Phys. Rev. Lett. **83**, 1854.
Sleight, A. W., and P. J. Bouchard, 1972, Proceedings of the Fifth Materials Research Symposium (unpublished), Vol. 364, p. 227.
Sleight, A. W., J. L. Gillson, J. F. Weiher, and W. Bindloss, 1974, Solid State Commun. **14**, 357.
Snyder, J., J. S. Slusky, R. J. Cava, and P. Schiffer, 2001, Nature (London) **413**, 48.
Snyder, J., J. S. Slusky, R. J. Cava, and P. Schiffer, 2002, Phys. Rev. B **66**, 064432.
Snyder, J., B. G. Ueland, A. Mizel, J. S. Slusky, H. Karunadasa, R. J. Cava, and P. Schiffer, 2004, Phys. Rev. B **70**, 184431.
Snyder, J., B. G. Ueland, J. S. Slusky, H. Karunadasa, R. J. Cava, A. Mizel, and P. Schiffer, 2003, Phys. Rev. Lett. **91**, 107201.
Snyder, J., B. G. Ueland, J. S. Slusky, H. Karunadasa, R. J. Cava, and P. Schiffer, 2004, Phys. Rev. B **69**, 064414.
Soderholm, L., J. E. Greedan, and M. F. Collins, 1980, J. Solid State Chem. **35**, 385.
Solovyev, I., 2003, Phys. Rev. B **67**, 174406
Sosin, S. S., L. A. Prozorova, A. I. Smirnov, P. Bonville, G. Jasmin-Le Bras, and O. A. Petrenko, 2008, Phys. Rev. B **77**, 104424.
Sosin, S. S., A. I. Smirnov, L. A. Prozorova, G. Balakrishnan, and M. E. Zhitomirsky, 2006, Phys. Rev. B **73**, 212402.
Sosin, S. S., A. I. Smirnov, L. A. Prozorova, O. A. Petrenko, M. E. Zhitomirsky, and J.-P. Sanchez, 2006, J. Magn. Magn. Mater. **310**, 1590.
Stevens, K. W. H., 1952, Proc. Phys. Soc., London, Sect. A **65**, 209.
Stewart, J. R., G. Ehlers, and J. S. Gardner, 2004, private communication.
Stewart, J. R., G. Ehlers, A. S. Wills, S. T. Bramwell, and J. S. Gardner, 2004, J. Phys.: Condens. Matter **16**, L321.
Subramanian, M. A., G. Aravamudan, and G. V. Subba Rao, 1983, Prog. Solid State Chem. **15**, 55.
Subramanian, M. A., and A. W. Sleight, 1993, in *Handbook on the Physics and Chemistry of Rare Earths*, edited by K. A. Gschneidner and L. Eyring (Elsevier Science, New York), p. 225.
Subramanian, M. A., B. H. Toby, A. P. Ramirez, W. J. Marshall, A. W. Sleight, and G. H. Kwei, 1996, Science **273**, 81.
Subramanian, M. A., C. C. Torardi, D. C. Johnson, J. Pannetier, and A. W. Sleight, 1988, J. Solid State Chem. **72**, 24.
Sushko, Yu., V. Y. Kubo, Y. Shimakawa, and T. Manako, 1996, Czech. J. Phys. **46**, 2003.
Sushkov, A. B., O. Tchernyshyov, W. Ratcliff, II, S. W. Cheong, and H. D. Drew, 2005, Phys. Rev. Lett. **94**, 137202.
Tabata, Y., H. Kadowaki, K. Matsuhira, Z. Hiroi, N. Aso, E. Ressouche, and B. Fåk, 2006, Phys. Rev. Lett. **97**, 257205.
Taguchi, Y., K. Ohgushi, and Y. Tokura, 2002, Phys. Rev. B **65**, 115102.
Taguchi, Y., Y. Oohara, H. Yoshizawa, N. Nagaosa, T. Sasaki, S. Awaji, Y. Iwasa, T. Tayama, T. Sakakibara, S. Iguchi, K. Ohgushi, T. Ito, and Y. Tokura, 2004, J. Phys.: Condens. Matter **16**, S599.
Taguchi, Y., Y. Oohara, H. Yoshizawa, N. Nagaosa, and Y. Tokura, 2001, Science **291**, 2573.
Taguchi, Y., and Y. Tokura, 1999, Phys. Rev. B **60**, 10280.
Taguchi, Y., and Y. Tokura, 2000, Physica B **284-288**, 1448.
Taira, N., M. Wakeshima, and Y. Hinatsu, 1999, J. Solid State Chem. **144**, 216.
Taira, N., M. Wakeshima, and Y. Hinatsu, 2001, J. Phys.: Condens. Matter **13**, 5527.
Taira, N., M. Wakeshima, Y. Hinatsu, A. Tobo, and K. Ohoyama, 2003, J. Solid State Chem. **176**, 165.
Tang, Z., C. Z. Li, D. Yin, B. P. Zhu, L. L. Wang, J. F. Wang, R. Xiong, Q. Q. Wang, and J. Shi, 2006, Acta Phys. Sin. **55**, 6532.
Tchernyshyov, O., R. Moessner, and S. L. Sondhi, 2002, Phys. Rev. B **66**, 064403.
Tchernyshyov, O., R. Moessner, and S. L. Sondhi, 2006, Europhys. Lett. **73**, 278.
Toulouse, G., 1977, Commun. Phys. (London) **2**, 115.

Troyanchuk, I. O., 1990, Inorg. Mater. **26**, 182.
Troyanchuk, I. O., and V. N. Derkachenko, 1988, Sov. Phys. Solid State **30**, 2003.
Troyanchuk, I. O., N. V. Kasper, D. D. Khalyavin, H. Szymczak, and A. Nabialek, 1998, Phys. Status Solidi A **167**, 151.
Tsuneishi, D., M. Ioki, and H. Kawamura, 2007, J. Phys.: Condens. Matter **19**, 145273.
Ueda, H., H. A. Katori, H. Mitamura, T. Goto, and H. Takagi, 2005, Phys. Rev. Lett. **94**, 047202.
Ueland, B. G., G. C. Lau, R. J. Cava, J. R. O'Brien, and P. Schiffer, 2006, Phys. Rev. Lett. **96**, 027216.
Ueland, B. G., G. C. Lau, R. S. Freitas, J. Snyder, M. L. Dahlberg, B. D. Muegge, E. L. Duncan, R. J. Cava, and P. Schiffer, 2008, Phys. Rev. B **77**, 144412.
van Duijn, J., N. Hur, J. W. Taylor, Y. Qiu, Q. Huang, S. W. Cheong, C. Broholm, and T. Perring, 2008, Phys. Rev. B **77**, 020405.
Velasco, P., J. A. Alonso, M. T. Casais, M. J. Martínez-Lope, J. L. Martínez, and M. T. Fernández-Díaz, 2002, Phys. Rev. B **66**, 174408.
Villain, J., 1977, J. Phys. C **10**, 1717.
Villain, J., 1979, Z. Phys. B: Condens. Matter **33**, 31.
von Gaertner, H. R., 1930, Neues Jb. Mineralog., Geol. Palaontol., Beilage-Bd. Abt. A **61**, 1.
Wang, R., and A. W. Sleight, 1998, Mater. Res. Bull. **33**, 1005.
Wannier, G. H., 1950, Phys. Rev. **79**, 357.
Wannier, G. H., 1973, Phys. Rev. B **7**, 5017.
White, S. J., M. R. Roser, J. Xu, J. T. van der Norrdaa, and L. R. Corruccini, 1993, Phys. Rev. Lett. **71**, 3553.
Wiebe, C. R., J. S. Gardner, S.-J. Kim, G. M. Luke, A. S. Wills, B. D. Gaulin, J. E. Greedan, I. Swainson, Y. Qiu, and C. Y. Jones, 2004, Phys. Rev. Lett. **93**, 076403.
Wills, A. S., R. Ballou, and C. Lacroix, 2002, Phys. Rev. B **66**, 144407.
Wills, A. S., M. E. Zhitomirsky, B. Canals, J. P. Sanchez, P. Bonville, P. Dalmas de Réotier, and A. Yaouanc, 2006, J. Phys.: Condens. Matter **18**, L37.
Wu, W., D. Bitko, T. F. Rosenbaum, and G. Aeppli, 1993, Phys. Rev. Lett. **71**, 1919.
Yafet, Y., and C. Kittel, 1952, Phys. Rev. **87**, 290.
Yamamoto, A., P. A. Sharma, Y. Okamoto, A. Nakao, H. A. Katori, S. Niitaka, D. Hashizume, and H. Takagi, 2007, J. Phys. Soc. Jpn. **76**, 043703.
Yamashita, Y., and K. Ueda, 2000, Phys. Rev. Lett. **85**, 4960.
Yanagishima, D., and Y. Maeno, 2001, J. Phys. Soc. Jpn. **70**, 2880.
Yaouanc, A., P. Dalmas de Réotier, V. Glazkov, C. Marin, P. Bonville, J. A. Hodges, P. C. M. Gubbens, S. Sakarya, and C. Baines, 2005, Phys. Rev. Lett. **95**, 047203.
Yasui, Y., S. Iikubo, H. Harashina, T. Kageyama, M. Ito, M. Sato, and K. Kakurai, 2003, J. Phys. Soc. Jpn. **72**, 865.
Yasui, Y., T. Kageyama, T. Moyoshi, H. Harashina, M. Soda, M. Sato, and K. Kakurai, 2006, J. Phys. Soc. Jpn. **75**, 084711.
Yasui, Y., M. Kanada, M. Ito, H. Harashina, M. Sato, H. Okumura, K. Kakurai, and H. Kadowaki, 2002, J. Phys. Soc. Jpn. **71**, 599.
Yasui, Y., Y. Kondo, M. Kanada, M. Ito, H. Harashina, M. Sato, and K. Kakurai, 2001, J. Phys. Soc. Jpn. **70**, 284.
Yasui, Y., M. Soda, S. Iikubo, M. Ito, M. Sato, N. Hamaguchi, T. Matsushita, N. Wada, T. Takeuchi, N. Aso, and K. Kakurai, 2003, J. Phys. Soc. Jpn. **72**, 3014.
Yavors'kii, T., W. Apel, and H.-U. Everts, 2007, Phys. Rev. B **76**, 064430.
Yavors'kii, T., M. Enjalran, and M. J. P. Gingras, 2006, Phys. Rev. Lett. **97**, 267203.
Yavors'kii, T., T. Fennell, M. J. P. Gingras, and S. T. Bramwell, 2008, Phys. Rev. Lett. **101**, 037204.
Yoshida, S.-i., K. Nemoto, and K. Wada, 2004, J. Phys. Soc. Jpn. **73**, 1619.
Yoshii, S., S. Iikubo, T. Kageyama, K. Oda, Y. Kondo, K. Murata, and M. Sato, 2000, J. Phys. Soc. Jpn. **69**, 3777.
Yoshii, S., and M. Sato, 1999, J. Phys. Soc. Jpn. **68**, 3034.
Zhang, F. X., J. Lian, U. Becker, R. C. Ewing, L. M. Wang, L. A. Boatner, J. Z. Hu, and S. Saxena, 2006, Phys. Rev. B **74**, 174116.
Zhang, F. X., J. Lian, U. Becker, L. M. Wang, J. Z. Hu, S. Saxena, and R. C. Ewing, 2007, Chem. Phys. Lett. **441**, 216.
Zhou, H. D., C. R. Wiebe, Y. J. Jo, L. Balicas, Y. Qiu, J. R. D. Copley, G. Ehlers, P. Fouquet, and J. S. Gardner, 2007, J. Phys.: Condens. Matter **10**, 342201.